FRA/TTC-82/07

RADIAL AXLE PASSENGER TRUCK EVALUATION;

LIFE TEST RESULTS

AND

VEHICLE PERFORMANCE PROBLEMS

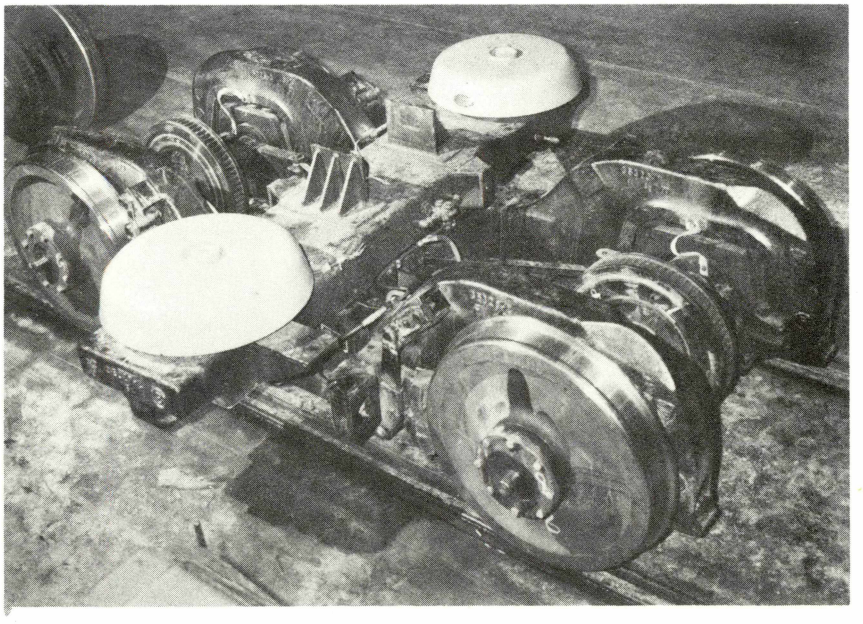

Final Report

03 - Rail Vehicles & Components

Technical Report Documentation Page

1. Report No.	2. Government Accession No.	3. Recipient's Catalog No.
FRA/TTC-82/07		

4. Title and Subtitle	5. Report Date
Radial Axle Passenger Truck Evaluation; Life Test Results and Vehicle Performance Problems	June 1982
	6. Performing Organization Code
	8. Performing Organization Report No.
7. Author(s) K. J. Simmonds	
9. Performing Organization Name and Address Boeing Services Intl., Inc. Transportation Test Center P.O. Box 11449 Pueblo, CO 81001	10. Work Unit No. (TRAIS)
	11. Contract or Grant No.
12. Sponsoring Agency Name and Address U.S. Department of Transportation Federal Railroad Administration Office of Research and Development, Office of Passenger Systems Washington, D.C. 20590	13. Type of Report and Period Covered Final Report May 1980 through June 1981
	14. Sponsoring Agency Code

15. Supplementary Notes

16. Abstract A pair of prototype radial-axle passenger trucks was tested at the Transportation Test Center, Pueblo, Co. With steering cross-links to provide yaw-angle compliance and axle stability, these trucks can execute axle radial alignment when negotiating curves; primary suspension is made up of separate vertical and horizontal springing.

Curving performance, stability, ride quality, braking performance, and component life were evaluated during extended service tests. This report covers vehicle safety, resolution of technical problems, wayside rail force data, and the extended service life testing. A separate report on the performance test phase has been prepared by Ensco, Inc. for the sponsoring agency (shown above); the Ensco report also cross-references this report. Safety factors considered were: overturning stability, wheel derailment, and equipment failure. A secondary suspension static instability was cured by doubling airspring roll stiffness. A running bias to the right, causing flanging, was solved by improving axle alignment, correcting axle lateral offset, and shimming the chevron primary springs. Vertical and lateral rail force data, compared to Pioneer III truck data, showed that the radial trucks generated less lateral force.

Life Test I was stopped when truck cross-link components failed; failures were analyzed. Life Test II began with the original wheel profiles and no speed restrictions. Wheelset hunting occurred at lower speeds as treads wore further. 'Effective Conicity' studies verified that critical speed decreased as effective conicity increased from wheel tread wear. Suspension stiffnesses, increased by spring modifications, were evaluated in curving and stability tests during Life Tests III and IV.

17. Key Words	18. Distribution Statement
radial-axle trucks effective conicity stability rail forces wheel tread wear curve performance	Document available through the National Information Service 5285 Port Royal Road Springfield, VA 22161

19. Security Classif. (of this report)	20. Security Classif. (of this page)	21. No. of Pages	22. Price
Unclassified	Unclassified	88	

Form DOT F 1700.7 (8-72) Reproduction of completed page authorized

This page left blank intentionally

TABLE OF CONTENTS

TABLE OF CONTENTS (CONTINUED)

LIST OF FIGURES

LIST OF FIGURES, CONTINUED.

LIST OF FIGURES, CONTINUED.

LIST OF TABLES

ACRONYMS

CTL	Component Test Laboratory
EDX	Energy Dispersive X-Ray
FAST	Facility for Accelerated Service Testing
FRA	Federal Railroad Administration
GSI	General Steel Industries
LH	left hand
NEC	Northeast Corridor
RAPT	Radial Axle Passenger Truck
RH	right hand
RTT	Railroad Test Track
SEM	Scanning Electron Microscopy
TTC	Transportation Test Center

ABBREVIATIONS AND METRIC CONVERSIONS

1',ft	foot	= 0.3048 m
g	gravity	
Hz	hertz	
",in	inch	= 25.4 mm
1 kip	1,000 lb	= 453.59 kg
kip-in	1,000 lb-in/degree	
lb	pound	= 453.59 g
m	meter	
mi/h	miles per hour	= 1.6094 km/h
mm	millimeter	
MN/m	Mega Newtons per meter	
MN/rad	Mega Newtons per radian	
mrad	milliradian	
ms	millisecond	
p-p	peak to peak	
psig	pounds per square inch gage	
s	second	

This page left blank intentionally

EXECUTIVE SUMMARY

This report describes the tests carried out on a pair of prototype radial-axle passenger trucks at the Transportation Test Center (TTC), Pueblo, Colorado, from May 1980 through June 1981. The trucks were designed and fabricated by General Steel Industries for Amtrak and were fitted to a standard Amcoach, car 21091. The principal feature of the trucks, which were designed for high speed, is a radial axle alignment capability during curve negotiation. This is accomplished by means of steering cross-links which connect the axles diagonally, to provide yaw angle compliance together with axle stability. An axle yaw damping feature was provided for test purposes only by hydraulic dampers which connected the axle ends horizontally to the truck frame. Primary suspension is provided by a two-part system which partially separates the vertical and horizontal springing. This system allows vertical springing to suit vehicle weight and suspension travel criteria, while permitting relatively soft horizontal shear springing for axle yaw compliance during curve negotiation.

The total test program encompassed curving performance, stability, ride quality, braking performance and component life evaluation through extended service testing. The Life Test Program was conducted by Boeing Services International, Inc. (BSI), the operations and maintenance contractor for the TTC. Ensco, Inc., had prime responsibility to the Federal Railroad Administration (FRA) for data collection, data processing, and analysis of the Performance Test. This report deals with tasks which were the responsibility of the TTC; these were vehicle safety, the resolution of technical problems that arose during early shakedown testing, and the extended service life testing.

Safety considerations addressed vehicle overturning stability, wheel derailment, and equipment failures. Overturning stability was examined and found not to be a potential problem, as cant deficiencies remained within acceptable limits at the highest test speeds. Of the possible modes of wheel derailment--wheel climb, rail rotation, or panel shifting--wheel climb was judged to be the only potential problem area due to the unknown dynamic stability characteristics of the truck. A means of monitoring L/V ratio (L = lateral, V = vertical load) was devised, using lateral suspension deflection and steering cross-link tension loads. Limiting values of lateral force were established to preclude wheel climb. Safety criteria for truck components and motions were established and monitored.

The problems that arose were a secondary suspension static instability caused by insufficient roll stiffness, flange contact due to poor initial axle alignment, premature failure of some of the truck components, and wheelset hunting. In the secondary suspension instability, the vehicle carbody rolled from bump stop to bump stop, due to the interaction of insufficient roll stiffness and slow leveling valve response. This rolling was cured by converting the suspension to a four-valve system, thereby doubling the air spring roll stiffness.

A flanging problem was discovered in early shakedown test runs, in which the wheelsets of the A truck displaced laterally on the track until flange

contact occurred. It was hypothesized that the problem was due to misalignment of the wheelsets. In a conventional truck the misalignment could be accommodated by the lateral flexibility of the wheelsets, but in the radial truck with increased lateral stiffness and control between axles, such self-correction was not possible. The theory was confirmed by modeling cases representing a conventional truck and a radial truck, using a non-linear curving prediction model for a curving situation with an infinitely large radius (10,000 m). The model predicts the wheel/rail forces, creepage, and lateral displacements which occur in a steady state curving situation. The model demonstrated the sensitivity of high lateral stiffness (i.e., radial truck) designs to axle misalignment. Alignment measurements were carried out on the problem truck using a highly accurate optical method developed at TTC. Correlating the actual measured axle misalignments with the computer predictions confirmed that the truck should develop wheel/rail contact in the flange root. Modifications were then made to the truck to improve the alignment; the steering cross-link length was adjusted to correct lateral offset, and the chevron springs were shimmed to correct radial misalignment. The flanging problem was corrected as a result of these changes.

As a part of the curving performance evaluation, vertical and lateral rail forces were measured at several strain-gaged track locations on the FAST (Facility for Accelerated Service Testing) track. The data were compared to the curving rail forces generated by the standard Amcoaches in the test consist that were equipped with Pioneer III trucks. The data were measured on the high rail only, and showed that both the leading and trailing radial trucks generated less lateral force than the conventional Pioneer trucks.

An extended service life test program was initiated, but the initial phase (designated Life Test I) was terminated after only 9,200 mi due to the failure of truck components. The failures were broken steering cross-links on the B truck, together with failed brake hangers; the tread brake cross-link attachment brackets were broken in several locations; and the disc brake fork bolts had cracks in four locations. A comprehensive analysis of the failures was carried out in the TTC Component Test Laboratory. The cross-link failures, which occurred at the spherical rod-end bearings, were caused by excessive tensile loads; the brake hangers, designed to flex to allow the brake shoes to align themselves with the wheel treads, failed in bending fatigue due to excessive wheelset hunting motion. Following the cross-link and brake hanger failures, the trucks were repaired, reassembled, and the life test, now designated Life Test II, was continued. The steering cross-links were redesigned with larger rod-end bearings; new brake hangers of the original design and redesigned disc brake fork bolts were fitted. Initial test runs were conducted at 120 mi/h around the track. Hunting was first noticed through the core area of the RTT (Railroad Test Track), and then spread to other areas of the track as the test progressed. As a result, speed limits had to be imposed on the test consist, at first through the core area and then over all of the RTT. As the wheel treads wore further, the speed limits were further reduced. Life Test II was concluded after approximately 31,000 miles of cumulative accelerated service operation which consisted of repeated New York-to-Washington, D.C. duty cycles.

As a result of the hunting phenomena, an 'effective conicity' study was implemented at TTC during Life Test II to determine whether the hunting

critical speed could be related to wheel/rail effective conicity changes caused by wheel tread wear. Wheel and rail profiles were measured using highly accurate profilometers, which measure the profile coordinates and relate them spatially to the mating wheel and rail. The data were processed by a computer program which effectively took a wheel profile pair and superimposed it on a corresponding rail profile pair, examining the rolling radius differences as the wheels were displaced laterally across the track. The resulting output, a rolling radius difference/lateral displacement plot, was then used to derive effective conicity values (defined as half the slope of the plot between the limits of root radius contact). Using a critical speed value from the test data and knowing the effective conicity for this test condition, a theoretical speed/conicity relationship was computed from a simplified hunting stability algorithm. Test data pairs, of critical speed and the effective conicity at the track station at which the speed was reported, were then superimposed on the theoretical plot. They showed reasonable agreement with the theoretical relationship, to within a 10 mi/h band of critical speed determination. It was concluded that increases in effective conicity resulting from wheel tread wear were the prime reason for the reduction in critical speed.

Two further service life tests, Life Test III and Life Test IV, were conducted. Each of these tests featured an increase in the horizontal shear stiffness and yaw stiffness of the truck primary suspension over the previous configuration, and wheel profiles turned, in an attempt to increase the critical speed/effective conicity relationship. For Life Test III, the horizontal rubber/steel sandwich elastomer springs were redesigned with a harder durometer rubber. Also, one of the three rubber layers was replaced by a steel spacer. For Life Test IV, the two-layer spring used previously was modified by drilling four holes through the top layer and pinning the steel layers together with steel dowels. This was done to isolate one layer of rubber. Although spring modifications yielded some incremental increases in critical speed the predominating effect remained that of wheel wear, giving rise to increased effective conicity and reduced critical speeds for the onset of wheelset hunting.

Curving and stability tests were carried out for the spring configurations used in Life Tests III and IV. High rail lateral forces were measured for each configuration over a 10 to 45 mi/h speed range on the FAST track. The data showed that there were no significant increases in lateral force due to increasing the primary yaw stiffness. Critical speed/effective conicity trends were developed from the stability data. These illustrated the improvement in critical speed due to the increased spring stiffness, but indicated that the truck design might have insufficient axle lateral stability to cope with the range of effective conicities that could be expected in service. As a result, a parametric study was proposed by the TTC, using curving performance and hunting stability math models to examine the effect of design changes on the radial axle design concept. The parametric study has not been funded at the time of publishing this report.

As a prerequisite to this study, a series of truck characterization tests was carried out to define the primary suspension characteristics, together with the torque required to overcome static bolster rotational friction. The tests defined the spring rates of the primary spring configurations evaluated in Life tests I through IV.

This page left blank intentionally

1.0 INTRODUCTION

The performance advantages of articulated trucks over the conventional three-piece North American freight trucks are well established and documented. Radial trucks exhibit improved curve negotiation performance, resulting in lower rates of wheel flange wear and reduced track gage and alignment maintenance. They offer stable guidance in high speed/light load freight operation, where conventional three-piece trucks are subject to the lateral limit-cycle oscillation phenomena commonly referred to as 'hunting'.

The application of radial steering concepts to high speed passenger applications is not so well established. The purpose of this test program was to evaluate a prototype radial axle passenger truck in this application and to determine if the claimed benefits of the radial axle concept can be realized. The potential advantages are:

- Improved curving performance, resulting in less wheel tread and flange wear, less rail wear, and reduced noise levels in the curves.
- Increased high speed stability and better ride quality.

The radial axle passenger trucks which are the subject of this evaluation were designed and fabricated by General Steel Industries (GSI). Two prototype trucks were purchased by Amtrak and fitted to a standard locomotive-hauled Amcoach, car 21091.

The Radial Axle Passenger Truck (RAPT) test program was sponsored by the Federal Railroad Administration (FRA), Office of Research and Development, Office of Passenger Systems, and was carried out at the Department of Transportation, Transportation Test Center (TTC), Pueblo, Colorado from May 1980 through June 1981. Operation of the test program was conducted for the FRA by ENSCO, Inc. during the performance tests and by Boeing Services International, Inc., the TTC operations and maintenance contractor, during the life tests; the TTC also had responsibility for test program safety. The prime data collection, processing, and analysis tasks were assigned to Ensco, Inc. during the performance tests. The TTC staff monitored several channels of information periodically during the life tests.

The test program scope included cutaway braking, stability, curving performance, ride quality tests, and component life evaluation through extended service testing. As the program progressed, various technical problems arose with the trucks. The problem areas included a secondary suspension static instability, poor tracking due to axle misalignment, truck hunting, and component failures.

This page left blank intentionally

2.0 THE RADIAL AXLE PASSENGER TRUCK

The following section contains a general description of the salient design features of the GSI prototype radial passenger truck, and continues with a discussion of the safety considerations and a description of two truck problem areas. The problems, which were identified and resolved in early shakedown test runs, were a static instability of the truck secondary suspension and poor tracking due to axle misalignment.

2.1 DESIGN FEATURES

The truck frame is a rigid, cast steel, H-frame design with inside journal bearings. A general view of the truck is shown in Figure 2-1. The axles are mounted to the truck frame by a two-part primary suspension system illustrated in Figure 2-2. The axle journal bearings are connected to upper journal boxes by means of elastomer/steel laminated springs. These have a high vertical spring rate, but have a low horizontal shear stiffness to provide the necessary compliance required for radial axle alignment. The upper journal boxes are in turn attached to the truck frame by a series of elastomer 'chevron' springs that provide vertical compliance with relatively high lateral and longitudinal stiffness. In this way, longitudinal/lateral and vertical stiffnesses can be, for all practical purposes, controlled independently. The chevron springs are supplemented by coil springs mounted between the top face of the upper journal boxes and the truck frame. The axle journals are coupled diagonally by two cross-links which provide the radial steering function. These provide direct transmission of stabilizing forces between wheelsets and improve stability at high operating speeds without interfering with the self-steering characteristics of the wheelsets. The cross-links can be seen in Figure 2-3. Radial motion (yaw) damping can be provided, as an option, by hydraulic dampers, mounted between bearings on the outside of the wheels and the truck frame (Figure 2-4); these were removed after an initial evaluation period. Braking is provided by a combination of disc brakes and tread brakes. A single disc unit is mounted at the center of each axle (also illustrated in Figure 2-3); tread brake units are mounted at the center of the truck side frame and operate against each wheel.

The need for radial motion of the wheelsets necessitated the provision of flexible spring steel brake hangers. These allow the brake shoes to align themselves with the wheel treads when the wheelsets are yawed radially during curve negotiation. The tread brakes and hangers are illustrated in Figure 2-5. Secondary suspension springing is provided by two air springs per truck, mounted between the carbody bolster and truck bolster. The truck bolster doubles as an air reservoir for the air springs. Load leveling valves compensate for passenger load and track irregularities to provide a constant ride height. Vertical secondary damping is provided by means of a restrictor in the air spring system. The bolster is located longitudinally by two radius rods that are resiliently-mounted between the truck bolster and the carbody underframe.

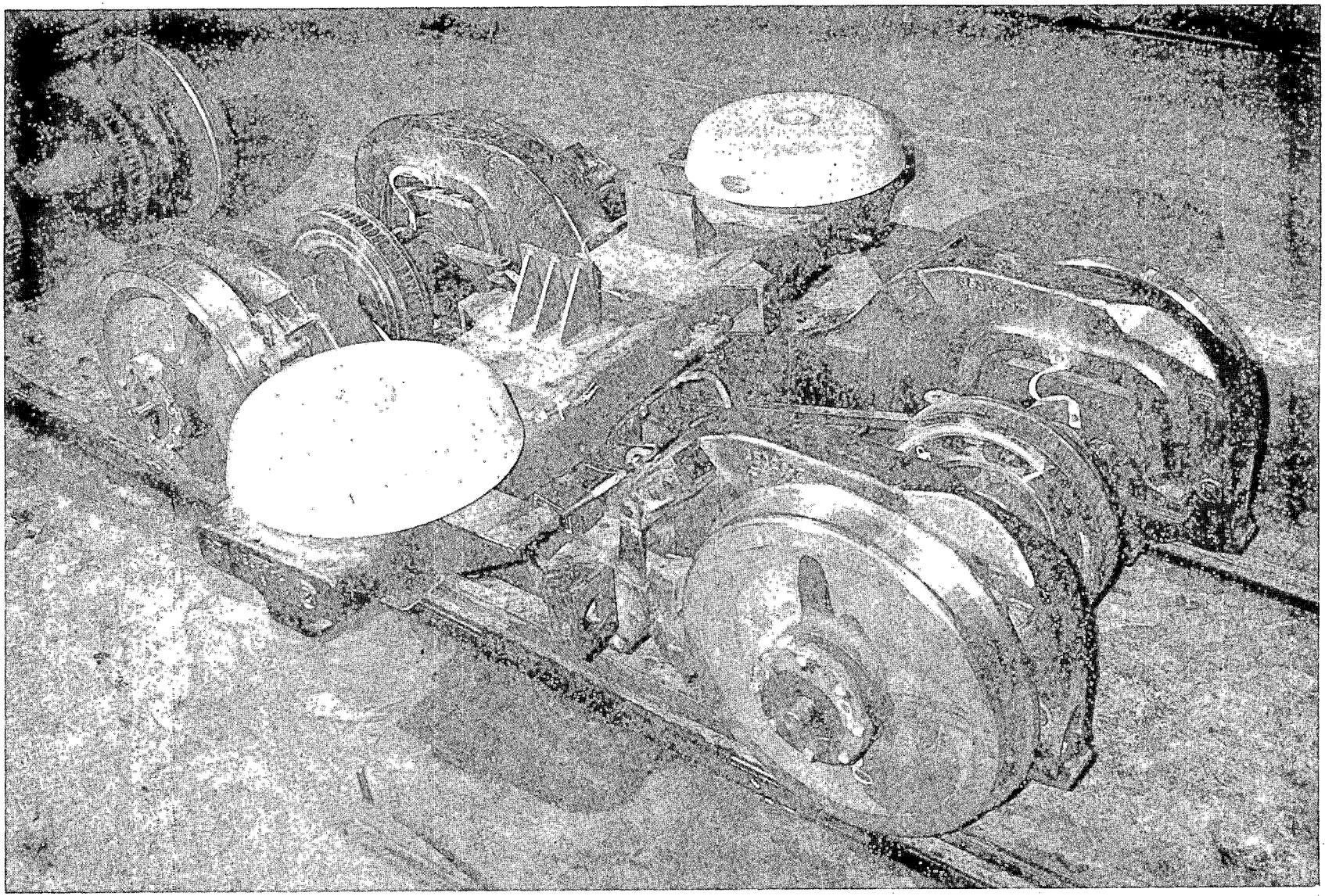

FIGURE 2-1. RADIAL AXLE PASSENGER TRUCK.

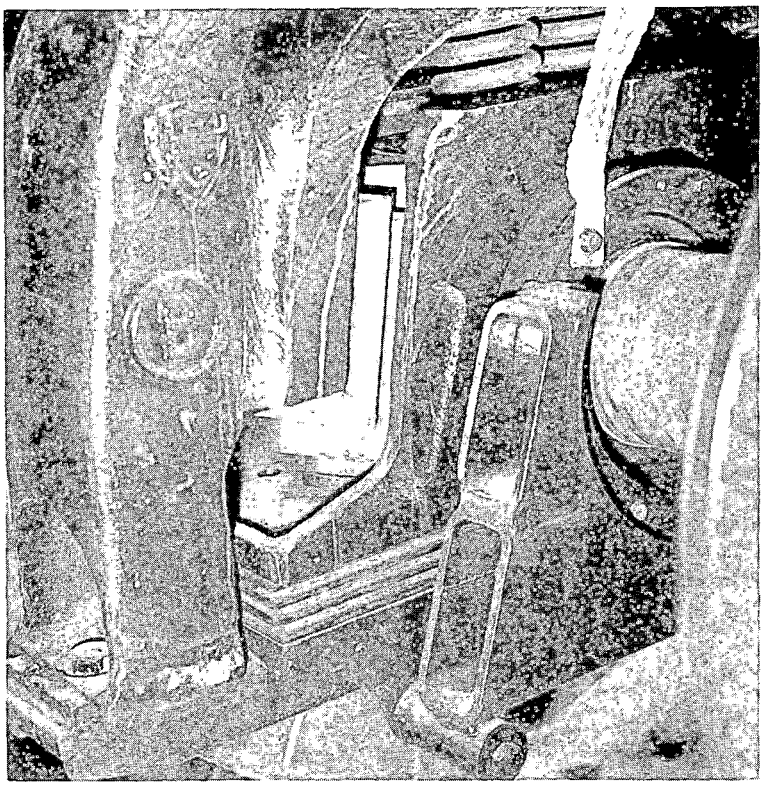

FIGURE 2-2. PRIMARY SUSPENSION.

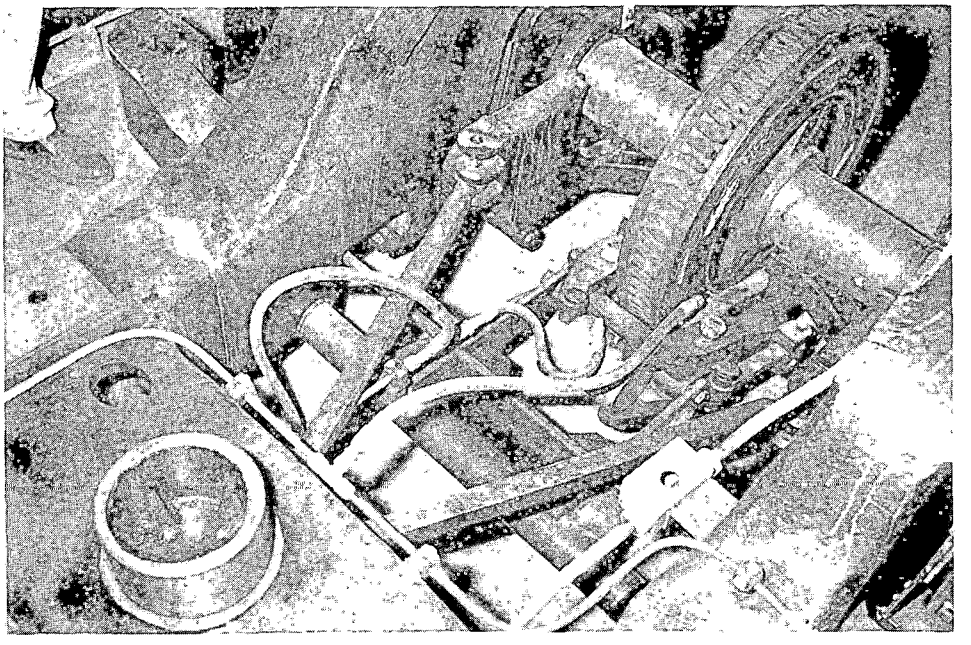

FIGURE 2-3. CROSS-LINKS AND DISC BRAKE.

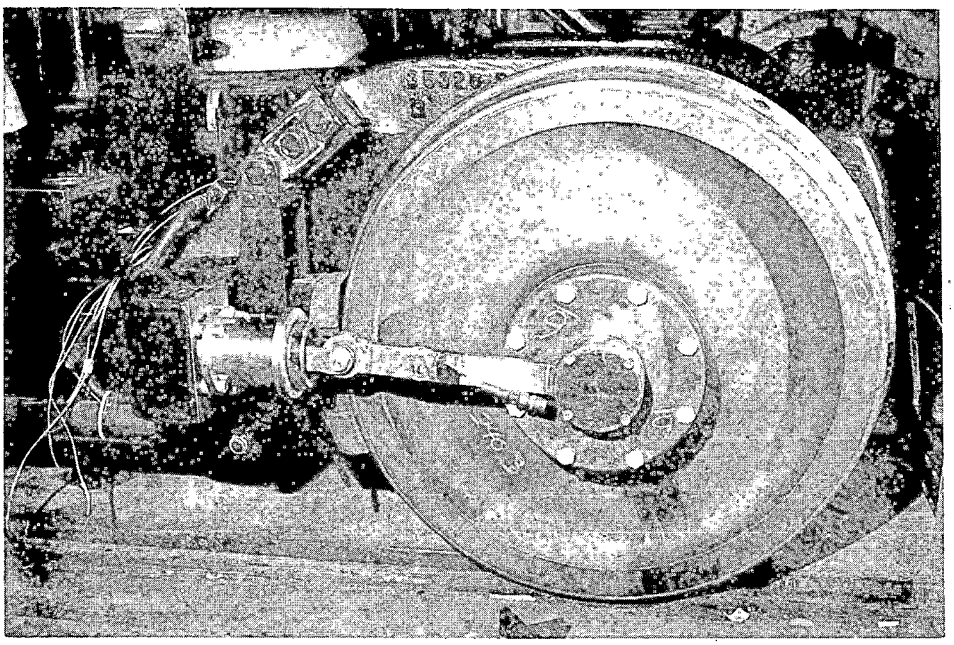

FIGURE 2-4. YAW DAMPERS.

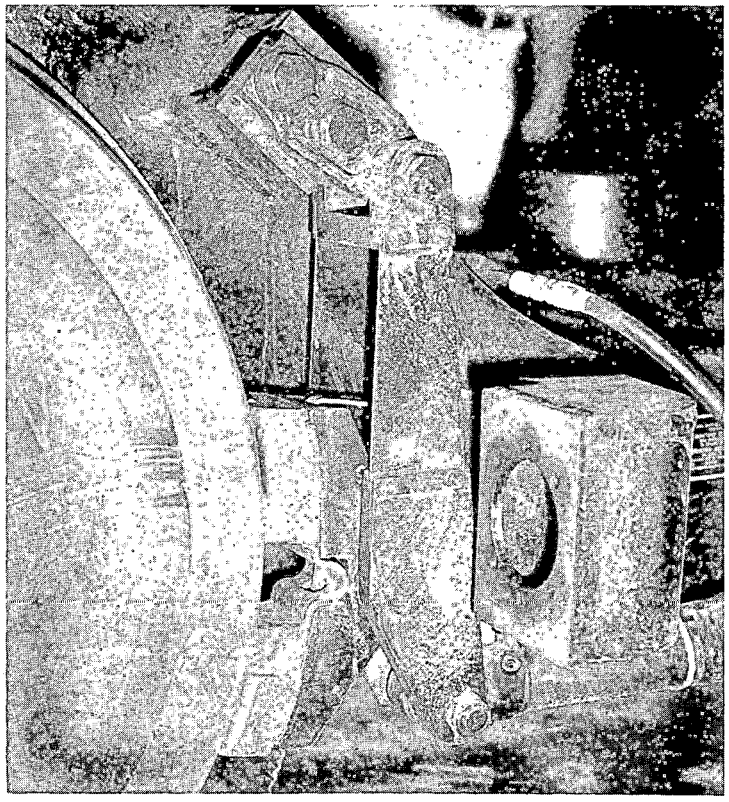

FIGURE 2-5. TREAD BRAKES AND HANGERS.

2.2 TEST PROGRAM SAFETY

2.2.1 Safety Considerations

Prior to the commencement of the test program, all aspects of test safety were carefully considered. These can be categorized in the following groups:

- Vehicle Overturning Stability
- Wheel Derailment
- Equipment Failures.

Each of these safety categories was considered in relation to the RAPT test program. A brief discussion of the conclusions is contained in the following paragraphs.

- Vehicle Overturning Stability. Vehicle overturning is caused primarily by the centrifugal forces resulting from curve negotiation at high speeds, with crosswind forces a significant contributer of much smaller magnitude. The RAPT program did not include operating at high cant deficiencies; i.e., beyond the three-inch unbalance limits established by FRA track safety standards. The limiting case, assuming availability of a high speed locomotive, was assumed to be test operations at speeds of 130 mi/h. At this speed on the 0° 50'curves of the Railroad Test Track (RTT), which have an uncompensated superelevation of 3.6 inches, the resultant vector of the centrifugal force and gravity vectors would intersect the plane of the rail heads approximately 10 inches from the high rail. Therefore, overturning stability was not a limiting safety consideration.

- Wheel Derailment. The primary concern during the safety planning stages of the program was with derailment, due to the unique nature of the truck design. Derailment normally results from wheel climb, rail rotation, or panel shifting. Each of these phenomena can be related to high lateral force to vertical force (L/V) ratios at the wheel/rail interface. Wheel climb was judged to be a potential problem area due to the unknown dynamic stability characteristics of the radial truck. Limit-cycle lateral oscillations, i.e., truck hunting, wheelset hunting, or carbody hunting were seen as the potential contributors to adverse L/V ratios when negotiating perturbations at high speed. Some means of measuring L/V ratio was considered to be essential to monitor truck stability; in addition, comparison of the curving performance of the RAPT vehicle to the Amcoach cars equipped with Pioneer III trucks, that were in the test consist, was suggested.

  Rail rotation, produced by high steady state L/V ratios, results in gage widening and subsequent derailment. This normally results from situations where vertical wheel unloading occurs simultaneously with high lateral loading. The radial truck was regarded as behaving in a similar manner to conventional trucks in this regard, and so rail rotation was not considered to be a significant hazard.

The steady state lateral forces produced by the Amcoach trucks were considered to be small in comparison to those developed by the locomotive. Therefore, the prime concern related to panel shifting was associated with the operation of the test locomotive at the high end of its speed range. The DOT-001 locomotive has been tested at speeds up to 130 mi/h on the RTT track, and the forces developed were considered to be less than the force required to produce panel shifting. Tests for locomotives similar to DOT-001 have shown a tendency for the locomotive to develop a yawing oscillation that can be related to high locomotive body accelerations. Lateral locomotive body acceleration was therefore a required safety parameter.

Due to the experimental nature of the RAPT vehicle, its steady state lateral and vertical forces were monitored until a level of confidence was obtained. Wheelset lateral forces were computed from primary suspension lateral displacement and cross-link loads. The lateral suspension was instrumented with displacement transducers, and the cross-links were strain gaged and calibrated as force transducers. Knowing the angle of the cross-links to the axle axes of rotation (Θ), wheelset lateral forces (L) were computed from:

$$L = (\text{primary lateral displacement} \times \text{primary lateral stiffness}) + (\text{cross-link axial force} \times \sin \Theta)$$

An operating limit of 12,240 lb lateral force was established, based on a European safety limit formula.

- Equipment Failure. A prime safety consideration from the equipment failure standpoint was the monitoring of stresses in components which play an important role in maintaining truck stability. Strain data from the steering cross-links and the yaw dampers were considered to be in this category. The strain data in the cross-links represent the forces in the links, and the time history signature of the strain data is an indicator of the degree of wear in the end fittings. The maintenance of consistent peak force levels in the dampers indicates that these are remaining effective and therefore contributing to dynamic vehicle stability.

2.2.2 Safety Limits

Safety limits were established and the critical data channels were monitored throughout the performance test program on oscillograph recorders. The established limits are shown in Table 2-1. A selected number of these channels were monitored periodically during the life tests.

2.3 SECONDARY SUSPENSION ROLL INSTABILITY

The Amcoach cars for the test consist were shipped to the TTC on their regular Pioneer III trucks. Then the bolster adaptors and radial trucks were

TABLE 2-1. RADIAL TRUCK SAFETY LIMITS.

Description	Frequency Range (Hz)	Limit
Lateral journal box acceleration, radial truck	0-50	20 g p-p
Lateral journal box acceleration, reference truck	0-50	20 g p-p
Vertical motion of primary suspension	0-50	0.75" up for seated loads
Lateral motion upper box to journal box displacement, radial truck	0-50	± 3/4"
Longitudinal primary frame to journal box displacement, radial truck	0-50	± 3/4"
Truck frame to bolster swivel, radial truck	0-20	1.5 x peak* average on reference truck
Truck frame to bolster swivel, reference truck	0-20	--
Angle of attack, radial truck	0-20	Not greater than reference truck
Angle of attack, reference truck	0-20	--
Consist speed	--	Table 4.3
Locomotive carbody lateral acceleration***	0-10	1.2 g p-p
Lateral force, radial truck, A-end lead axle*	0-20	12,240 lb**
Lateral force, radial truck, A-end trailing axle*	0-20	12,240 lb**
Axle box tilt, A truck	0-10	± 3 degrees
Lateral Acceleration on carbody, radial truck***	0-10	1.0 g p-p
Lateral Acceleration on carbody, reference truck***	0-10	1.0 g p-p

* No undamped oscillations
** Based on 50 ms pulse duration.
*** At speeds below 80 mi/h on the RTT, these channels may be replaced by two carbody roll channels and one carbody lateral displacement on radial truck car.

installed on Amcoach car 21091. During a static (0 mi/h) inflation test of the assembled truck, bolster, and air springs, a secondary suspension stability problem was observed. A combination of insufficient secondary suspension roll stiffness, high center of gravity, and leveling valve response time produced an unstable secondary suspension system with the vehicle stationary. Insufficient roll stiffness allowed the carbody to roll over to the limit of the suspension stops. The leveling valves then acted to increase the pressure differential in the air springs, to correct the body roll. However, when the carbody started to right itself, the pressure differential (retained by the slow response of the leveling valves) acted to drive the carbody to the other extreme of its roll travel. The leveling valves then acted as a low response servo system to correct the new roll situation, and the cycle was repeated, creating a slow response instability.

The initial RAPT configuration used a three-valve leveling system, in which two air springs at one end of the car, each controlled by a leveling valve, provided all the roll stiffness for the vehicle. The other springs were cross-connected and controlled by a single valve; they maintained a constant floor height above the rail but provided no contribution to roll stiffness or cross-level correction. The system was modified by removing the cross-connection and adopting a four-valve leveling system. This allowed all the air springs to contribute to roll stiffness, effectively doubling the vehicle roll stiffness. Enough roll stiffness was then provided to overcome the 'pendulum' effect of the carbody mass acting about the center of lower sway, and stabilize the system.

A further problem relating to roll stiffness was encountered during early testing, following the modification to a four-valve leveling system. The carbody rolled to the inside of the curve when operating on a 6-inch superelevation, resulting in the mechanical failure of the high side leveling control valves. An exact analysis would require access to design data for the car and the trucks. However, it would appear that the restoring force of the airbags, even with the four-valve leveling arrangement, barely exceeds the out-of-balance resulting from the carbody tilt, with the result that dynamic track input causes a loss of carbody roll control. An interim 'fix' was implemented by removing a 15 psig limit on airbag differential pressure and the 4 second time delay characteristic of the leveling valves. While this was expedient for the test program, it removed the protection against a burst airbag due to excessive pressure or a faulty leveling valve, and is not recommended as a permanent modification. A reduction in air spring volume was suggested as the most promising solution, although this would increase both the effective roll stiffness and the effective vertical stiffness of the system. Obviously, a modification of this nature would require a comprehensive design study.

2.4 AXLE ALIGNMENT OVERVIEW.

During early shakedown of the RAPT vehicle, it was noted that the wheelsets of both trucks had a tendency to roll towards flange contact. Subsequent investigation showed that the original wheel profiles had been incorrectly machined (to an effective negative conicity) due to a template error. The error in the template was corrected and the wheels were reprofiled

accordingly. The vehicle was once more checked for roll symmetry and it was discovered that, while the B truck now centralized itself on the tangent track, the A truck still rolled towards flange contact. Engineers at TTC theorized that the flanging problem was due to axle misalignment on that truck. In a conventional truck, such misalignment could be accommodated by the lateral flexibility between wheelsets. However the diagonal steering arms of the radial truck significantly increase the shear stiffness between the wheelsets, making realignment more difficult. In order to test the hypothesis, several cases were modeled using a nonlinear curving prediction math model. The model predicts the wheel/rail forces, creepage, and displacements that occur in a steady state curving situation. While not duplicating the RAPT problem, the model demonstrated the sensitivity of curving performance to wheelset lateral stiffness, and showed that a high lateral stiffness design was more susceptible to flanging problems due to axle misalignment. Axle alignment measurements were made using an extremely precise optical procedure developed at the TTC. The results of the alignment tests confirmed that the axles of the problem "A" truck were misaligned; analysis of these data, using the math model for the tangent track situation, confirmed the hypothesis that flanging would occur with such misalignments. Modifications were then made to the A truck to correct the misalignment problems. The lateral offset misalignment was corrected by altering the length of the cross-links, and subsequently the radial misalignment was corrected by shimming the chevron primary springs. The axle alignment problems and their resolution are discussed in detail in the following sections.

2.4.1 The Flanging Problem

The tendency of the A truck to displace laterally to the right when pulled from the A end is illustrated in Figure 2-6. The displacement resulted in wheel/rail contact at the flange root.

Typical alignment situations are illustrated in Figure 2-7; Θ_1, and Θ_2 denote the angles of the axles with respect to perpendiculars to the rail. Angular misalignment, the most common type of misalignment, usually results in flange contact at wheels on diagonally opposite corners. The misalignment shown in case B, where $\Theta_1 = \Theta_2$ is equivalent to the axles being misaligned laterally with respect to each other. This does not normally create problems in conventional trucks, because there is usually sufficient lateral shear flexibility between wheelsets to allow them to correct themselves. However the radial steering cross arms have the effect of significantly increasing the shear stiffness between the wheelsets, which results in higher realignment force requirements.

In order to test the hypothesis, hypothetical cases were examined using a nonlinear curving prediction model. This model predicts the wheel/rail forces, creepages, and displacements which occur in a steady state curving situation.[1] Two truck types were modeled, the first of conventional design

---

[1] Numbered references are listed at the end of this report.

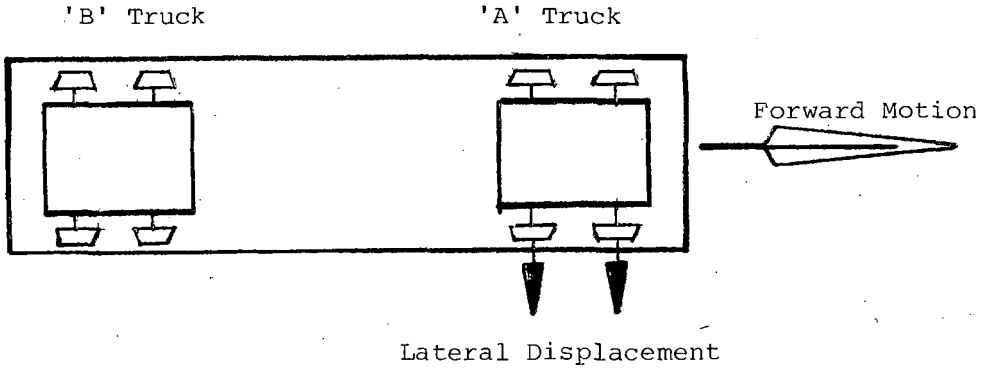

FIGURE 2-6. FLANGING PROBLEM CHARACTERISTICS.

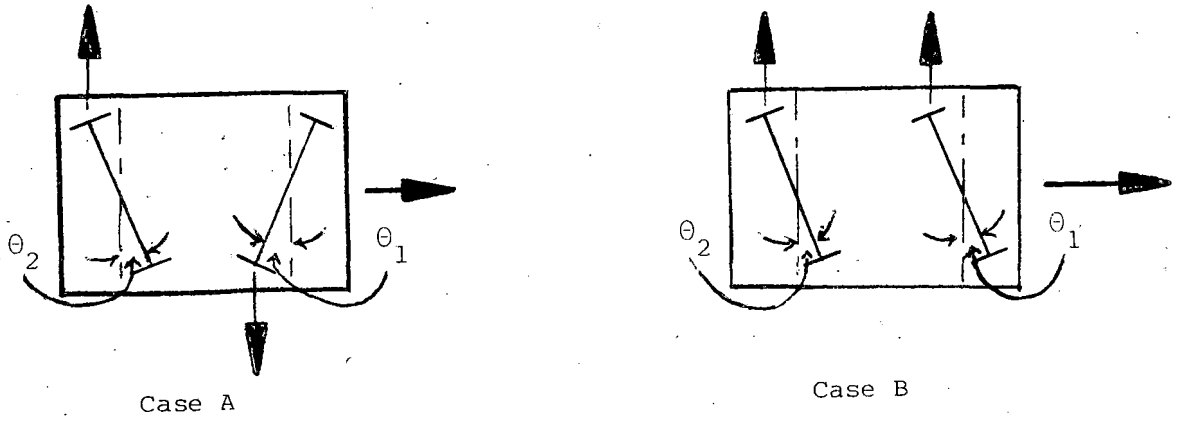

FIGURE 2-7. TYPICAL MISALIGNMENT SITUATIONS.

with low primary lateral shear stiffness 3 MN/m* and low primary yaw stiffness 3 MN/m. Other parameters used were typical of passenger service trucks. For the second case, the same parameters were used except that a shear stiffness of 20 MN/m was used. Both cases used conventional wheel/rail geometry data, new AAR 1:20 wheel profiles on new rail, canted to 1 in 40. Several cases of misalignment, i.e., various values of θ_1 and θ_2 were modeled for curve negotiation through a large radius curve (10,000 m). At that time the program was not able to model the tangent track situation, therefore a large curve case was chosen.

For the $\theta_1 = \theta_2$ case (i.e., the RAPT case), with θ being varied from 0.25 to 2.0 milliradians (mrad) the wheelset lateral displacement trends are illustrated in Figure 2-8. The vertical axis of the graph represents the amount of lateral displacement of the wheelset from a centralized condition to achieve steady state equilibrium. The horizontal axis represents axle misalignment, θ. The trends show that the truck with the higher shear stiffness displaces laterally more than a truck with conventional stiffness, for the same lateral axle misalignment. For the assumed wheel and rail profiles and truck parameters, the model shows that flange contact could occur for 2.0 mrad of misalignment; $\theta_1 = \theta_2 = 2.0$ mrad is equivalent to a lateral misalignment of one axle with respect to the other of only 5.2 mm.

It should be emphasized that the modeling exercise did not duplicate the RAPT problem, since the truck parameters were assumed values and not actual ones. The high conicity wheel profile geometry was not available to the computer program, and the truck design stiffness parameters were considered proprietary information by the manufacturer. However, the parametric study identified the sensitivity of the radial-type concept to lateral misalignment.

2.4.2 Alignment Measurements

Axle alignment measurements were carried out using an optical method. The wheelsets of a truck were supported on two air bearings, as shown in Figure 2-9; when 'floated' by applying compressed air to the tables, each wheelset was relieved of the external forces acting on it and was free to take up an unstrained position. The air tables were then deactivated and precision scales were placed against the machined rim faces of the wheels on one side. The wheels were previously positioned to provide points of equal lateral runout at the scales, so that errors due to wheel machining eccentricities were eliminated. Figure 2-10 shows the scales in place against the wheel rims. The scales were then sighted with a highly accurate optical transit, which can be seen left of center in Figure 2-9. The transit gave precise measurements of the distance of the wheel rim points from an optical datum plane; knowing these dimensions and the distances between the scales, the relative angles of the wheelsets were calculated by simple triangulation. A diagram showing the measurements taken and the calculations made is shown in Figure 2-11. The test procedure was repeated three times to gain some measure of confidence in

---

* MN/m = Mega Newtons per meter.

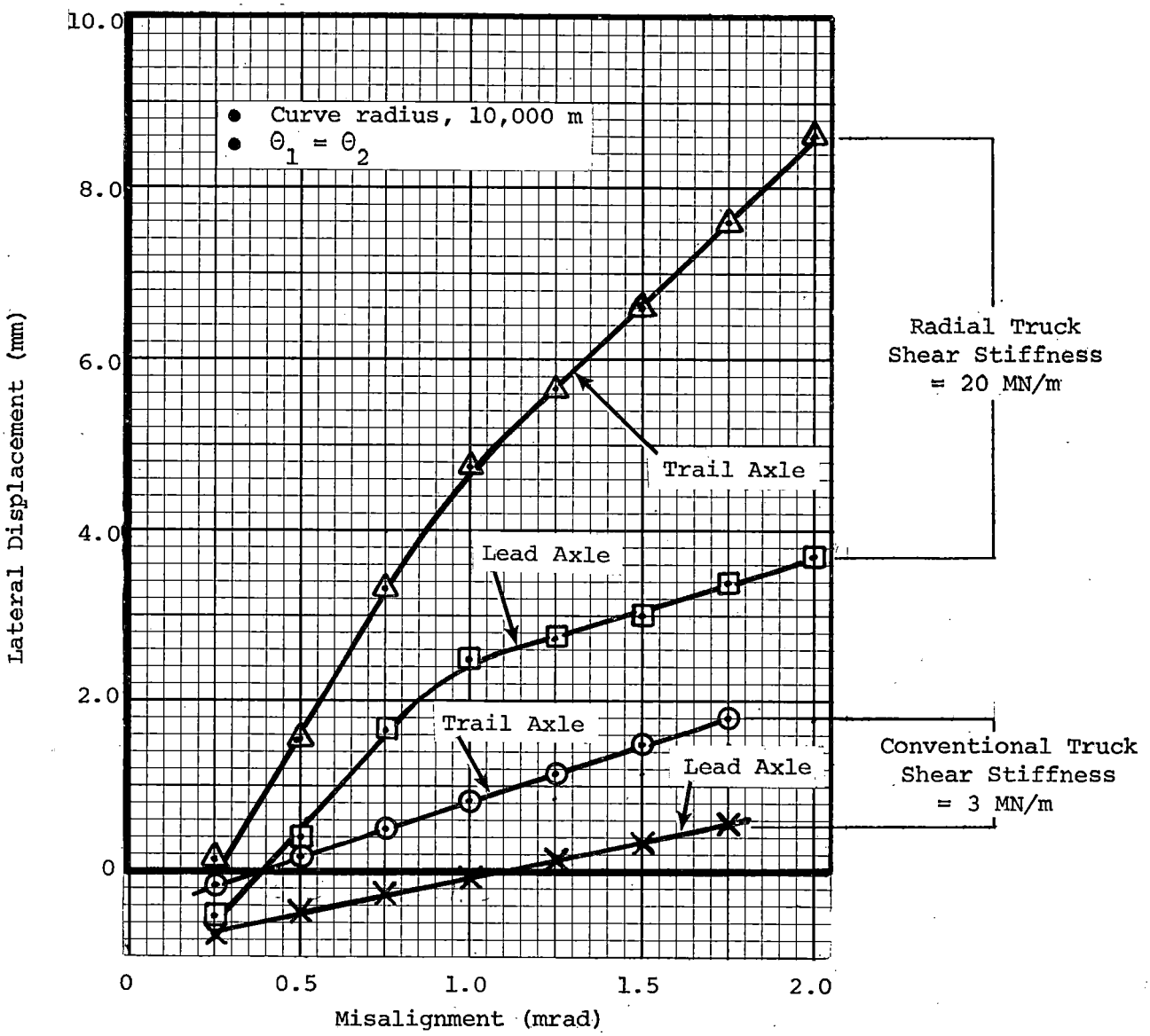

FIGURE 2-8. WHEELSET LATERAL DISPLACEMENT/EQUAL-ANGLE MISALIGNMENT TRENDS.

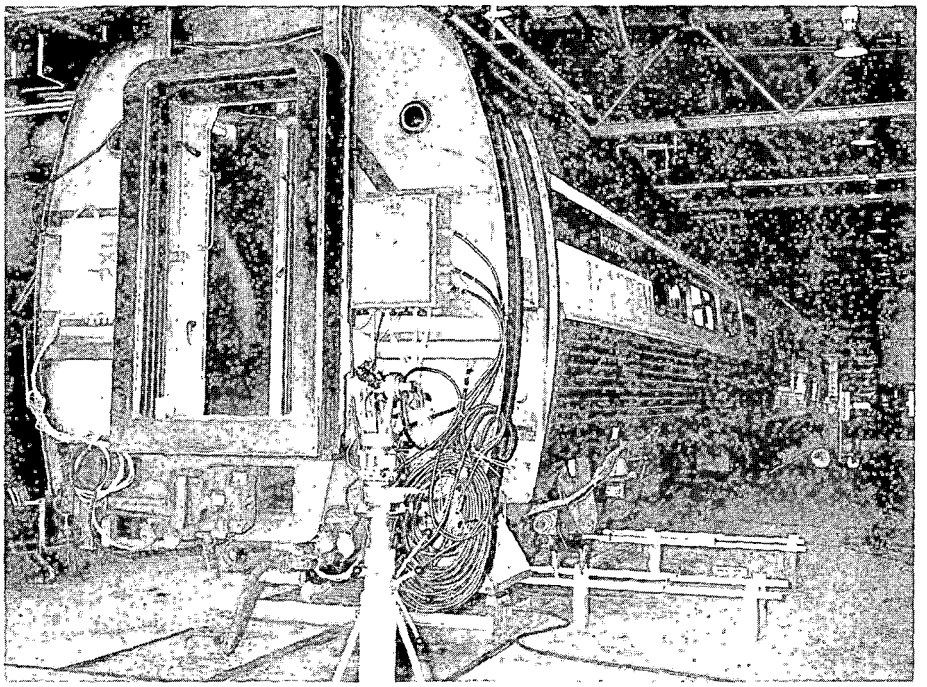

FIGURE 2-9. ALIGNMENT MEASUREMENTS, TEST SETUP.

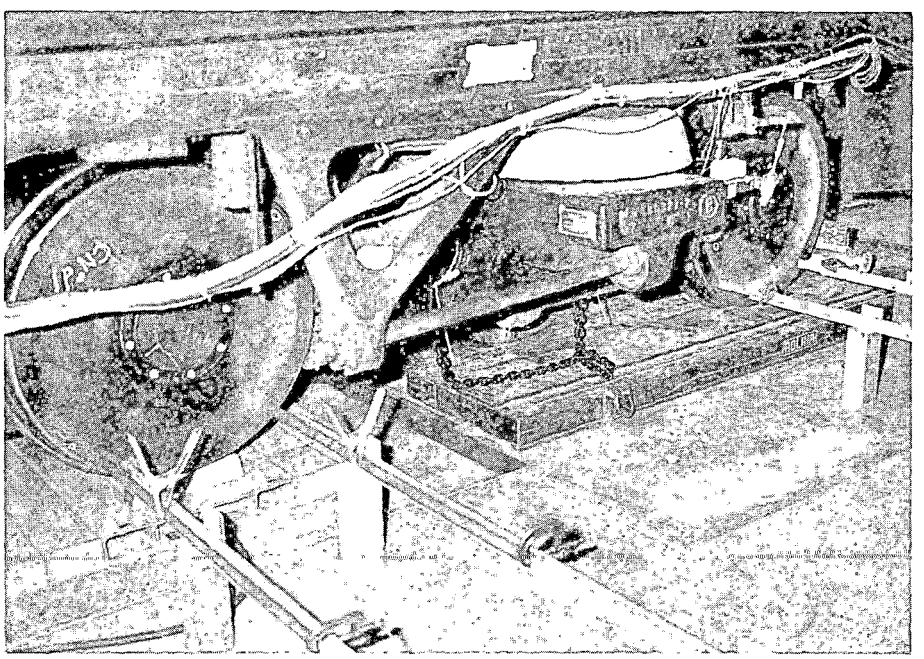

FIGURE 2-10. SCALE POSITIONING.

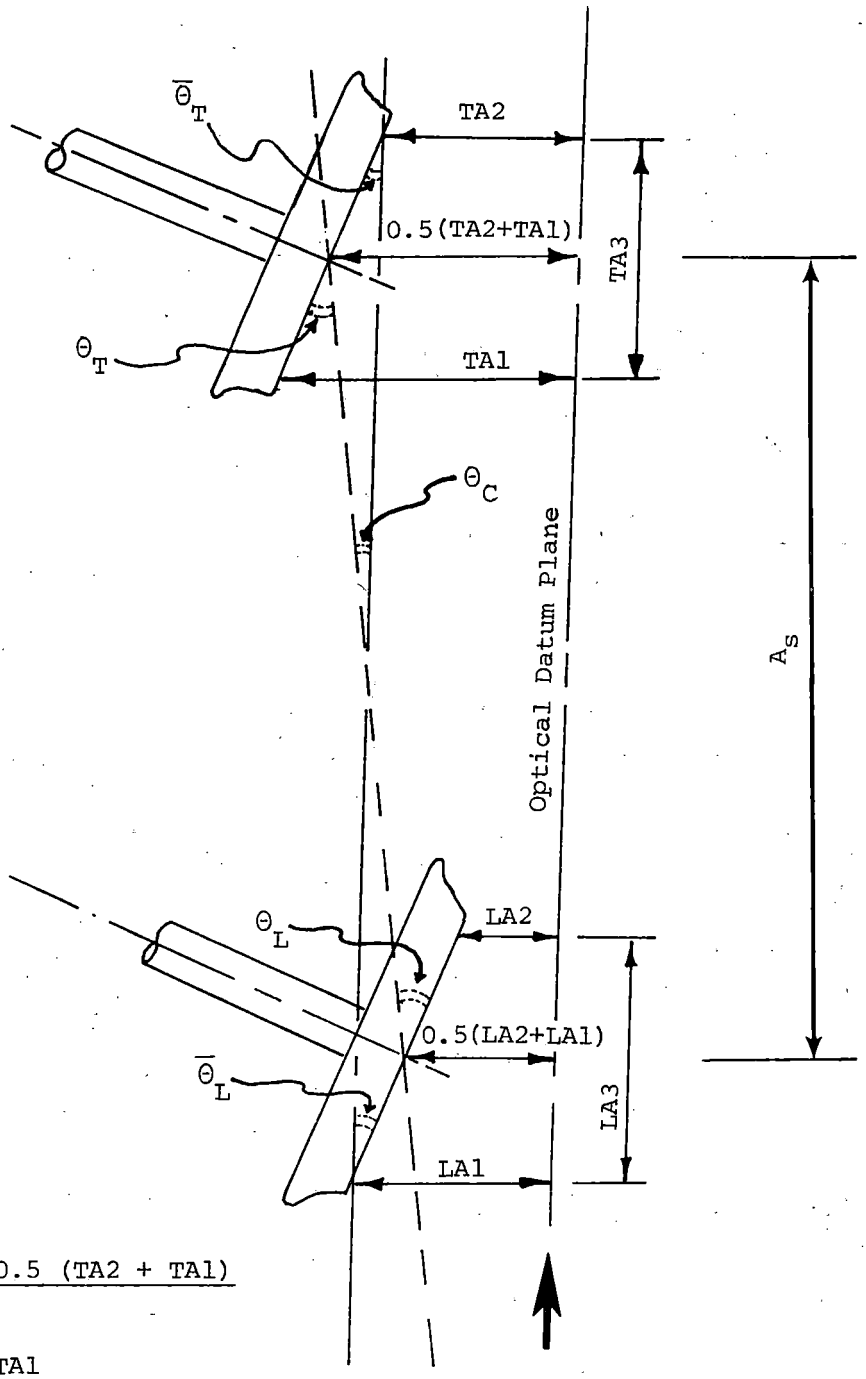

OBJECTIVE:

calculate Θ_T and Θ_L

$$\Theta_T = \overline{\Theta}_T - \Theta_C$$

$$\Theta_L = \overline{\Theta}_L - \Theta_C$$

Where:

$$\overline{\Theta}_T = \frac{(TA1 - TA2)}{TA3}$$

$$\overline{\Theta}_L = \frac{(LA1 - LA2)}{LA3}$$

$$\Theta_C = \frac{0.5\ (LA2 + LA1) - 0.5\ (TA2 + TA1)}{A_S}$$

$$= \frac{LA2 + LA1 - TA2 - TA1}{2A_S}$$

FIGURE 2-11. ALIGNMENT MEASUREMENTS AND CALCULATIONS.

the data. The A and B trucks were both measured for axle alignment, and the A truck was also examined with the cross-links disconnected.

The results of the tests are contained in Table 2-2. Θ_T and Θ_L represent the angles of each wheelset to a line drawn through the centers of both wheels. Thus the angles represent the deviation of each axle from its perfect alignment position; i.e., orthogonal to the truck longitudinal centerline and parallel to the other axle on the same truck.

TABLE 2-2. CALCULATED ALIGNMENT ANGLES.

Case 1. A Truck - Cross-Links Connected

	$\bar{\Theta}_T$	$\bar{\Theta}_L$	Θ_C	Θ_T	Θ_L
Measurement 1*	+0.24	+2.92	-0.88	+1.12	+3.80
Measurement 2	+0.38	+2.97	-0.85	+1.23	+3.82
Measurement 3**	-	-	-	-	-

Case 2. B Truck - Cross-Links Connected

	$\bar{\Theta}_T$	$\bar{\Theta}_L$	Θ_C	Θ_T	Θ_L
Measurement 1	-0.40	+0.23	-0.33	+0.06	+0.56
Measurement 2	-0-	+0.41	-0.23	+0.23	+0.64
Measurement 3	+0.04	+0.13	-0.27	+0.32	+0.41

Case 3. A Truck - Cross-Links Disconnected

	$\bar{\Theta}_T$	$\bar{\Theta}_L$	Θ_C	Θ_T	Θ_L
Measurement 1	+0.28	+3.19	-0.22	+0.49	+3.41
Measurement 2	+1.00	+3.53	-0.29	+1.03	+3.56
Measurement 3	+0.05	+2.73	-0.21	+0.25	+2.93

* All angles are in milliradians.
** The brakes were on for this measurement and the data are invalid.
Sign Convention: When viewed from above, clockwise displacements are positive angles.

The data showed that the B truck was relatively well aligned whereas the A truck, which had the flanging problem, was badly aligned. The mean alignment angles for each configuration are presented in Figure 2-12. The results are shown graphically and are explained by considering case 1. Alignment angles of Θ_T = +1.17 mrad and Θ_L = +3.81 mrad are shown on the left side. To aid interpretation of these results, it is shown that this misalignment can be resolved into two components. These components are:

Case A: A truck, cross-links connected;

Θ_T = +1.17 mrad Θ_L = +3.81 mrad

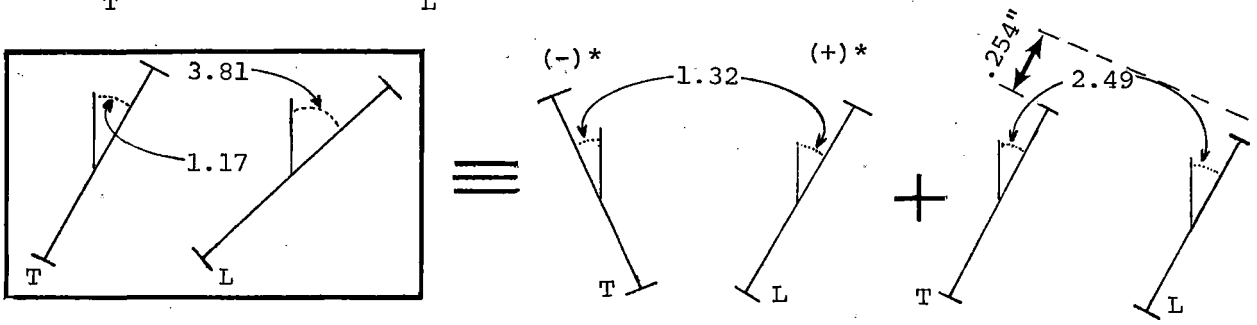

Case B: B truck, cross-links connected;

Θ_T = +0.20 mrad Θ_L = +0.54 mrad

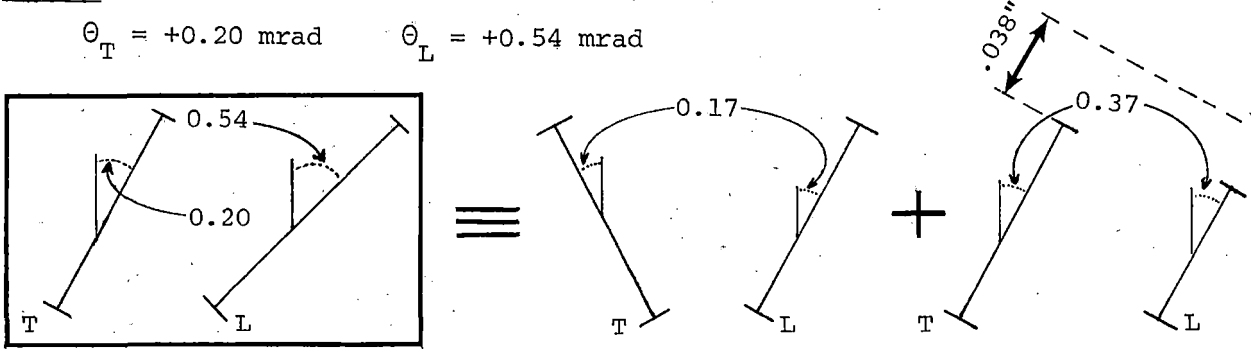

Case C: A truck, cross-links disconnected

Θ_T = +0.59 mrad Θ_L = +3.30 mrad

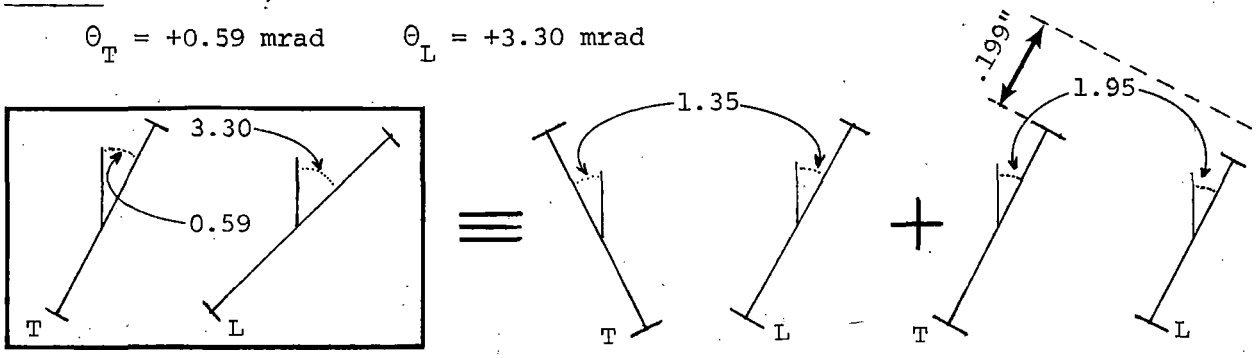

* Sign Convention: clockwise rotations are positive.

FIGURE 2-12. MEAN VALUES OF ALIGNMENT.

- Angles equal to ± 0.5 (3.81 - 1.17) = + 1.32 mrad (such that the axles have equal and opposite misalignments), and

- Equal angles of the same sign (3.81 - 1.32) or (1.17 + 1.32) = + 2.49 mrad.

The latter case (axles parallel to each other but at an angle to the correct orthogonal position) is equivalent to a lateral misalignment of one axle with respect to the other. This misalignment displacement was obtained by multiplying the angle (2.49 mrad) by the nominal truck wheelbase (102").

Therefore, with the cross-links connected, the A truck misalignment was equivalent to an equal and opposite misalignment angle of 1.32 mrad plus a lateral offset of 0.254"; truck B's misalignment was an order of magnitude smaller than this. The results substantiate the hypothesis that the flanging problem on truck A was due to misalignment. The measurements made on truck A with the cross-links disconnected showed little change from case 1, indicating that the cross-links themselves were not the major cause of the lateral offset.

The lateral misalignment of truck A, measured at 0.254", could be corrected by changing the length of one of the cross-links by approximately 0.2". However, this would have no significant effect on the equal and opposite angular misalignment.

In order to find the likely effect of these misalignments, some further hypothetical cases were run. The non-linear curving prediction method referred to earlier was used, modified to model a tangent track situation. Again, two types of trucks were considered. The first was of conventional design, with low primary lateral stiffness (3 MN/m) and low primary yaw stiffness (3.0 MN/mrad). The second was a radial truck with the same parameters, except that a lateral shear stiffness between the wheelsets of 20 MN/m had been added. This was an estimate of the constraint provided by the cross-links of the RAPT truck.

Computer runs were made for the two types of misalignment, $\Theta_L = \Theta_T$ and $\Theta_L = -\Theta_T$, for straight track. The results of the former case of are shown in Figure 2-13. This case was a repeat of the one modeled previously, except that a straight track simulation was used. Previously the simulation was carried out for a 10,000 meter radius curve. The results for the second case, i.e., $\Theta_L = -\Theta_T$, are shown in Figure 2-14. It can be seen that the radial type of truck was much more susceptible to misalignment than the conventional truck. Also, the angular misalignment was more serious than lateral misalignment. Only 0.75 mrad of misalignment was necessary to give flange contact on the leading wheelset, compared with 1.75 mrad on the trailing wheelset. The ± 1.32 mrad of misalignment measured on truck A was considered likely to induce flange contact, based on the modeling trends.

It must be emphasized that these results have been obtained using a hypothetical model of the truck, as the true parameters were not available. Given the actual parameters, more accurate estimates of the effects of these misalignments could be made. This would enable establishment of the necessary tolerances to which the alignment should be set.

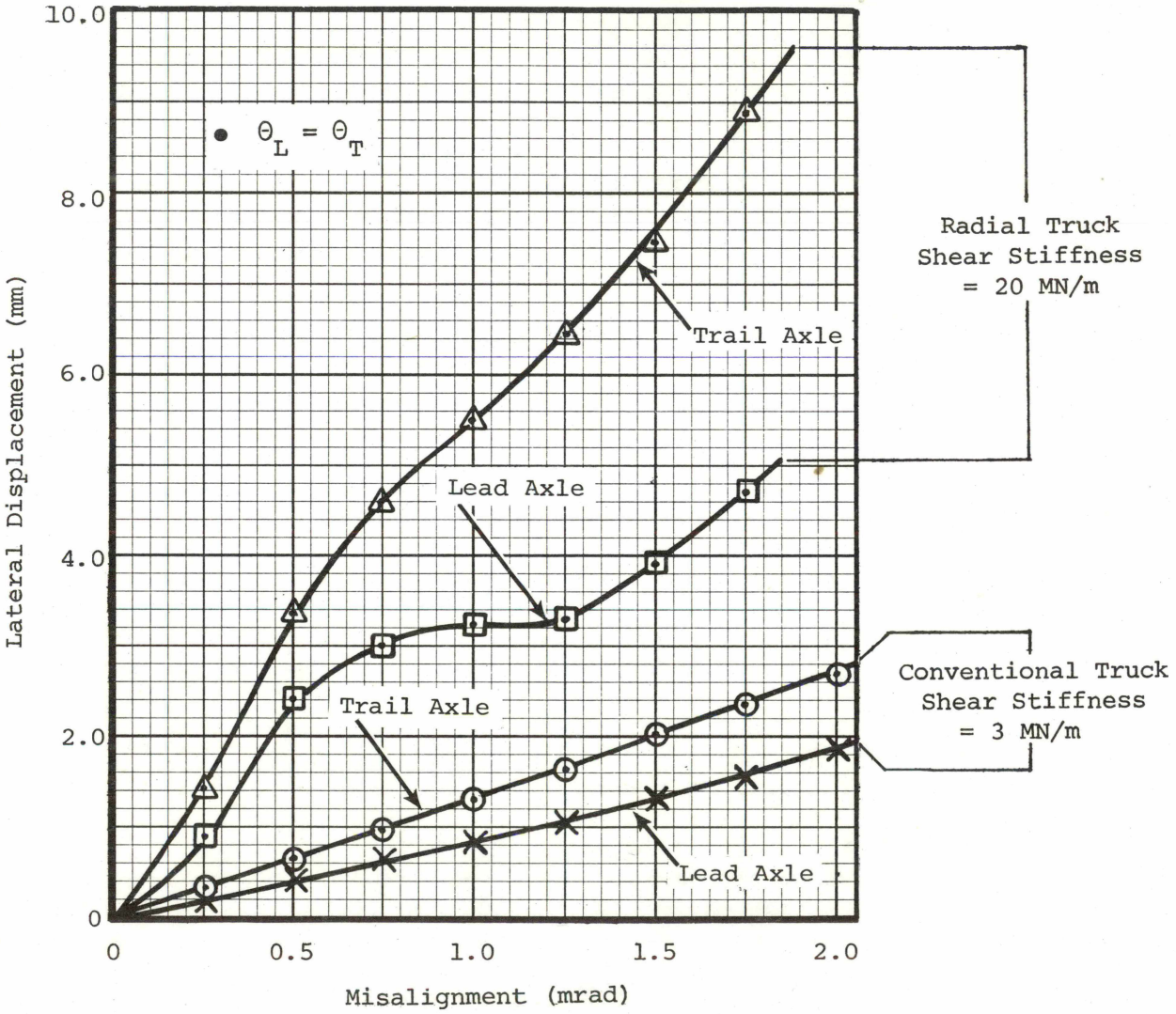

FIGURE 2-13. WHEELSET LATERAL DISPLACEMENT/EQUAL-ANGLE MISALIGNMENT TRENDS, TANGENT TRACK.

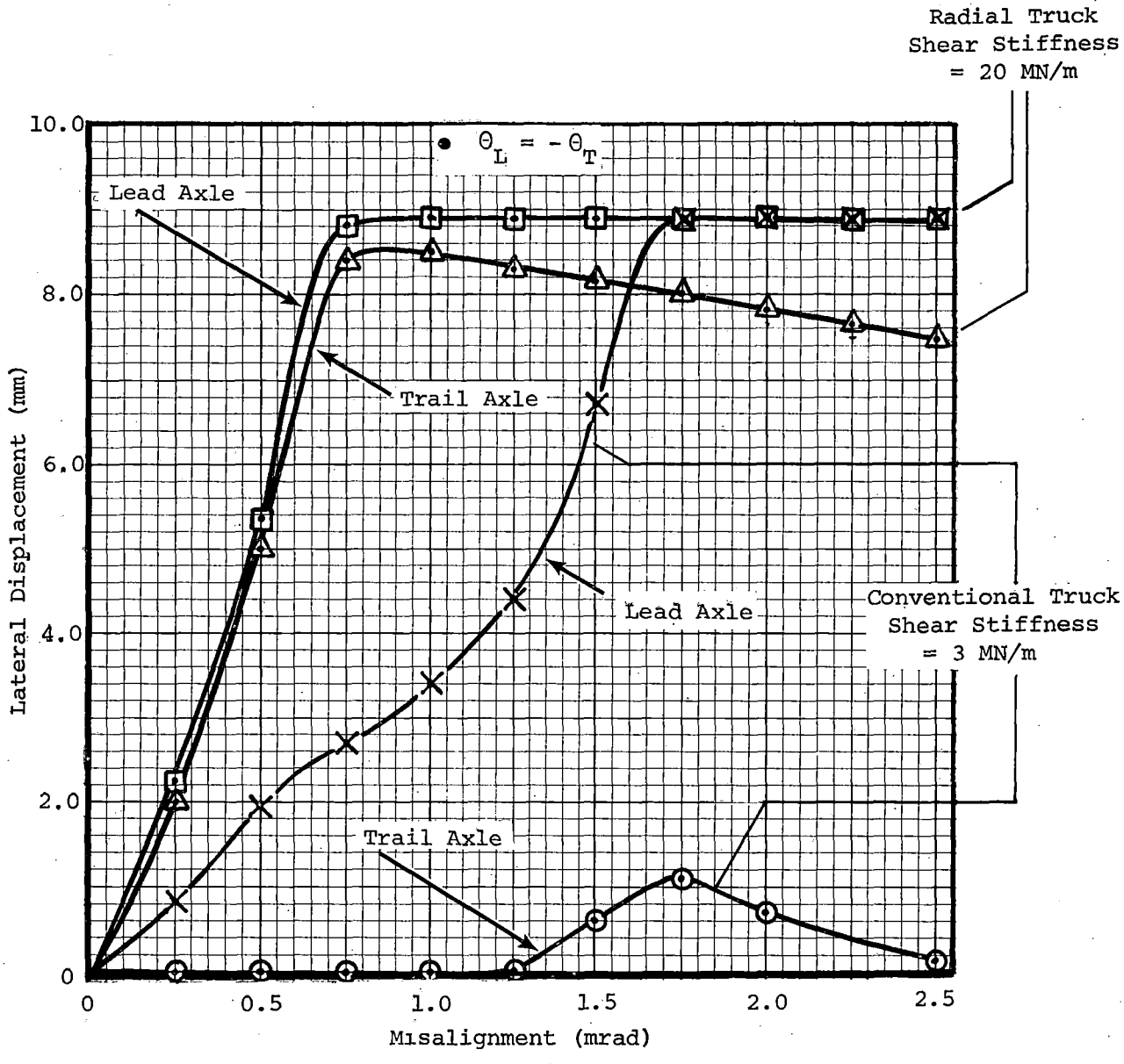

FIGURE 2-14. WHEELSET LATERAL DISPLACEMENT/EQUAL AND OPPOSITE MISALIGNMENT TRENDS, TANGENT TRACK.

2.5 VERTICAL AND LATERAL CURVING FORCES

The curving performance evaluation of the radial axle trucks included an investigation of the vertical and lateral forces exerted on the track during curve negotiation. The forces were compared to the forces generated by a similar coach equipped with conventional trucks. The evaluation was made by operating the test consist, which included the RAPT-equipped Amcoach and the reference Amcoach fitted with regular Pioneer III trucks, over a section of the FAST track containing four strain-gaged rail sections. The tests were conducted in Section 07, which is a 5° curve with four inches of superelevation; the section is constructed from 140 lb/yd rail on wood ties. Data were collected from the strain gage bridges on the high rail only, at tie locations 07-0214, 0277, 0325, and 0377.

The lateral and vertical force strain gage bridge configurations were similar to those illustrated in Figures 2-15 and 2-16, respectively. Lateral force gages were positioned on the heel of the rail at an angle of 45° to the web, in four locations spaced equidistantly between two ties. Vertical force gages were positioned on the rail web, on the neutral axis, and at 45° to the heel; eight gages were used at two locations between ties. The gages at each location were connected electrically, so as to cancel outputs due to strain caused by forces and moments other than pure lateral or vertical bending. Initial calibration of strain gage locations was made by applying point loads by means of hydraulic fixtures attached to a calibration car; calibration loads were measured by load cells attached to the cylinders. The initial calibration was correlated to a shunt resistor calibration, in which the strain gage bridge is artificially unbalanced by shunting one arm of the bridge with a fixed resistor. The resulting electrical output can be equated to a strain level from the load calibration. Thereafter the bridge conditioning/amplifying equipment can be checked for gain by shunting the bridge with the same resistor. Check system calibrations during the RAPT test program were made using the shunt calibration method to establish bridge sensitivities.

Test runs were made through the strain gaged test section at speeds of 10, 20, 33, 40, and 45 mi/h in both clockwise and counterclockwise directions of travel around the track. All runs were made with the RAPT and reference car A trucks leading. The signal outputs from the four strain gage locations were recorded continuously on analog tape and an oscillograph recorder at a wayside data acquisition van. Maximum vertical and lateral loads, corresponding to the passage of the truck axles over the strain gage locations, were tabulated from the oscillograph records for each run. The data from each pass-by speed were averaged from the four locations to improve their statistical reliability.

The high rail lateral force trends with speed are presented in Figures 2-17 and 2-18. Radial truck and conventional truck performances are compared for each axle. In both clockwise and counterclockwise directions of travel, the RAPT lead axle high rail lateral forces were considerably lower than those of the reference car; trailing axle forces were of similar magnitude for both radial and conventional truck types. High rail vertical force trends are presented in Figures 2-19 and 2-20 for clockwise and counterclockwise travel, respectively. The data were plotted versus speed squared, since cant deficiency/excess, and therefore high rail vertical force, is proportional to velocity squared, ignoring second order creep and gyroscopic effects.

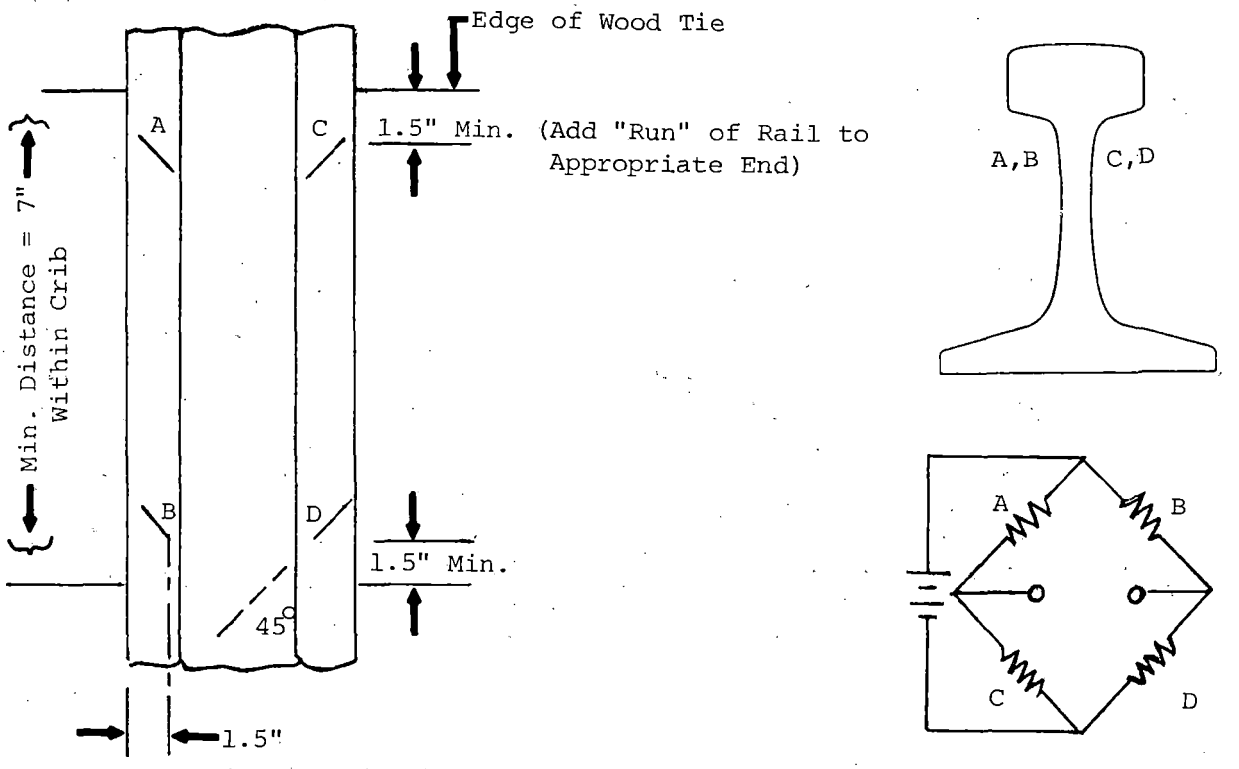

FIGURE 2-15. LATERAL LOAD-MEASURING CIRCUIT.

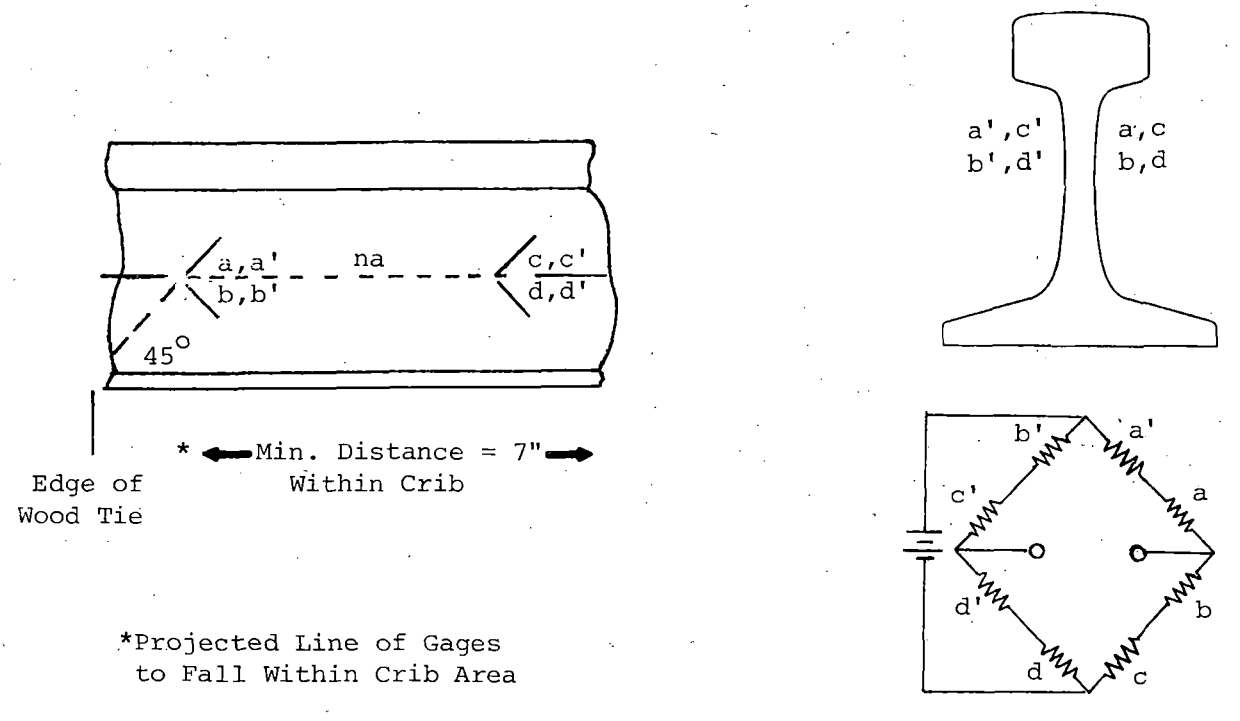

*Projected Line of Gages to Fall Within Crib Area

FIGURE 2-16. VERTICAL LOAD-MEASURING CIRCUIT.

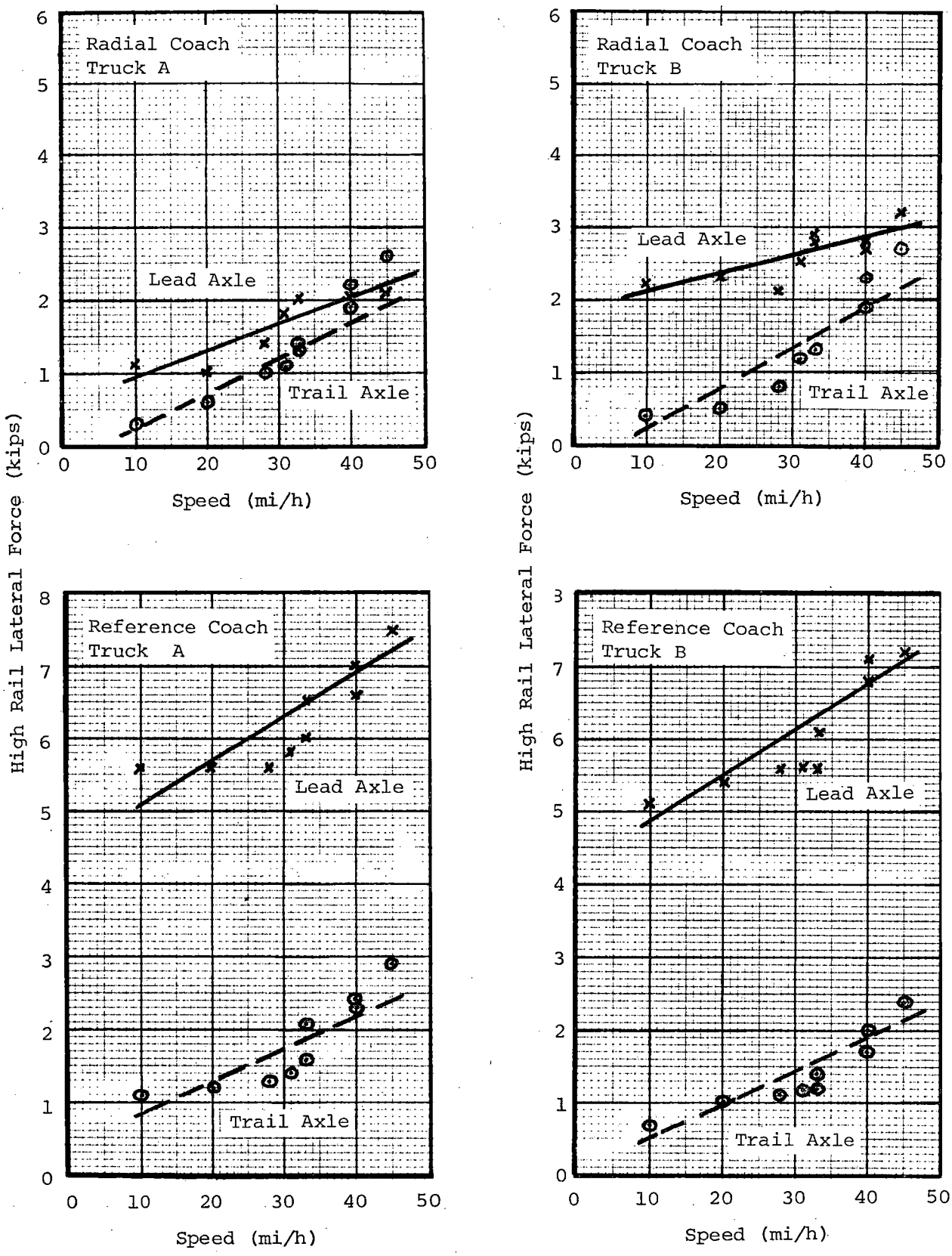

FIGURE 2-17. HIGH RAIL LATERAL FORCES, CLOCKWISE RUNNING.

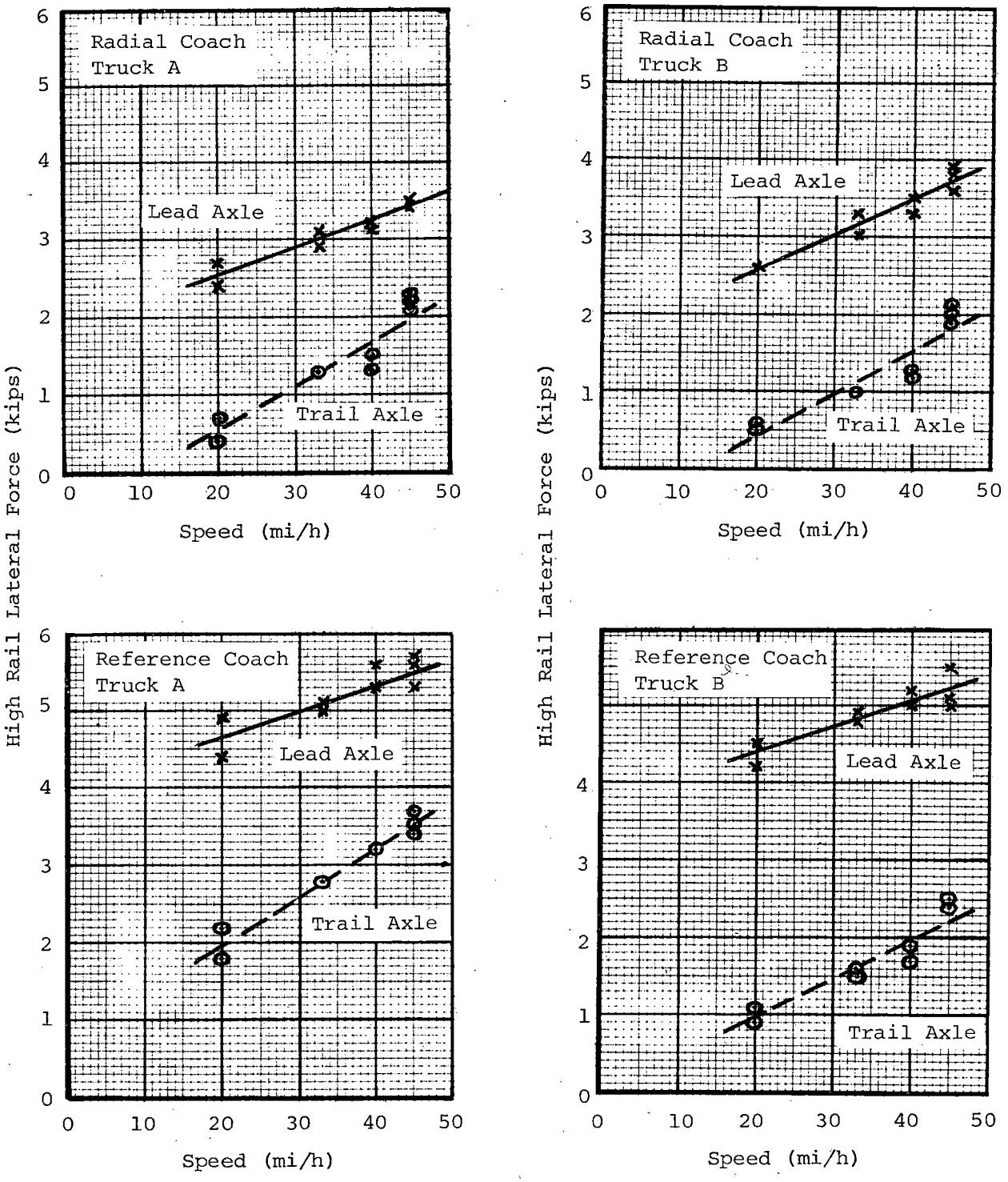

FIGURE 2-18. HIGH RAIL LATERAL FORCES, COUNTERCLOCKWISE RUNNING.

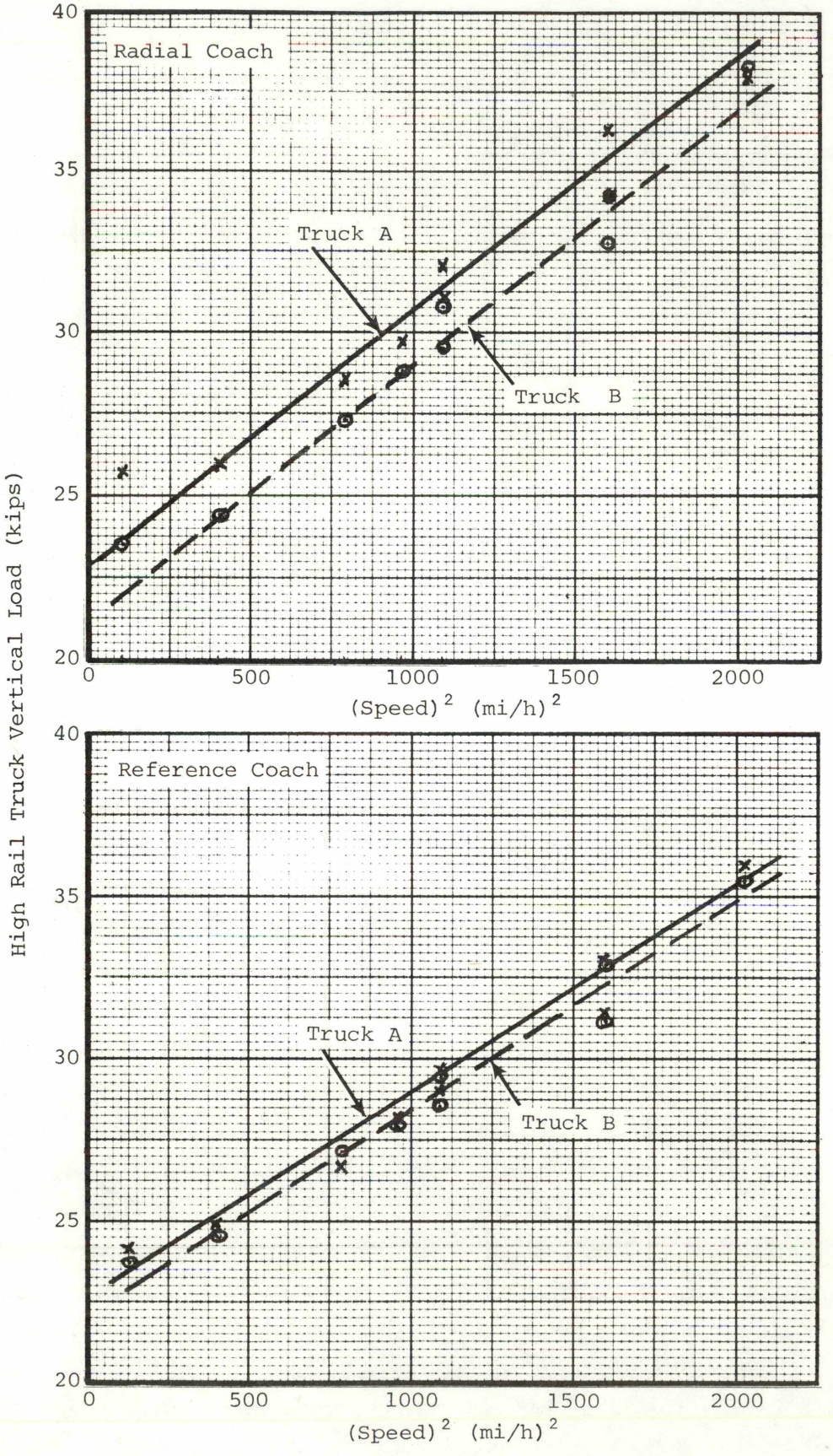

FIGURE 2-19. HIGH RAIL VERTICAL FORCES, CLOCKWISE RUNNING.

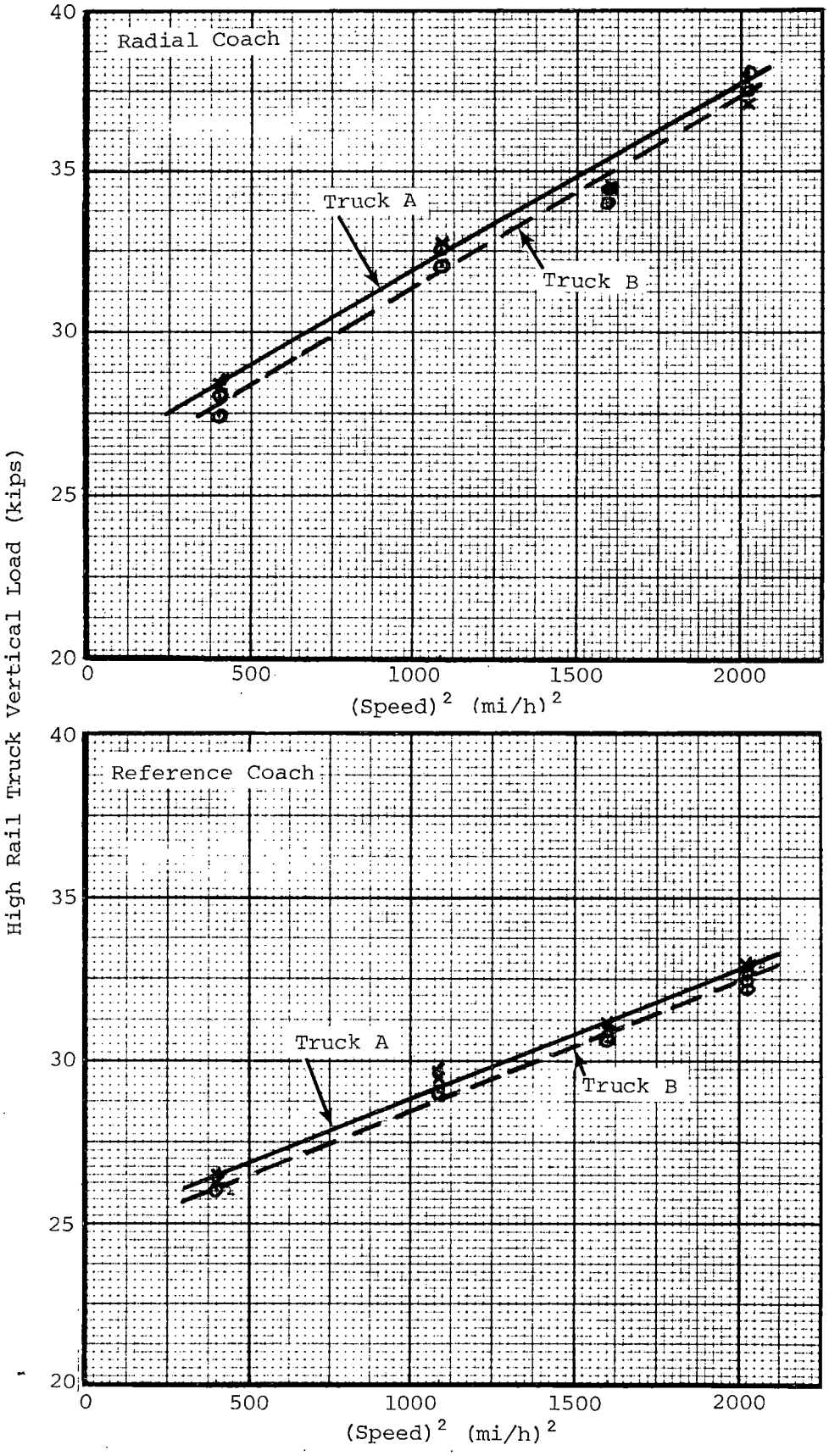

FIGURE 2-20. HIGH RAIL VERTICAL FORCES, COUNTERCLOCKWISE RUNNING.

This page left blank intentionally

3.0 LIFE TESTS

The following section describes the life tests which were carried out on the radial axle trucks to determine if they were subject to any long-term wear or structural problems. Life testing was started in late November, 1980, following the initial shakedown, cut-away braking, stability performance, curving performance, and ride quality test phases. The life test program was complicated by truck dynamic stability problems, wheel tread wear component failures, and configuration changes. The program, as it evolved, was divided into four phases, each phase representing a major configuration change as a result of a component failure or dynamic stability modification. The following chronology is provided to guide the reader through the major events of these test phases, which are then described in more detail in the subsequent sections.

3.1 CHRONOLOGY

The first phase of the life test program, designated Life Test I, was conducted with the trucks in their original primary suspension spring configuration. The primary longitudinal springs were of a three-layer rubber/steel elastomeric type; the axle alignment and secondary suspension leveling valve modifications were incorporated as detailed in Section 2.0. The test was terminated after 9,237 miles due to the failure of major truck components, including brake hangers, and steering cross-links. The failures and the failure analysis conducted by the TTC are documented in Section 3.2.

Following a rebuild of the trucks, which included the fitting of redesigned, stronger components, the life test program was continued as Life Test II. The new truck components are described and illustrated in Section 3.3. Further tread brake hanger failures occurred early in this test phase, but the characteristic feature of Life Test II was the deterioration of truck stability with increasing mileage. Observation of the truck behavior with video cameras showed the instability to be due to truck hunting. This was thought to be caused by increases in effective conicity due to wheel tread wear. As a result, an effective conicity study was conducted which included an evaluation of typical effective conicities experienced by Amtrak equipment operating on the Northeast Corridor. The study, described in Section 3.4, used a computer program that determined the change in wheel effective rolling radius with lateral displacement of the wheelset on the rails; new and worn wheel and rail profile data were measured and used in the study. Effective conicities (one half the slope of the rolling radius difference/lateral displacement plot), together with critical speeds for axle hunting determined from the test, were used in a simplified hunting stability algorithm to establish effective conicity/critical speed trends. Life Test II was concluded after 30,785 mi of operation.

For the next phase, Life Test III, the yaw stiffness of the axles was increased by increasing the longitudinal shear stiffness of the primary suspension. The steel/rubber elastomeric sandwich springs which provide the

longitudinal spring stiffness were redesigned, as detailed in Section 3.5. Life Test III was concluded after 13,617 miles of testing because of tread wear and truck hunting; an additional 543 miles was accumulated during curving, performance, and stability tests.

For the final test phase, Life Test IV, the primary longitudinal springs used in Life Test III were again modified to increase the axle yaw stiffness further and, potentially, to gain additional wheelset stability. This configuration is also described in detail in Section 3.5. A total of 5,388 miles of endurance testing was accomplished during Life Test IV, which concluded the RAPT test program.

Between Life Tests III and IV, curving and truck characterization tests were carried out. The curving and stability tests are reported in Section 3.6. High rail lateral force loads for the Life Test III and IV configurations are compared to the original RAPT configuration, and to loads for the Pioneer III truck. In addition, critical speed/effective conicity trends, based on test and wheel profile data for the two configuations, are compared to trends derived previously for the original RAPT configuation. The methods described in Section 3.4. are used.

The Truck Characterization Tests were a series of static load/deflection tests carried out to define the truck primary suspension stiffnesses. The tests and the test results are discussed in Section 3.7. The requirement to determine the spring rates was dictated by the need to define the truck configurations and to provide input for the truck stability parametric studies, using math modeling techniques.

The chronological order of the events of the life test program is contained in Table 3-1. The technical problems and analyses discussed in the following sections are dealt with in the order in which they occurred.

3.2 BRAKE HANGER AND STEERING CROSS-LINK FAILURES (LIFE TEST I)

On December 1, following a routine vehicle inspection, it was discovered that all of the tread brake hangers on the B truck of the RAPT test vehicle had failed. Further inspection showed that the two steering cross-link end-fittings had also failed, together with three fork bolts on the disc brake calipers. Serious thermal cracking of a brake disc was also noted. The failures were documented with photographs (Table 3-2) and the failed components were removed and inspected. Dye penetrant was applied to any part suspected of failure. The following failures were found:

- The steering cross-link end-fittings on the B truck were broken (Figures 3-1 and 3-2) at the spherical bearings adjacent to journals L-1 and L-2. Locations are identified in the following description by side (R=right hand, L=left hand) and axle number (1,2,3, or 4).

- The brake hangers on the B truck had failed at their upper or lower ends where they attach to the tread brake assembly (Figures 3-3 and 3-4).

TABLE 3-1. CHRONOLOGY.

Date	Event	Total Miles	Reference Section
Nov. 7, 1980	Start Life Test I.	3,350*	
Nov. 30, 1980	Car 21091: left side disc pads changed at 10,265 mi; remaining at 11,479 mi. Minor hunting reported at 120 mi/h. Car 21018: all disc pads replaced. Significant disc brake thermal cracks observed.	11,650	
Dec. 1, 1980	Car 21091: brake hanger and steering cross-link end-fitting failure.	12,587	3.2
	Life Test I terminated because of of cross-link end-fitting damage		
	Truck rebuild with redesigned components.		3.3
Jan. 29, 1981	Start Life Test II. (Note: Wheels not turned.)	12,587	3.4
Jan. 30, 1981	Tread brake hanger failure, #1 axle.	14,451	3.2
Feb. 4, 1981	Tread brake hanger failure, #4 axle (left hand side).	17,009	
Feb. 5, 1981	Speed restrictions due to stability problems at 110 mi/h.	18,241	
Feb. 11, 1981	Speed restrictions due to stability problems: 90 mi/h at stations R70-R75; otherwise, 100 mi/h.	22,256	
	Effective conicity study.		3.4
Feb. 13, 1981	Lateral secondary suspension arm loose (right hand side) A truck: removed.	24,352	
Feb. 26, 1981	Life Test II terminated because hunting speed down to 95 mi/h.	33,034	
Apr.9-16,1981	Speed upgrade and stability tests.		

* Milage accumulated during the initial performance tests (May 19 - Nov 6, 1980).

TABLE 3-1. CHRONOLOGY, CONTINUED.

Date	Event	Total Miles	Reference Section
Apr. 17, 1981	Start Life Test III. New primary suspension longitudinal/lateral sandwich spring. Wheels turned.	33,854	3.5
Apr. 21, 1981	Mild truck hunting reported; no restrictions.	37,290	
May 1, 1981	110 mi/h restriction through core area due to hunting.	42,959	
May 5, 1981	Overall 105 mi/h restriction; 95 mi/h between stations R70 to R75 (Figure 3-14 to be presented later).	45,438	
May 7, 1981	Life Test III terminated because hunting speed down to 85 mi/h.	47,397	
June 8-14,1981	Curving and stability tests of one- and two-layer springs		3.7
June 15, 1981	Start Life Test IV Modification to lateral/longitudinal primary springs (wheels turned).	47,962	3.5
June 19, 1981	Speed restricted to 110 mi/h through core area.	50,800	
June 22, 1981	Speed restricted to 100 mi/h overall.	52,677	
June 26, 1981	Life Test IV concluded.	53,348* 60,434**	
	Truck Characterization		3.6

* Car 21091 (Radial Car)

** Car 21018 (Reference Car) The Reference Car accumulated greater mileage because it was used in the AEM-7 Locomotive Test consist while the radial truck was being repaired.

TABLE 3-2. PHOTOGRAPHS OF COMPONENT FAILURES.

Negative Number	Description
80-3274	L-2 cross-link; spherical rod-end showing fracture.
80-3275	L-2 disc brake caliper; failed/missing pivot bolt.
80-3276	R-2 tread brake cross-link; failed bracket.
80-3277	R-1 tread brake bracket; sheared pin.
80-3278	L-1 tread brake cross-link; lugs failed on brake hanger.
80-3279 (3-1)*	L-1 cross-link; fractured rod-end.
80-3280 (3-3)	L-2 brake shoe assembly; general view showing failed hangers.
80-3281	L-1 brake shoe assembly; general view showing failed hangers.
80-3282	R-1 brake shoe assembly; general view showing failed hangers.
80-3283	R-2 brake shoe assembly; general view showing failed hangers.
80-3284	L-1 cross-link; rod-end fracture.
80-3285 (3-2)	L-2 cross-link; rod-end fracture.
80-3286	L-2 tread brake shoe; abnormal wear on flange side.
80-3287 (3-5)	L-2 brake disc; large radial crack.
80-3288 (3-6)	R-2 brake disc; multiple thermal radial cracks.
80-3289	R-1 brake disc; multiple thermal radial cracks.
80-3290	R-1 brake disc; multiple thermal radial cracks.
80-3291	L-3 brake disc; multiple thermal radial cracks.
80-3292	L-4 brake disc; multiple thermal radial cracks.
80-3293	R-1 tread brake; cross-link bracket.
80-3295	R-1 brake shoe assembly; fracture of hanger at clamp.
80-3296	L-1 brake disc caliper; sheared pivot bolt.
80-3297	L-1 brake shoe assembly; fracture at clamp.
80-3298	#2 axle tread brake cross-link; fretting wear.
80-3299 (3-4)	L-1 brake shoe assembly; hanger faces at failure line.
80-3300	R-2 disc brake caliper; pivot bolt failed/missing.
80-3301	R-2 brake shoe assembly; close-up of fracture.
80-3302	R-2 brake shoe assembly; close-up of fracture.
80-3306	Disc brake fork bolt; cracks in base at weld.
80-3307	Disc brake fork bolt; general view.
80-3308	L-2 disc brake rotor; large radial crack.
80-3309	R-2 disc brake rotor; radial thermal cracks.
80-3310	L-1 disc brake rotor; radial thermal cracks.
80-3311	R-4 disc brake rotor; radial thermal cracks.
80-3312	R-3 disc brake rotor; radial thermal cracks.
80-3317	R-1 steering cross-link.
80-3318	R-3 steering cross-link; close-up of unfailed rod-end.
80-3319	L-3 steering cross-link; close-up of unfailed rod-end.
80-3320	R-4 steering cross-link; close-up of unfailed rod-end.
80-3376	L-3 steering cross-link; close-up of unfailed rod-end.

* (3-1), etc.: figure numbers

FIGURE 3-1. L-1 CROSS-LINK; FRACTURED ROD-END BEARING.

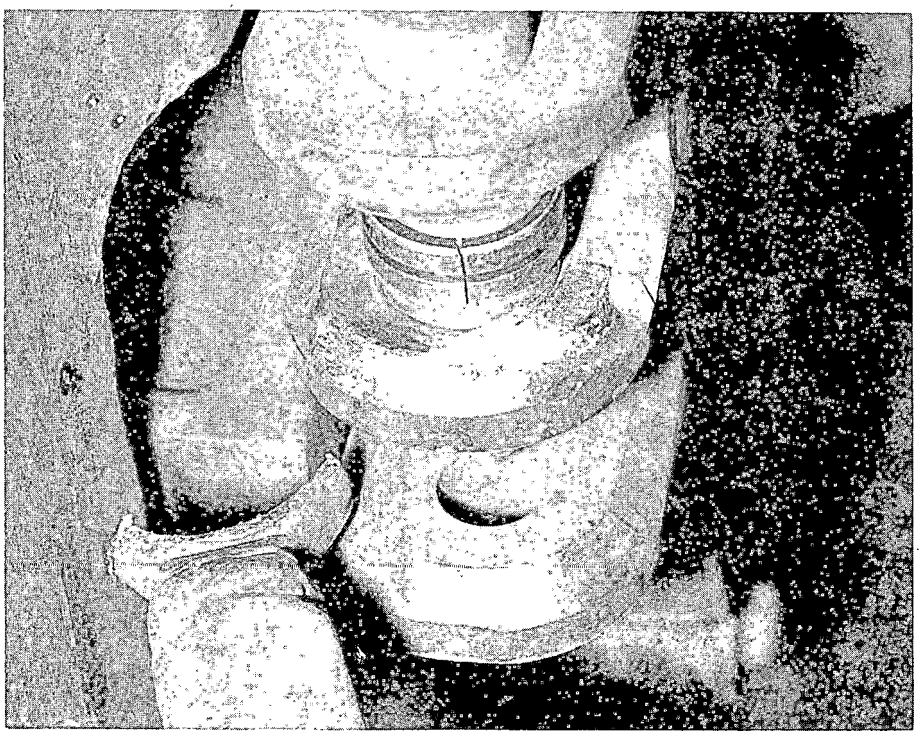

FIGURE 3-2. L-2 CROSS-LINK; FRACTURED ROD-END BEARING.

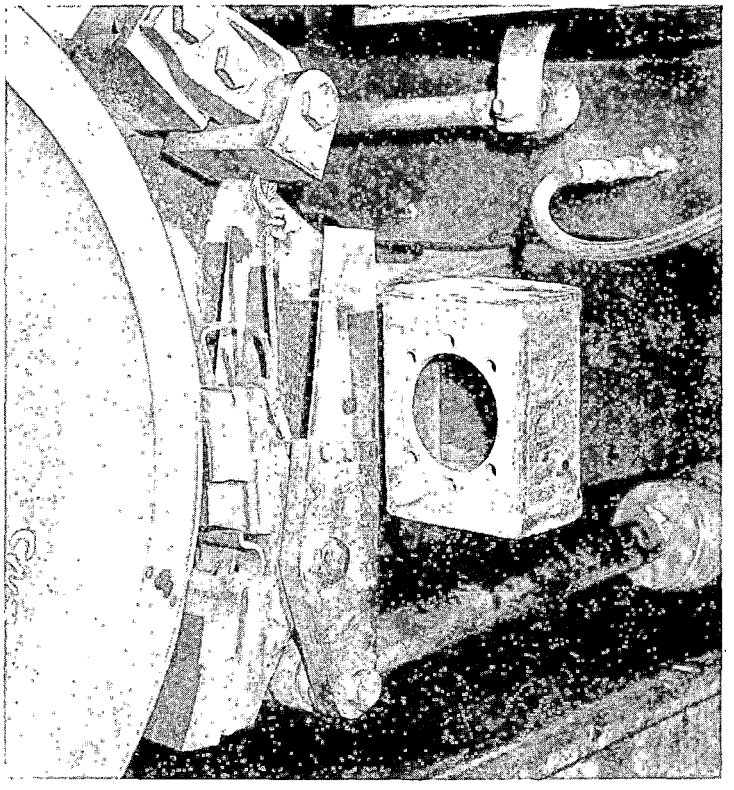

FIGURE 3-3. L-2 BRAKE SHOE ASSEMBLY, SHOWING FAILED BRAKE HANGERS.

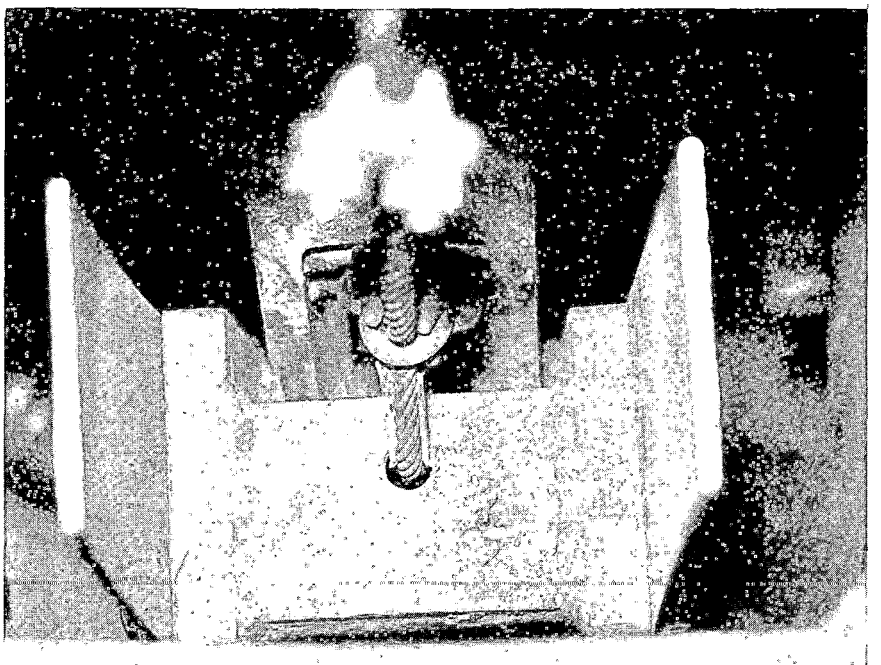

FIGURE 3-4. L-1 BRAKE HANGER; HANGER FACES AT FAILURE LINE.

- The tread brake cross-link attachment brackets were broken at R-1, R-2, and L-2. The #2 axle link had broken away completely and was found on the the track.

- The fork bolts holding the disc brake caliper assembly were missing at locations L-1, R-2, and L-4.

- Fork bolts on the disc brake calipers at L-2, R-1, R-3, R-4, and L-3 had cracks at the weld between the fork and the bolt shank. There were indications that slag was present in the welds.

- The disc brake rotor on axle #2 had a large radial crack. All other rotors showed a considerable number of small radial surface cracks (Figures 3-5 and 3-6).

- Following the failure of the hanger, surface scratches were caused by the brake shoe back plate riding on the rim face of the R-1 wheel.

Following the failure of these components, analyses of the steering cross-link end-fittings and brake hanger failures were carried out by personnel of the Component Test Laboratory (CTL) at TTC. The conclusions of these analyses are described in the following subsections.

3.2.1 Failure Analysis of the Steering Cross-Link End-fittings

Three pieces of the spherical rod-end bearings, two failed and one deformed, were submitted to the CTL for failure analysis. The following examinations were performed on these samples:

- Visual and Macroscopy Inspections. The two failed bearings were inspected visually and with a stereoscope, to identify the failure locations and locate any fatigue cracks.

- Non-Destructive Testing. A dye penetrant examination was performed on the deformed rod-end bearing to detect any cracks in the part.

- Scanning Electron Microscopy (SEM) and Energy Dispersive X-Ray Analysis (EDX). SEM examination of the failed component surfaces gave further clues as to the mode of failure. Since the manufacturer did not provide the chemical composition of the part, an EDX analysis was performed to identify the type of material.

- Metallography and Microhardness Measurements. In order to examine microstructural features and measure the Knoop hardness, one of the failed end-fittings was sectioned and cold mounted. The specimen was ground, polished, and then etched with 2% nital; typical microstructure and slightly work-hardened surfaces were revealed. No indications of decarburization (excessive ferrite) were observed. Knoop hardness indentations were taken through the thickness starting from the outer edge of the bar. Several indentations were made near the edge, and the hardness numbers were in the 215 to 220 range.

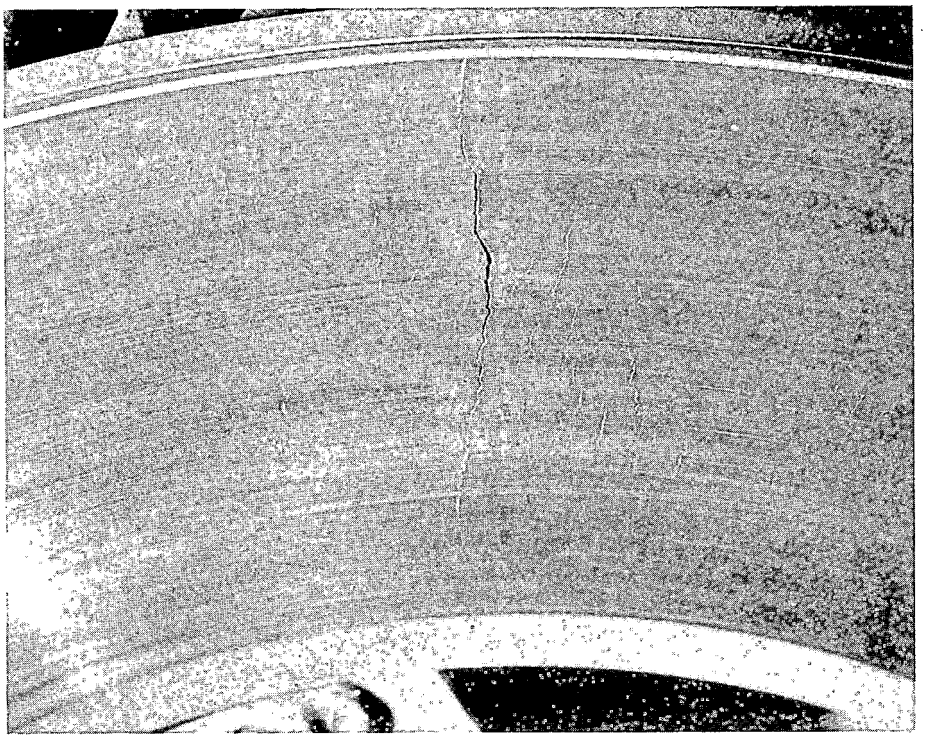

FIGURE 3-5. L-2 DISC BRAKE ROTOR; LARGE RADIAL CRACK.

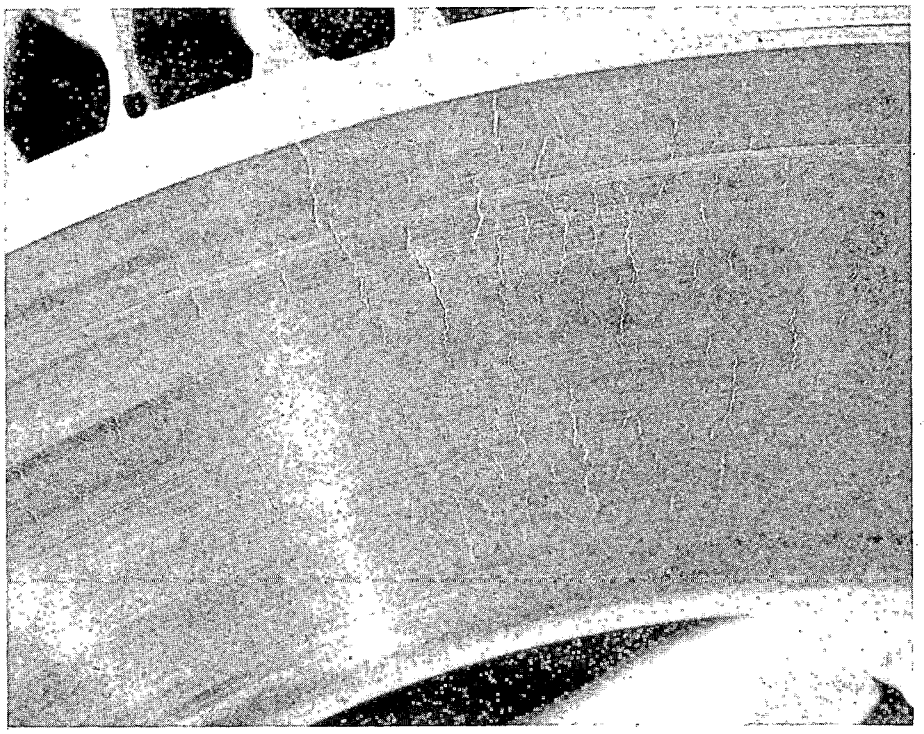

FIGURE 3-6. R-2 DISC BRAKE ROTOR; MULTIPLE THERMAL CRACKS.

- Strength Assessment. The tests show that there were no signs of metal fatigue, and the following estimates show that the failures were caused by axial loads which exceeded the design limits. Of the failed components examined, one failed through a threaded grease fitting and the other through the cross-section perpendicular to the loading direction. No cracks were found with the dye penetrant. The SEM of the failure surfaces show tensile dimples, indicative of tensile overloading. From the EDX analysis, metallography, and hardness data, the material was estimated to be a carbon steel with 0.20% carbon, 0.60% to 0.70% manganese, and 0.15% to 0.20% silicon (i.e., 1020 steel).

Estimates were made of the axial load necessary to produce failures, both for failure at the threaded hole and through a section at 90° to the load. In the analysis used[2], the stress level is considered greatest at the inner radius of the end-fitting and is a function of ratio of outer to inner radii (R/r), angle from the load axis (θ), presence or absence of stress raisers, and the ratio of pin clearance to inner radius (e/r) of the bearing. Since the clearance was unknown, estimates were made assuming zero and 0.010" clearances.

- Failure at 90° Section. The basic formula for stress (at inner radius for zero clearance) is:

$$S_T = \frac{W\phi}{LR}$$

where,

S_T = tensile stress, pounds per square inch
W = axial load, pounds
L = width of the eye bar, inches
R = outer radius, inches.
ϕ = dimensionless design factor which is dependent on R/r and θ.

For θ = 90° and extrapolating to R/r = 1.35, gives ϕ = 3.50. From the hardness data the ultimate tensile strength of the material is approximately 85,000 psi. Solving for W, at zero clearance,

$$W = \frac{S_T LR}{\phi} = \frac{85{,}000 \times 0.669 \times 1.063}{3.50} = 17{,}271 \text{ lb} \qquad (1)$$

With a clearance of 0.010",

$$e/r = \frac{0.010}{0.787} = 0.0127$$

and,

$$\phi = 4.75.$$

In that instance,

$$W = \frac{85,000 \times 0.669 \times 1.063}{4.75} = 12,720 \text{ lb}$$

- Failure at Threaded Hole. In calculating stress at this location, a stress concentration factor (k) must be introduced into equation (1). Timoshenko[3] indicates that for the condition of ratio of width of section to hole diameter of 0.669/0.157=4.25, the appropriate stress concentration factor is 3.2. For a hole located at $\Theta = 55°$, $\phi = 0.80$, hence;

$$W = \frac{S_T LR}{\phi k} = \frac{85,000 \times 0.512 \times 1.063}{0.80 \times 3.2} = 18,071 \text{ lb}$$

With 0.010-in clearance, ϕ would become

$$\frac{4.75}{3.50} \times 0.80 = 1.085$$

and

$$W = \frac{S_T LR}{\phi k} = \frac{85,000 \times 0.512 \times 1.063}{1.085 \times 3.2} = 13,300 \text{ lb}$$

It should be noted at this point that these loads are well above the rated design loads for the spherical rod-end fittings, which are: static design load = 10,000 lb; dynamic design load = 3,050 lb.

3.2.2 Failure Analysis of the Brake Hangers

The range of axle yaw angles expected as a result of the radial axle design required that some lateral freedom be allowed for in the design of the brake hangers. This was necessary to allow the brake shoes to align themselves with the wheel treads during curve negotiotion. The required freedom was accomplished by designing the brake hangers with two thin, spring steel plates, mounted on each side of the brake shoe (Figure 2-5); the plates act as flexures, allowing brake shoe alignment with the wheel tread through their torsional and bending deflections. The plates are attached to reinforcing members at their upper and lower edges by through-bolts and clamping pieces. The design of a single plate is illustrated in Figure 3-7.

Following the truck component failure of December 1, pieces of the failed brake hangers were submitted to the CTL for analysis. The actual failures are shown in Figures 3-8 and 3-9. As with the steering cross-links the analysis covered visual and dye penetrant inspection, microstructure examination, and hardness testing. In addition, the observation of brake hanger motion from a

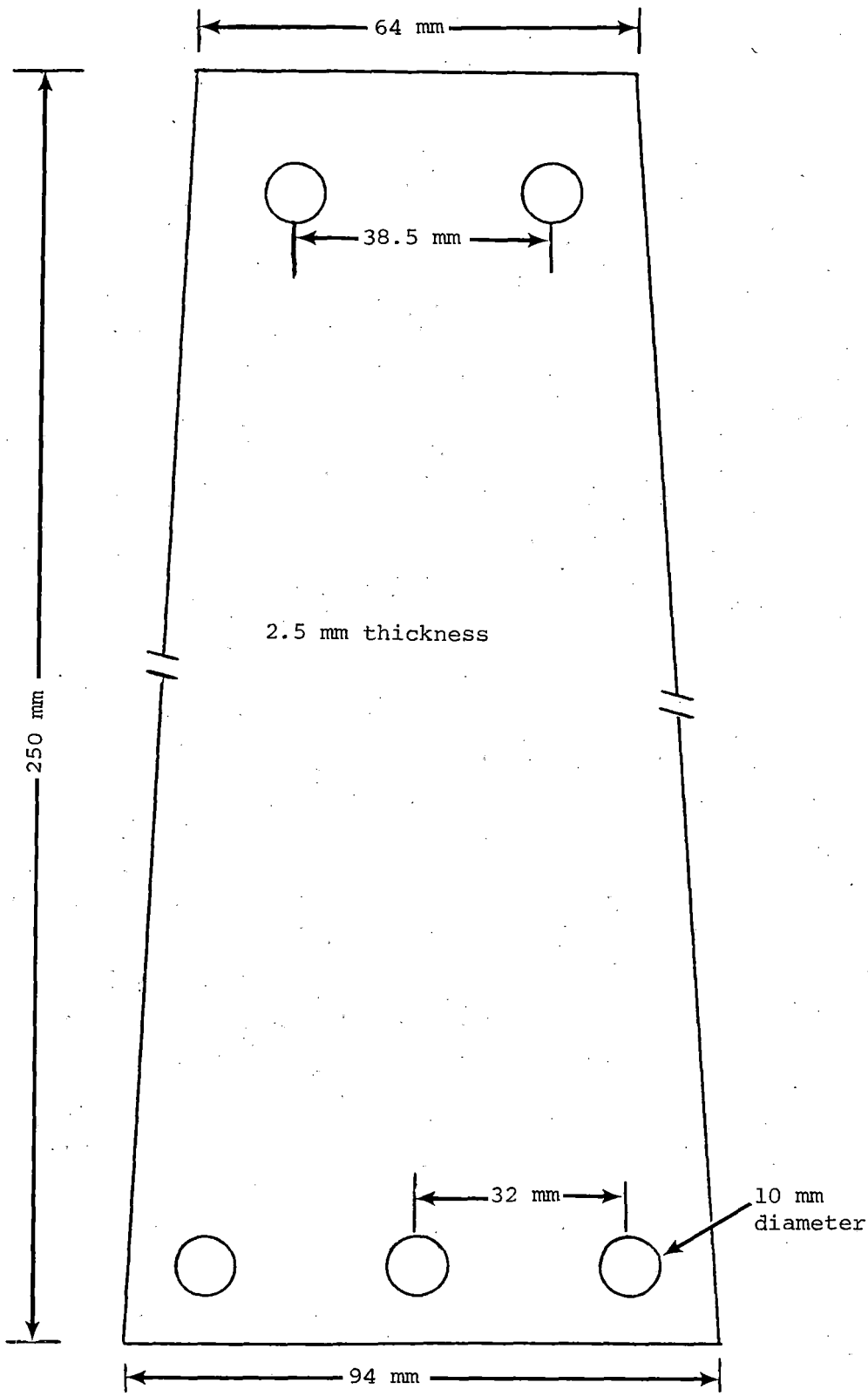

Figure 3-7. DESIGN OF BRAKE HANGERS.

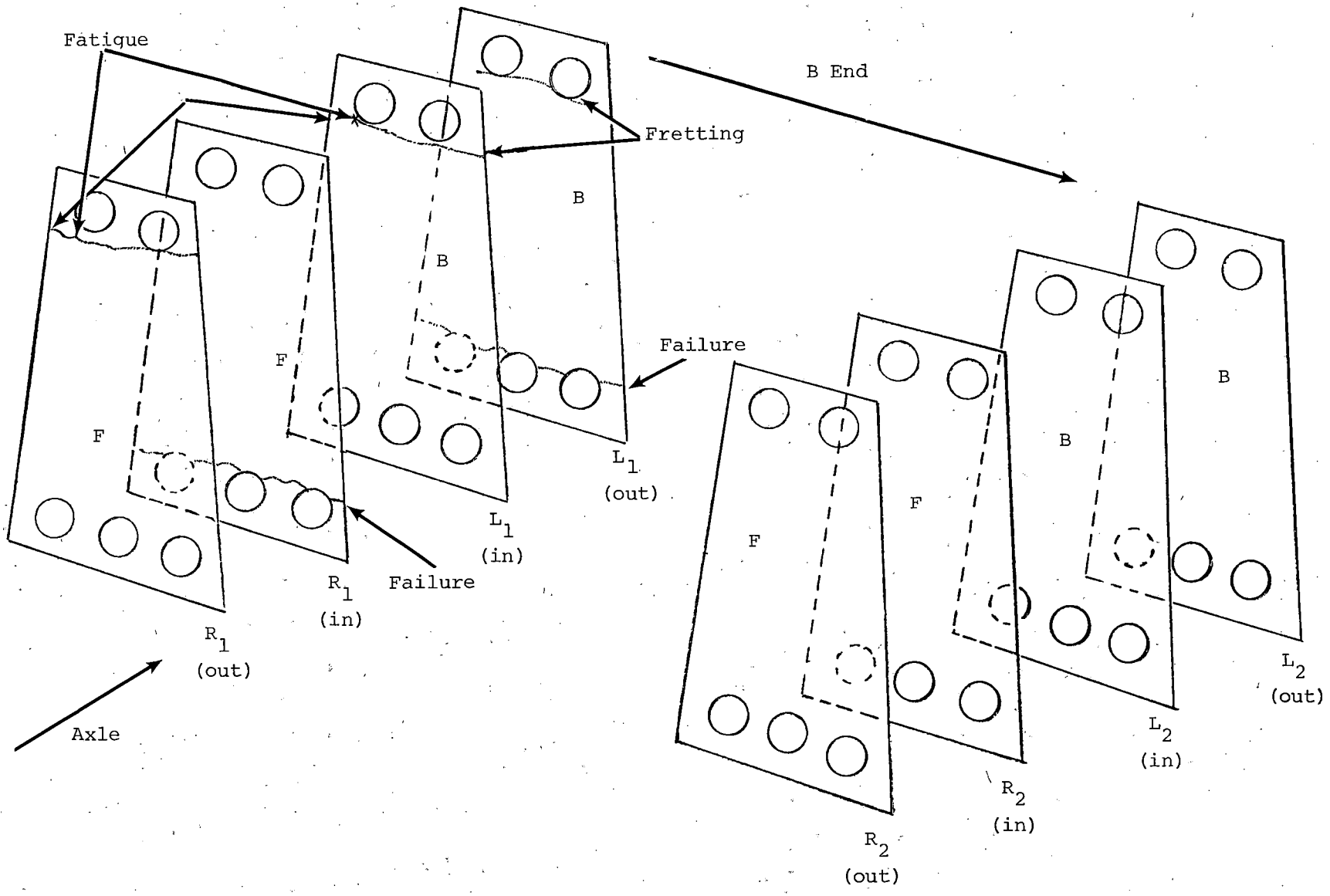

FIGURE 3-8. BRAKE HANGER FAILURE MODES, AXLES #1 AND #2 FROM RIGHT HAND SIDE.

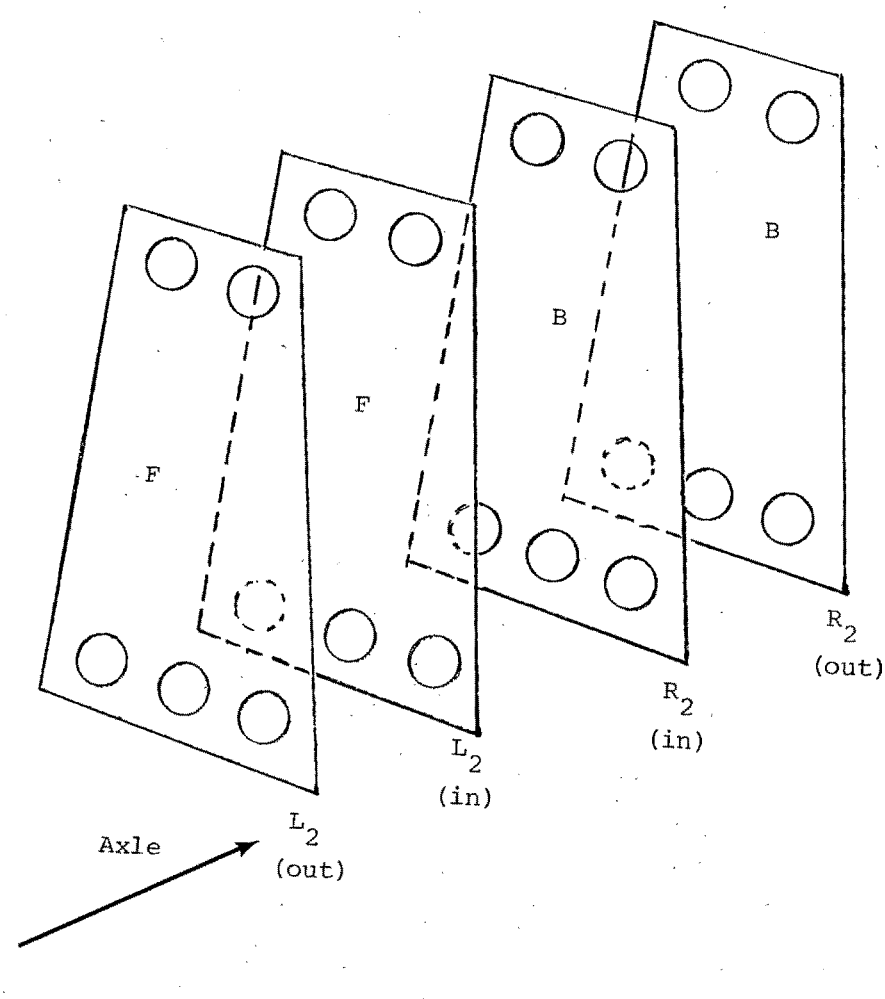

FIGURE 3-9. BRAKE HANGER FAILURE MODES,

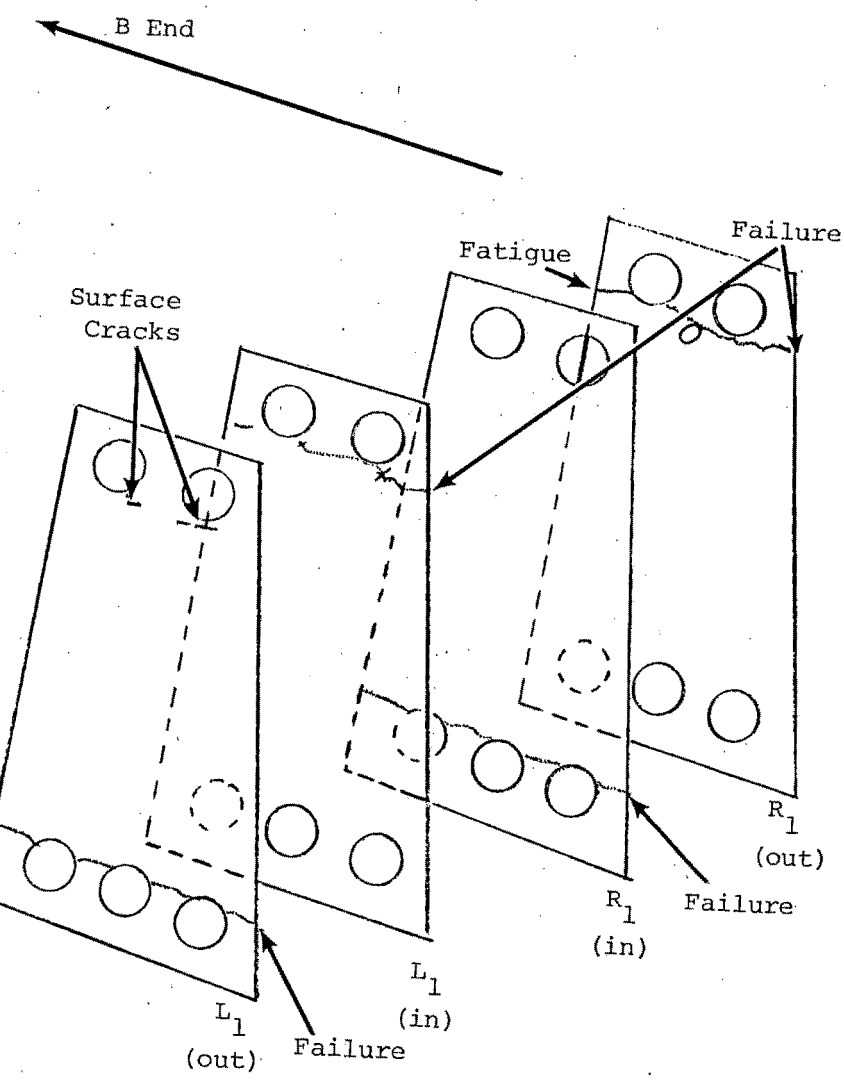

AXLES #1 AND #2 FROM LEFT HAND SIDE.

video tape allowed an estimation of the frequency and amplitude of the hanger bending cycles.

Visual examination showed that fretting of the plates took place in all failure cases, and in most cases, the fretting crossed the inner edge of the bolt holes. From the fretting marks it was evident that the clamps did not contact the surface of the hanger plates evenly. Fatigue cracks were observed in most fracture surfaces. For example, the hanger from wheel L-4 showed multiple fatigue cracks with several growth directions throughout the thickness and width of the plate. The fracture surfaces in one of the hanger plates in each pair were partially battered. This indicated that the sequence of the failure was such that the plates with battered fracture surfaces failed first, causing the other hanger plate of the pair to fail due to overloading in cyclic bending. Metallographic examination and hardness measurements indicated that the microstructure was 100% tempered martensite, as expected for the plate material, and that hardness numbers were in the expected range.

A review of a video tape of brake shoe motion at 110 to 115 mi/h showed that the brake shoe deflection was approximately ± 1", well above the design deflection of ± 9/16". The deflection was estimated from a reference mark on the TV screen. At speeds of 110 to 115 mi/h, the frequency of oscillation of the hangers was estimated to be 2.4 to 3.6 Hz, which equates to 8,600 to 13,000 cycles per hour.

In summary, the hanger failures were due to fatigue, primarily associated with fretting where the clamps contact the hangers. In addition, hardness tests revealed a soft area near the surface and adjacent to a fatigue crack origin on one of the hangers. The TTC considered that temporary fixes could be adopted to alleviate the local fretting problem by generating even clamping pressure, but suggested that the long term solution might be to redesign the brake hangers. A design incorporating spherical ball joint ends would allow the necessary brake shoe freedom without requiring that the brake hanger be torsionally flexible.

3.3 TRUCK REBUILD

Following the failure of the brake hangers and cross-links, the RAPT truck was rebuilt using some redesigned components supplied by the truck manufacturer, as follows:

- New steering cross-links were fabricated with substantially stronger rod-end bearings.
- New brackets were fabricated for the steering cross-arms.
- New disc brake fork bolt assemblies were designed and fabricated.
- New tread brake cross-link brackets were fabricated and welded to the tread brake assembly.
- The brake discs were turned to their machining limits to eliminate the

thermal cracks. The large radial crack in the disc rotor of axle #2 remained, however.

The redesigned and fabricated components are illustrated in Figures 3-10 through 3-13. A complete list of photographs documenting the redesigned hardware is to be found in Table 3-3. New brake hanger plates of the original design were fitted to replace those broken in the previous test phase. The test was restarted with the RAPT vehicle in this configuration.

3.4 LIFE TEST II AND EFFECTIVE CONICITY STUDY

Life testing (Life test II) was resumed on January 29, 1981 following the rebuild of the RAPT vehicle. After only 1,864 miles of operation, all four tread brake hangers on axle #1 failed again. The hangers were replaced and video cameras were mounted on the truck frame to monitor the tread brake environment during high speed operation. Since sporadic wheelset hunting had been reported by observers riding the vehicle, the video cameras were mounted on the truck frame to view the brake hangers and shoes, and the wheel/rail interface.

TABLE 3-3. PHOTOGRAPHS OF REDESIGNED TRUCK HARDWARE.

Negative Number	Description
81 - 0054	Spherical rod-end bearing, fork bolt assembly.
81 - 0055 (3-10)*	Fork bolt assembly, disk brake.
81 - 0116 (3-11)	Fork bolt assembled on disc brake caliper.
81 - 0117 (3-12)	Steering cross-link; new brackets and rod-end bearing prior to welding.
81 - 0118 (3-13)	Cross-link bearing prior to welding.
81 - 0119	Components of cross-link bearing assembly.
81 - 0120	New brackets for tread brake cross-link.
81 - 1037	Disc brake rotor, axle #2, radial thermal track after machining.

* (3-10), etc.: figure number

A high speed test was carried out on February 5, monitoring hanger and wheel/rail activity with the video system. At this time the vehicle had completed a total of 13,749 miles of life testing. From the video observations it was apparent that the wheelsets were hunting at speeds over 115 mi/h over at least 70% of the RTT. This represented a considerable deterioration in vehicle stability since the beginning of the life test. Hunting was observed to occur at different speeds over different sections of track, which suggested that wheel/rail effective conicity was playing a prominent role in the instability phenomenon. In order to validate this assumption, wheel and rail cross-sectional profiles were measured and effective conicities were calculated from these data for several locations around the track. This section of the report presents the wheel and rail test data and the resulting

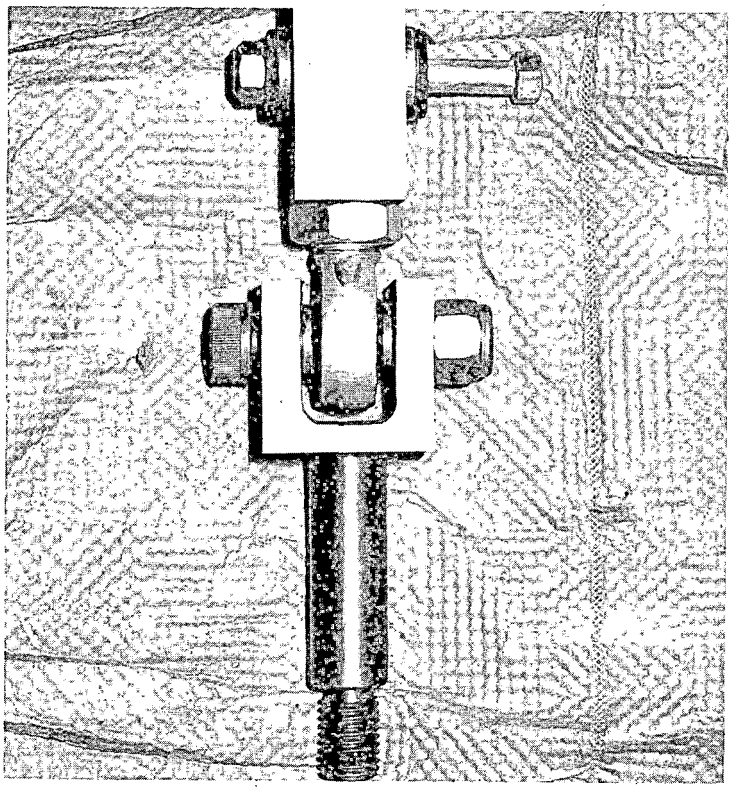

FIGURE 3-10. NEW DISC BRAKE FORK BOLT ASSEMBLY.

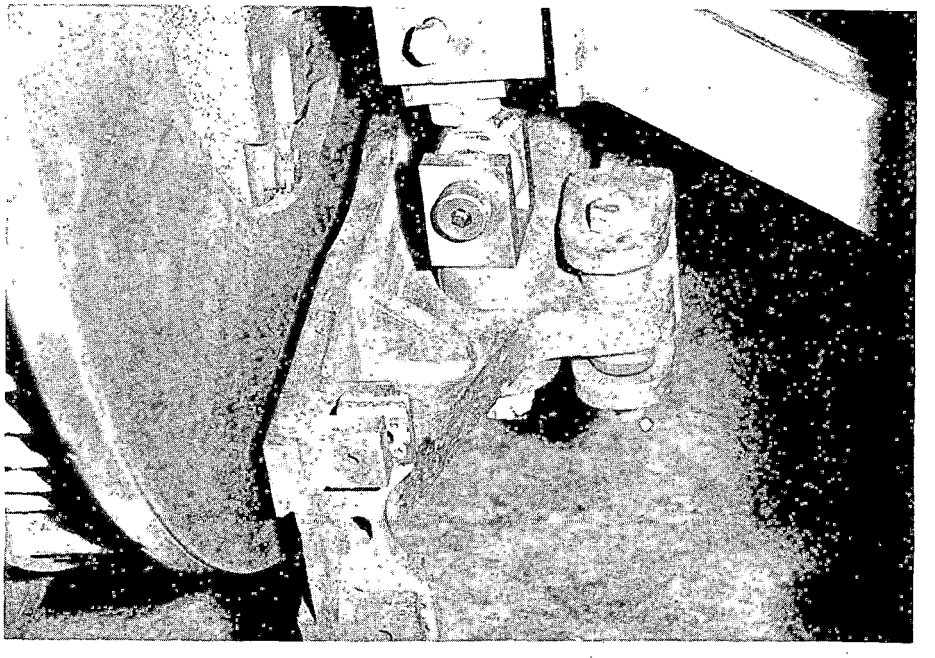

FIGURE 3-11. FORK BOLT ASSEMBLED ON DISC BRAKE CALIPER.

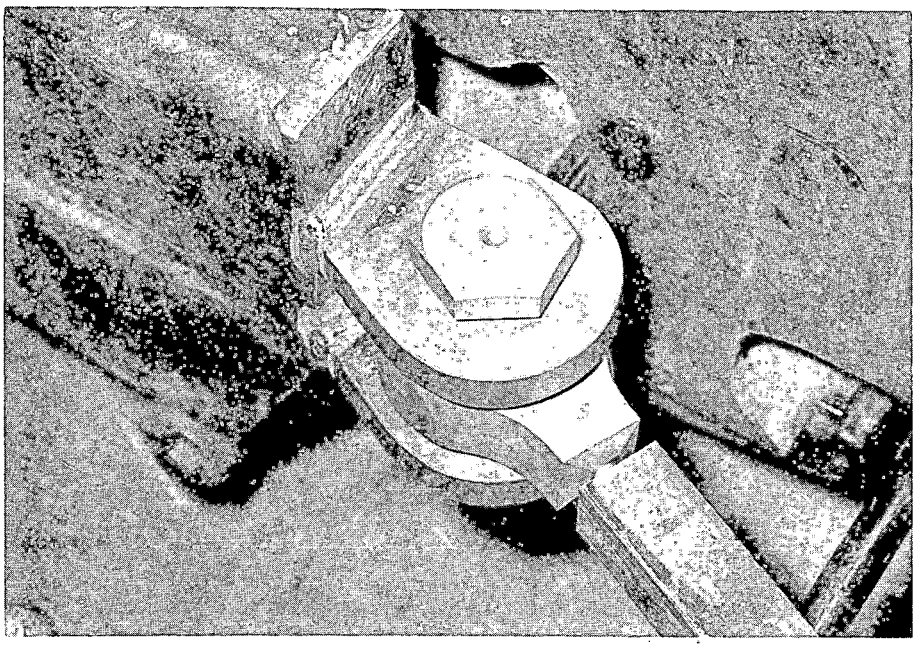

FIGURE 3-12. REDESIGNED CROSS-LINK ARM; NEW BRACKETS AND ROD-END BEARING PRIOR TO WELDING.

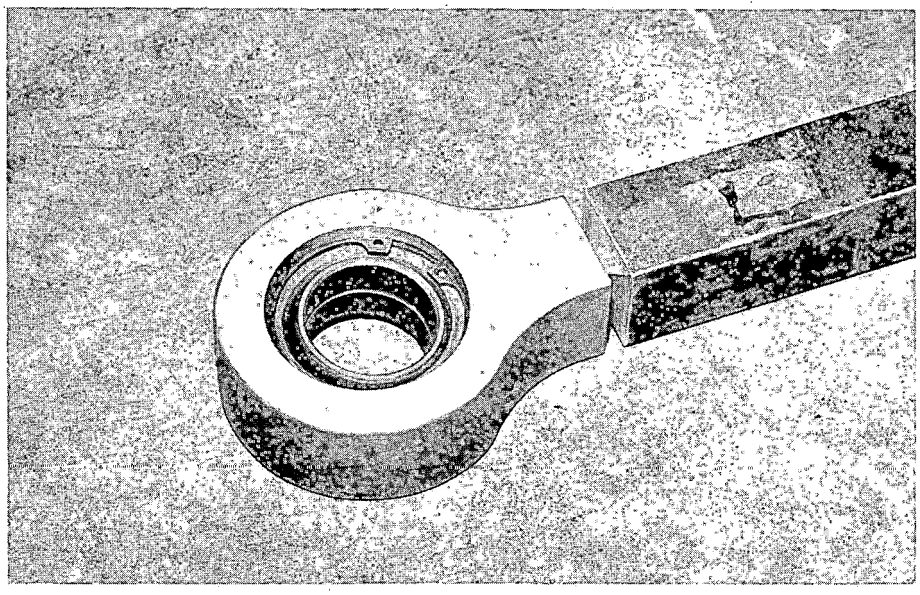

FIGURE 3-13. CLOSE UP OF NEW CROSS-LINK ROD-END BEARING.

effective conicities. The trends are discussed in relation to established wheelset hunting theory, and a relationship between the critical speed for wheelset stability and effective conicity is presented. Recommendations for design modifications to the truck primary suspension are suggested, in order to raise the critical speed of the system over the expected range of effective conicities resulting from wheel tread wear.

3.4.1 Test Observations

Video cameras were mounted on the B truck to monitor the brake shoe and the wheel/rail interface at the leading left side wheel (L-1). On the A truck cameras monitored the wheel and rail at the L-3 wheel and the tread brake system was removed. Laps of the RTT were made with the A truck leading in the counterclockwise direction of travel; constant speeds were maintained, starting at 100 mi/h and increasing in 5 mi/h increments up to 120 mi/h. At all speeds, continuous lateral oscillation of the wheels relative to the rail (wheelset hunting) was observed between stations R73 and R70 (see Figure 3-14). At 110 mi/h, hunting occurred over approximately 15% of the track; at 115 mi/h, hunting became markedly worse and was observed over 70% of the track. Further deterioration of the stability was noted at 120 mi/h. Vehicle stability was not considered hazardous, although the incidence of axle hunting had increased from that at the beginning of the life test, and critical speeds had dropped. A speed limit of 110 mi/h was placed on the test consist at this point.

The video test was repeated on February 12 with both cameras mounted at the L-1 axle. One camera viewed the brake hanger and wheel as before, and the second camera was positioned to view the wheel/rail interface, looking directly along the rail. The truck had accumulated 4,891 miles since the first video observations were made. The hunting characteristics were consistent with those observed previously; however, the critical speeds had dropped by approximately 10 mi/h throughout the speed range. Primary suspension yaw dampers (as illustrated in Figure 2-4) were fitted for some test runs, and these raised the critical speeds by 5 to 10 mi/h. Visual inspection of the wheels indicated that the treads were wearing in a hollow profile.

A third video test was made on February 19, after a further 5,679 miles of operation. Critical speeds were again reduced, and operation with the yaw dampers gave critical speeds of less than 90 mi/h between track stations R75 and R70, and 95 to 100 mi/h around the remainder of the RTT.

3.4.2 Wheel and Rail Profile Measurements

Observation of the reduction of wheelset critical speeds with time and accumulated mileage lead to the supposition that the rapid deterioration in stability was probably due to wheel tread wear. Initial wear would bring about a reduction in critical speed and give rise to some hunting. The hunting action would then tend to wear the treads at an accelerated rate; this wear would increase the effective conicity and give rise to increased instability and further hunting, thus further accelerating the process. In order to

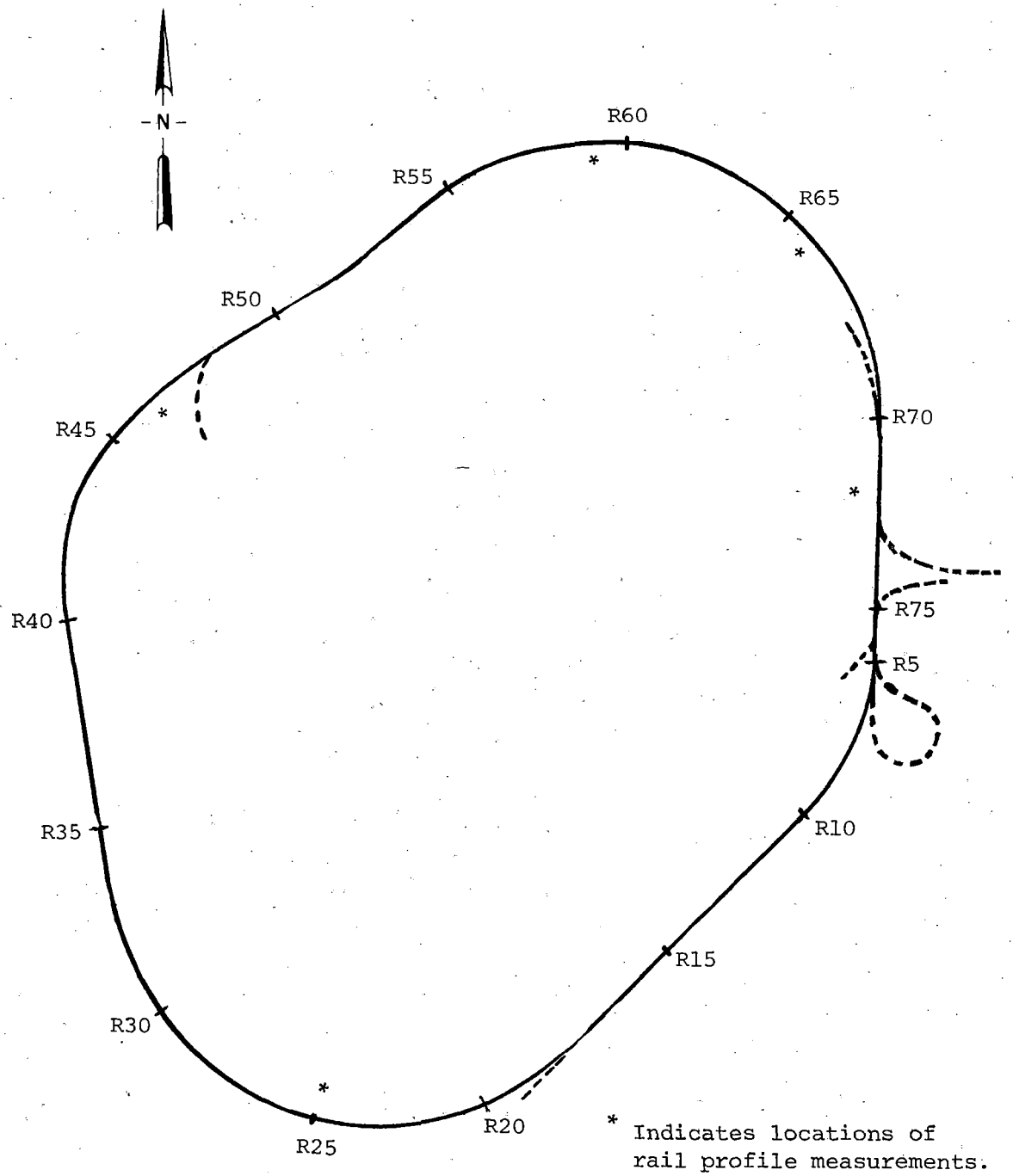

FIGURE 3-14. STATION LOCATIONS OF RTT.

test the hypothesis, five locations on the RTT were chosen for an effective conicity study. The locations and the critical speed of the RAPT vehicle over them, without yaw dampers, are shown in Table 3-4.

TABLE 3-4. RTT CRITICAL SPEEDS.

RTT Stations	Critical Speed (mi/h)	
	2/5/81	2/12/81
R25 - R27	110 - 115	97 - 103
R46 - R48	120	100 - 105
R58 - R60	105 - 110	102 - 108
R67 - R68	115 - 120	102 - 108
R71 - R73	100	87 - 93

Wheel and rail profile data were obtained using precision profilometers that have been described in previous literature.[1] The profilometers measure wheel and rail profiles by means of dial gage indicators which traverse the wheel or rail in a circular arc. A series of incremental radius readings (R) are obtained for each increment of angle (Θ) around the profile. Since the profilometers, by design, reference these measurements to a datum at the mating wheel or rail, the profiles generated are related geometrically in space with respect to each other. The R and Θ readings are tabulated together with calibration, flange-back spacing or rail gage, and wheel diameter data where appropriate.

The wheel profiles were measured prior to the start of the life test and were repeated when this conicity study was initiated. Axles #1 and #3 were considered in the study. Axle #1 had 20,823 miles accumulated on its wheel treads at the time of the study, and axle #3 had 19,693 miles.

The R and Θ wheel profile data were converted into X and Y coordinate format by computer and stored on file. Hard copy plots of the profiles were obtained and are presented in Figures 3-15 through 3-18. An indication of the tread wear can be obtained from Figure 3-19, which is an overlay of the new and worn profiles of the wheels on axle #3. The hollow tread wear can be seen; the absence of measurable flange wear, an indication of good curving performance, can also be observed.

Rail profiles were taken at five locations around the RTT; at each location profiles were taken at three adjacent sites. For each location, the three rail profile sets were inspected for consistency, and one was chosen for processing. The sites chosen were at stations R25, R47, R59, R67, and R72. Computer generated X - Y coordinate plots derived from the profilometer R, Θ tabulations are presented in Figures 3-20 through 3-24.

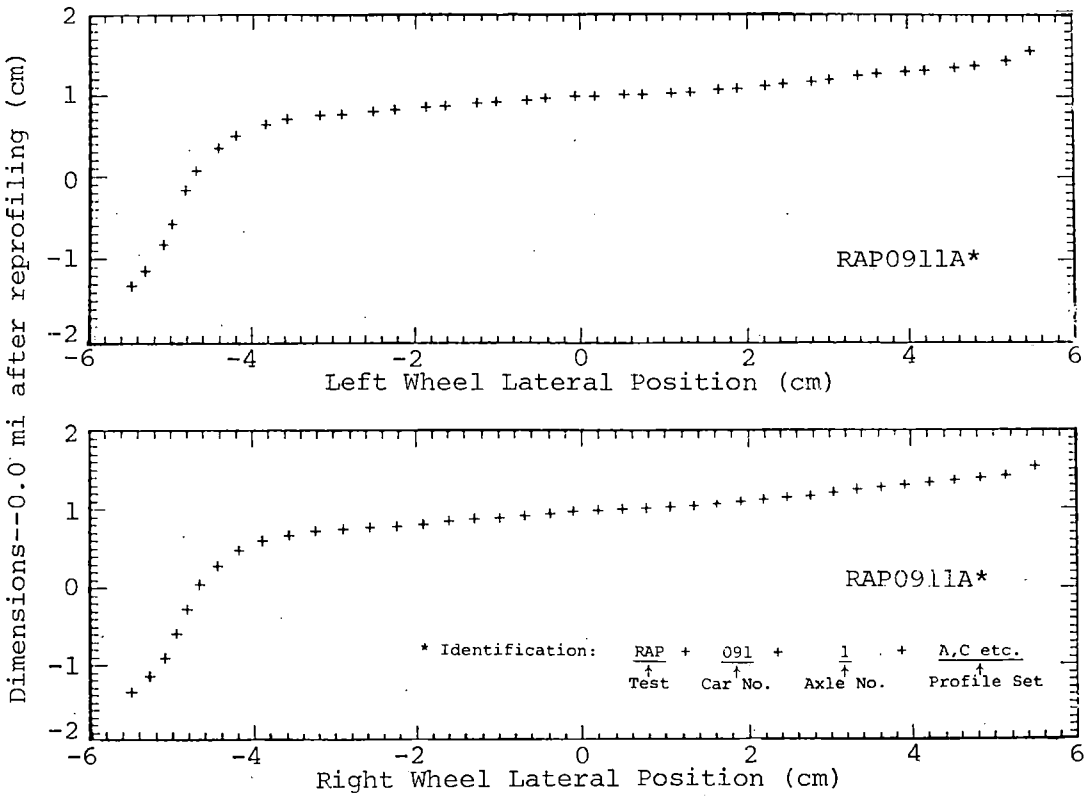

FIGURE 3-15. RAPT AXLE #1 WHEEL PROFILES ON 10-24-80.

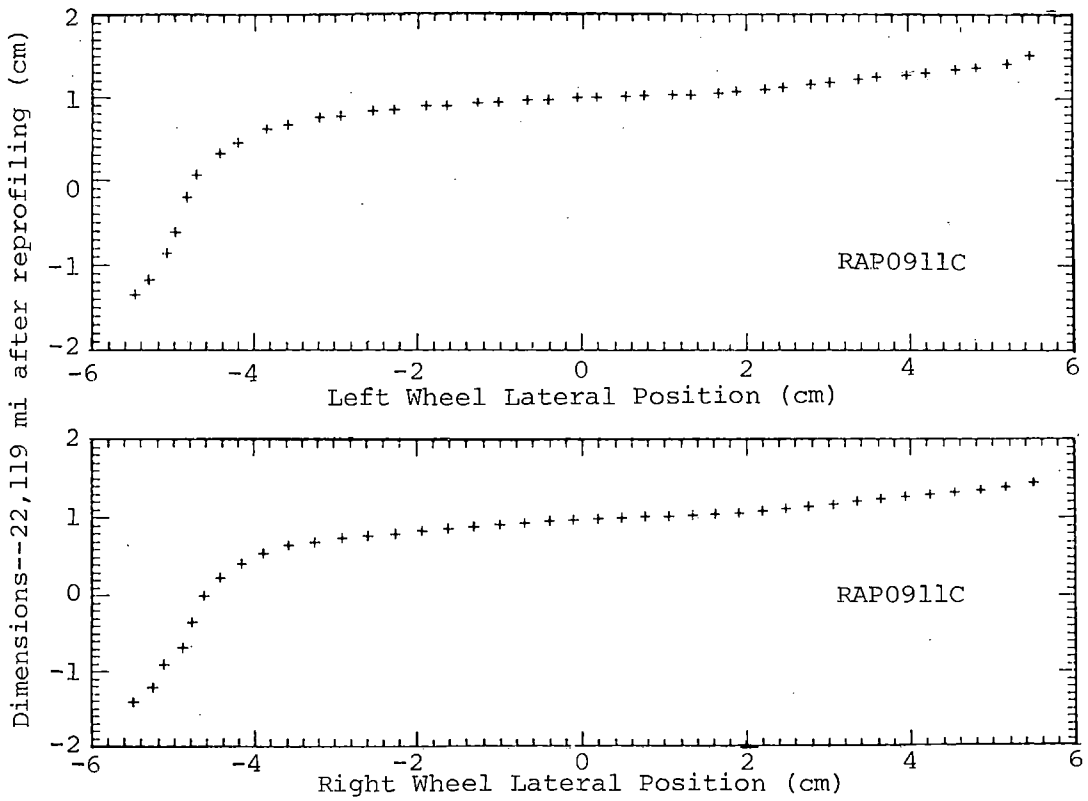

FIGURE 3-16. RAPT AXLE #1 WHEEL PROFILES ON 2-16-81.

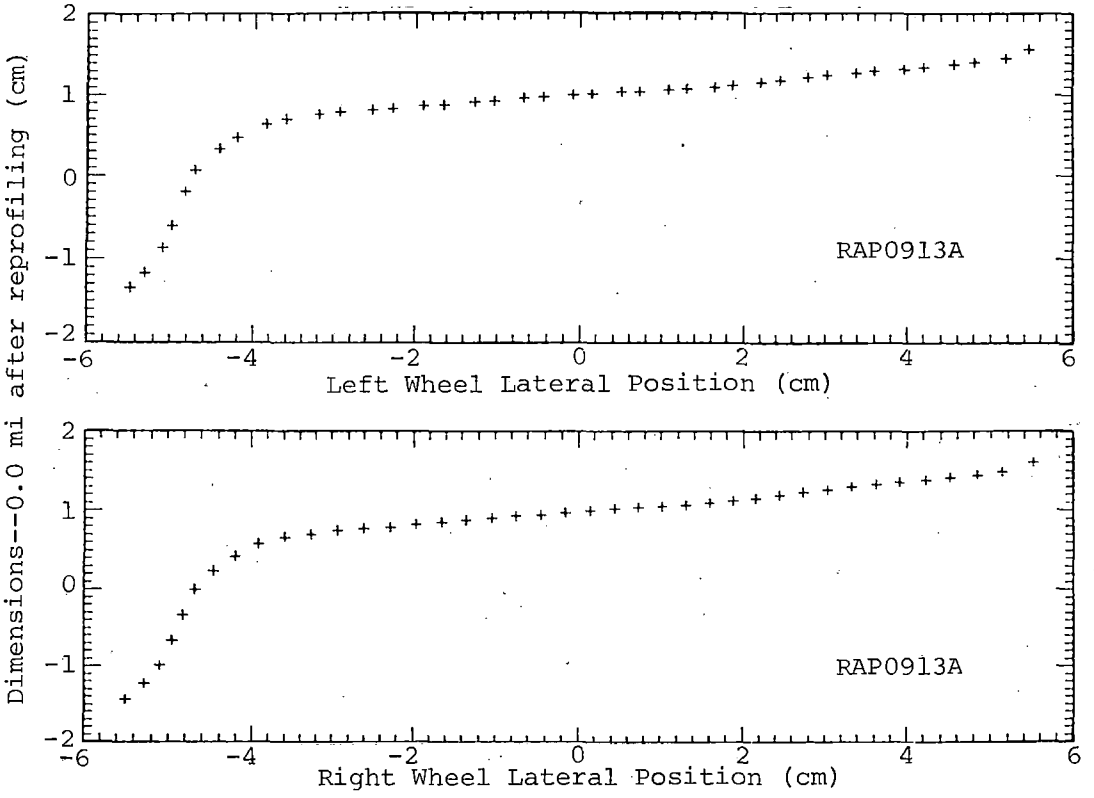

FIGURE 3-17. RAPT AXLE #3 WHEEL PROFILES ON 10-24-80.

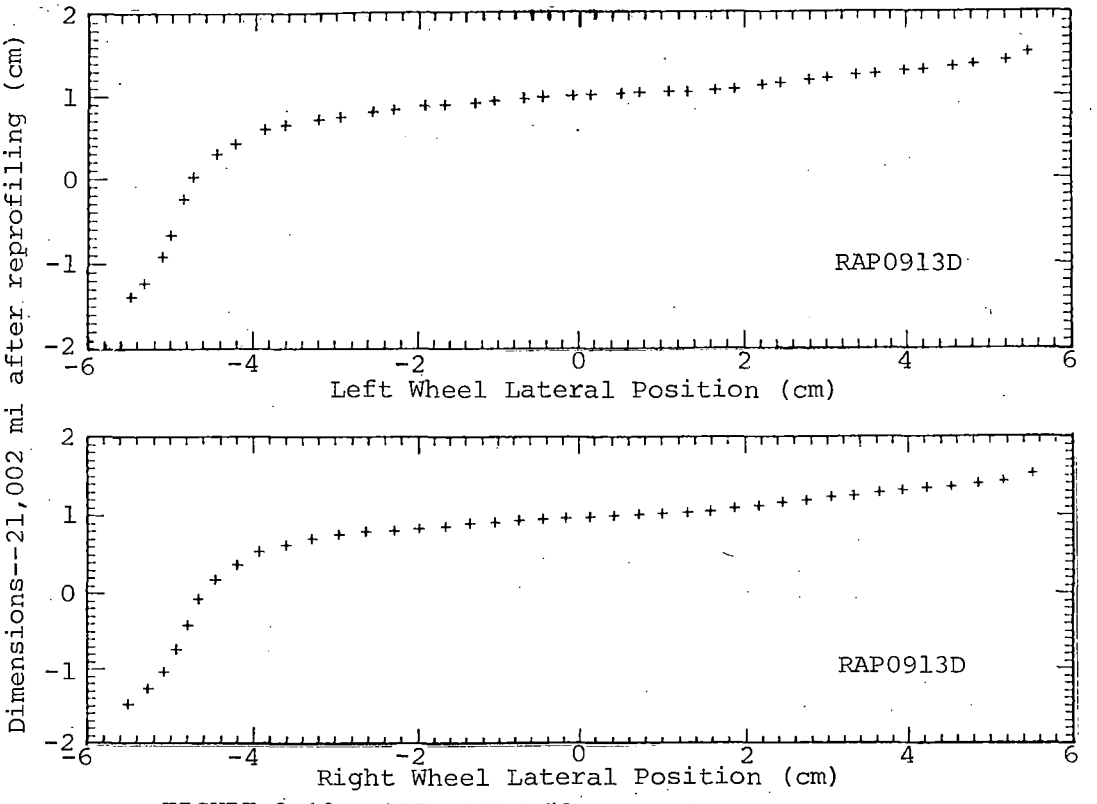

FIGURE 3-18. RAPT AXLE #3 WHEEL PROFILES ON 2-13-81.

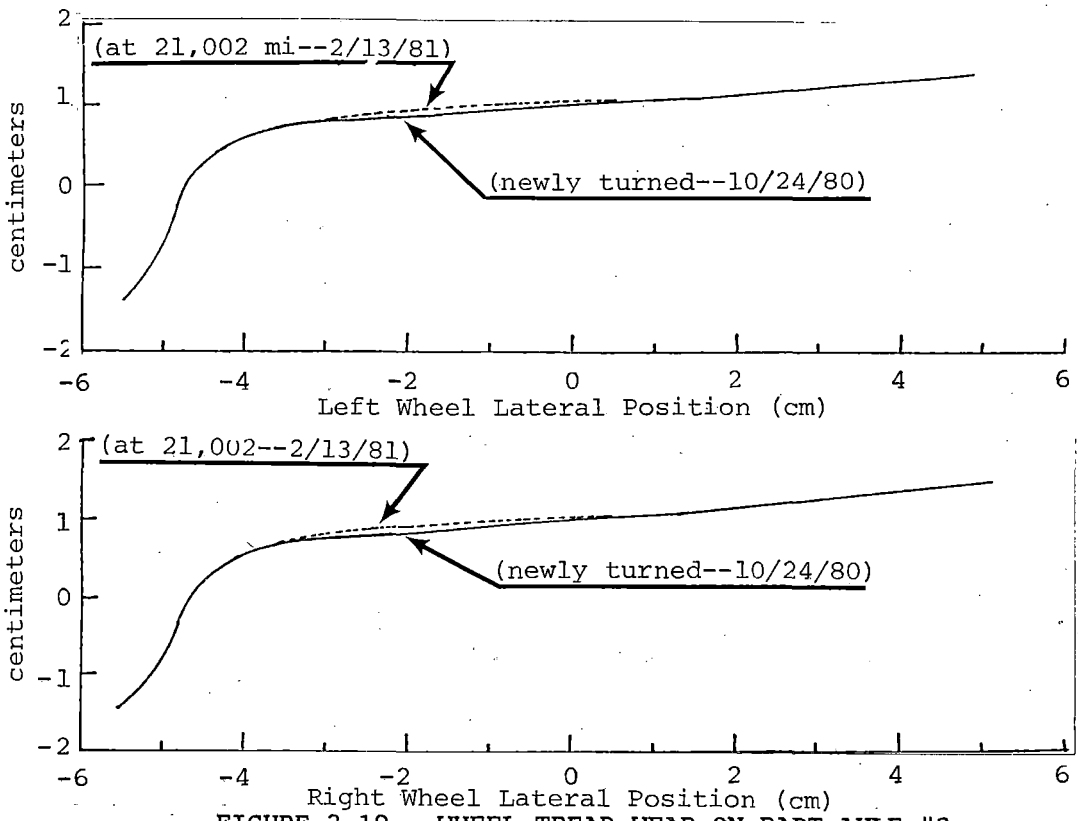

FIGURE 3-19. WHEEL TREAD WEAR ON RAPT AXLE #3.

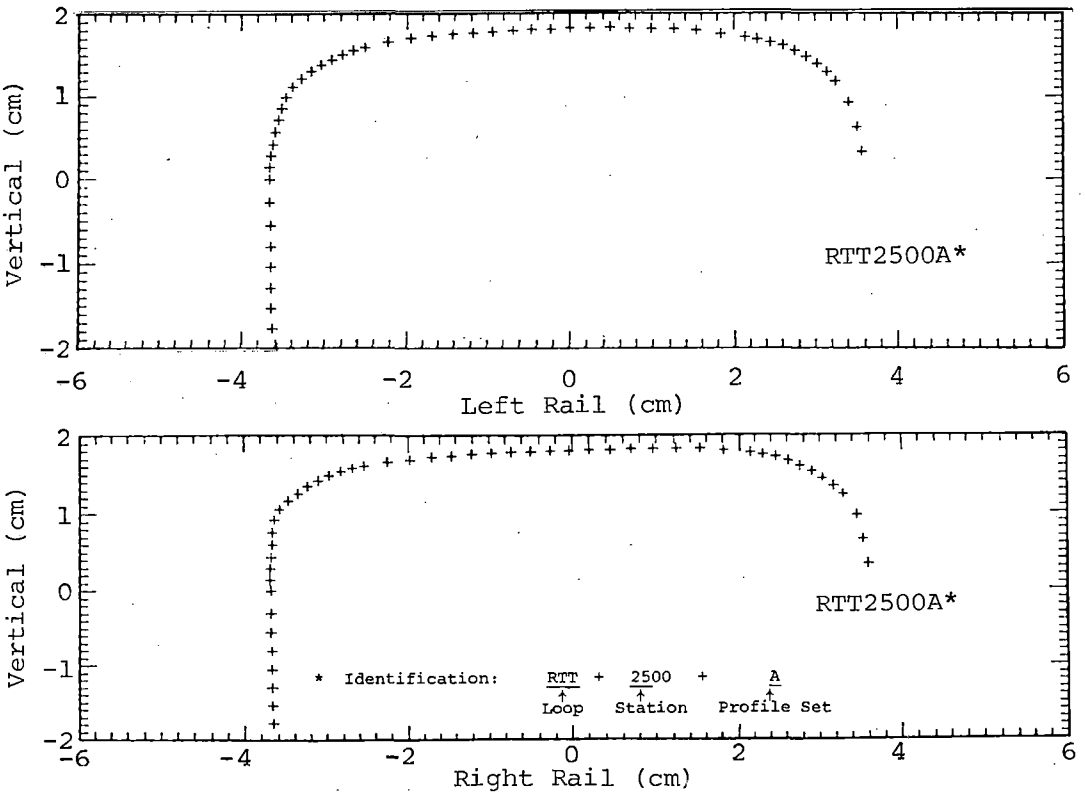

FIGURE 3-20. RTT RAIL PROFILES AT STATION R25.

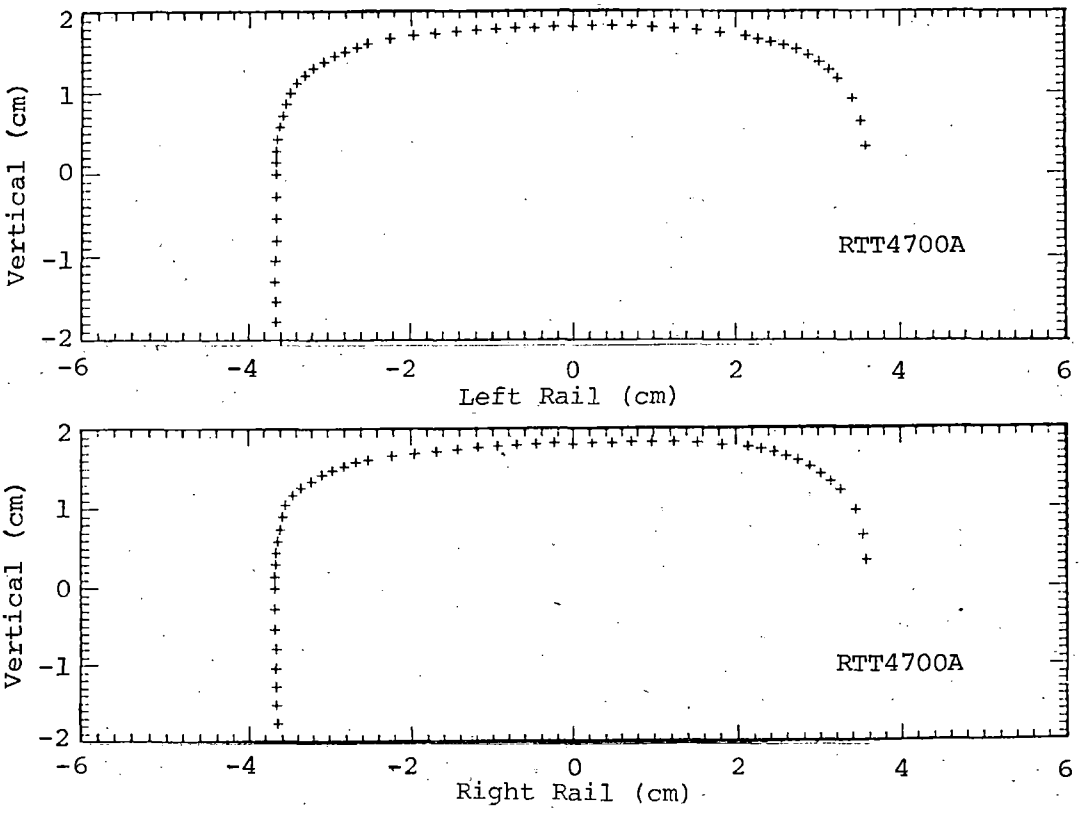

FIGURE 3-21. RTT RAIL PROFILES AT STATION R47.

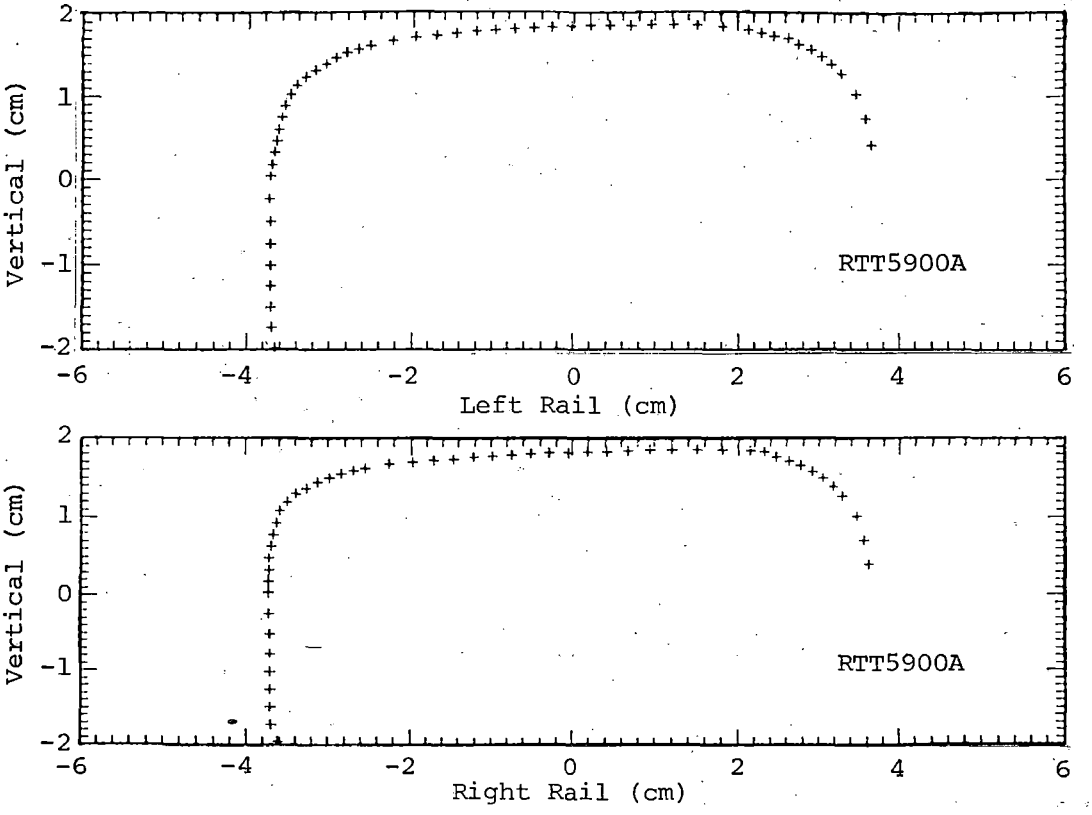

FIGURE 3-22. RTT RAIL PROFILES AT STATION R59.

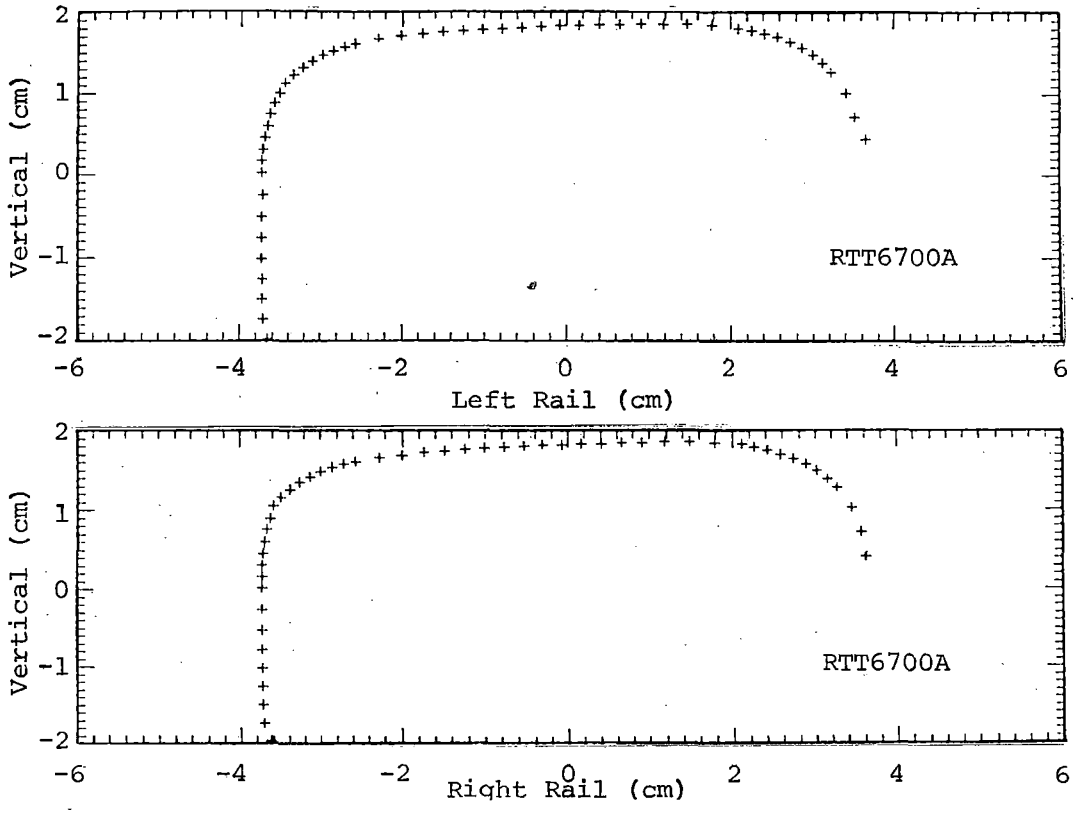

FIGURE 3-23. RTT RAIL PROFILES AT STATION R67.

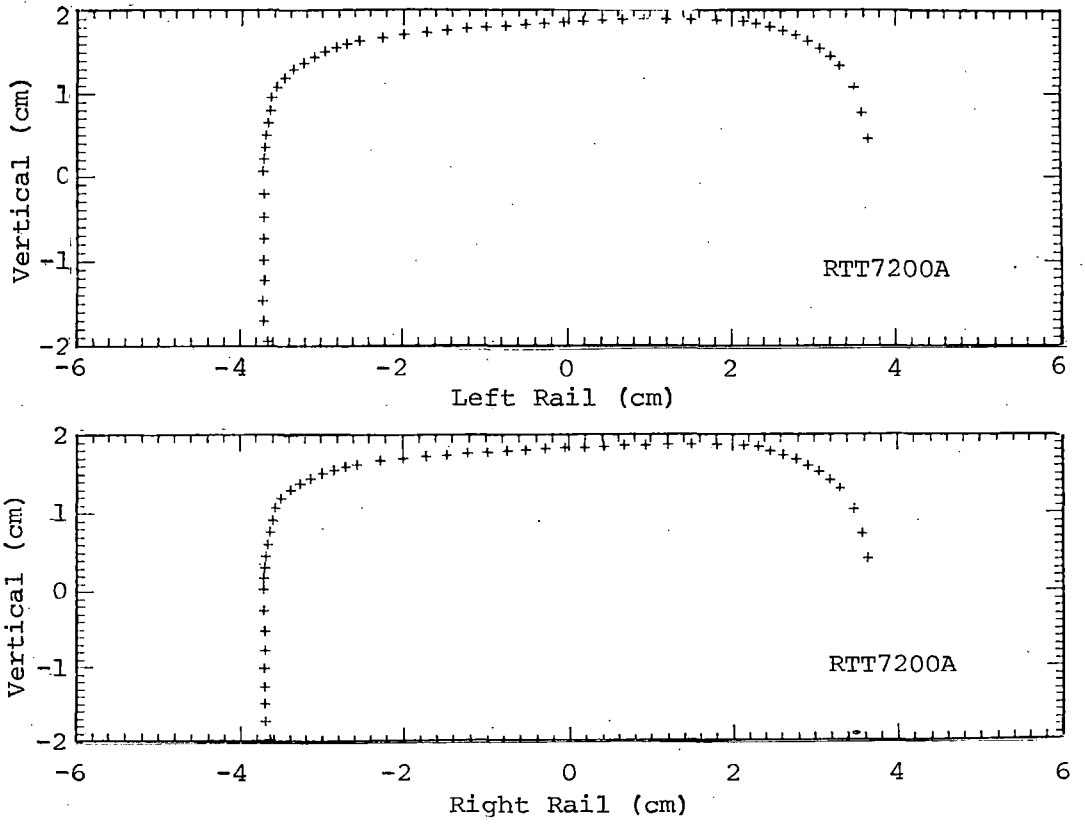

FIGURE 3-24. RTT RAIL PROFILES AT STATION R72.

3.4.3 Discussion of Effective Conicity/Critical Speed Relationships

Effective conicity values for a wheelset on a pair of rails can be determined from an understanding of the rolling radius difference between two wheels on an axle, for incremental lateral displacements of the wheelset relative to the track. Consider the graph of rolling radius difference versus lateral wheel/rail displacement shown in Figure 3-25. This is an idealized relationship, but a similar graph could be obtained from a wheelset with equal tread tapers.

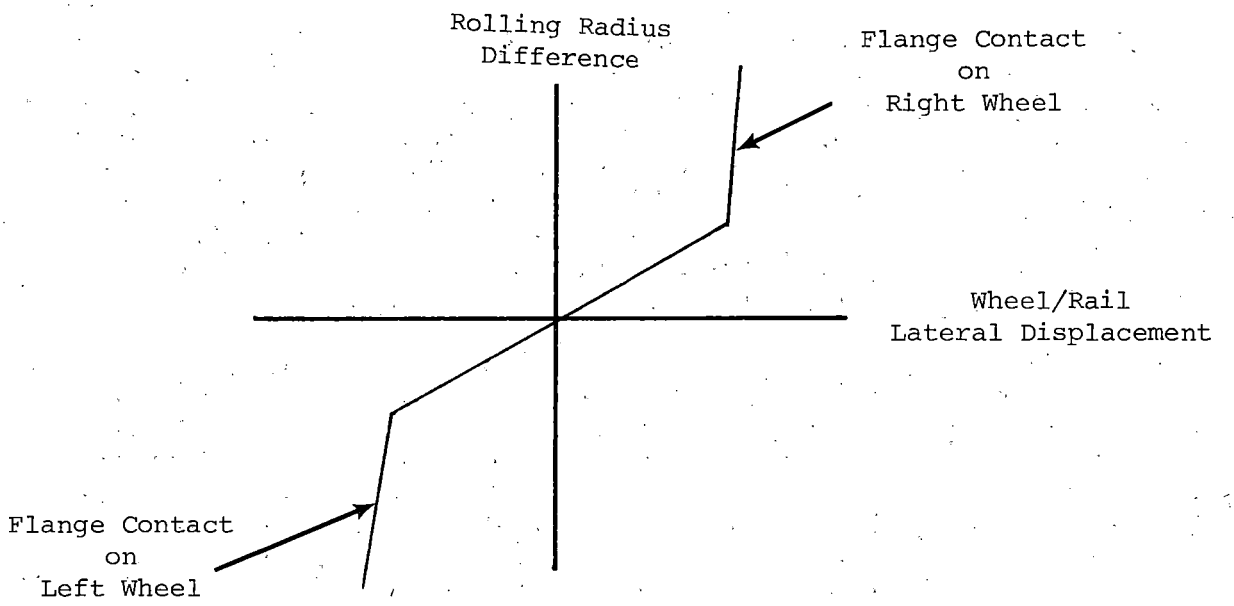

FIGURE 3-25. ROLLING RADIUS DIFFERENCE/LATERAL DISPLACEMENT TRENDS.

Obviously, as soon as flange contact occurs, the rolling radius difference will increase sharply with small lateral displacements. The portion between flange contacts is used to calculate effective conicity. Effective conicity is defined as half of the slope of the tread contact portion of the rolling radius difference/lateral displacement graph.

It can be shown[4] that the relationship between critical speed and effective conicity can be simplified to the form:

$$V_C^2 = \frac{m}{\lambda}$$

where,

V_C = critical speed,
λ = effective conicity,

and m = a constant, dependent upon primary stiffness, mass, and inertial properties and associated with the particulars of a given vehicle design, wherein suspension spring stiffness, damping mass, and inertial properties are fixed, as in the case of the RAPT vehicle operating on the RTT.

If we consider one critical speed and effective conicity data pair from the test data, we can determine a value for m; i.e.,

$$m = \lambda V_c^2$$

Knowing m, we can substitute a range of values of effective conicity λ in the original expression and derive a theoretical relationship between critical speed and effective conicity.

3.4.4 Correlation of Effective Conicity with Critical Speed

The computer program used at the TTC to calculate effective conicities is that developed by Acorn Associates.[5] Using the X and Y coordinates of the wheel and rail profiles, produced as described in 3.4.2, together with the data required to locate them spatially, the computer software mounts the wheelset on a pair of rails and moves the wheelset laterally across the rails. At each lateral position, the contact points on the wheels and rails are determined together with the wheel radii at each point.

Figures 3-26 through 3-31 are examples of the computer outputs for the axle #3 profiles and a pair of design case rails of 136 lb/yd with a rail gage reading of 56.510"; i.e., very near to nominal gage. The rail profiles used are from the TTC's Roll Dynamics Unit (its rollers having precisely correct profiles, inclined at the appropriate cant angle). In Figure 3-26, the vertical axis represents the wheelset lateral displacement, and the horizontal axis represents the distance across the left wheel or rail surface. Thus, the left hand plot shows how the contact point moves across the wheel as the wheelset is laterally displaced across the rails. Similarly, the right hand plot shows the contact point movement across the rail. Figure 3-27 shows data trends for the right wheel and rail.

The calculated effective conicities for the 'nearly new' and 'worn' wheel profiles on axles #1 and #3 at the five selected rail sites are tabulated in Tables 3-5 and 3-6. In all cases the effective conicities with the worn profiles are higher than with the nearly new ones, and this increase was undoubtedly a major reason for the deterioration of wheelset stability as the life test progressed. At stations R59 and R67, the effective conicity increased by less than the 50% value quoted previously, whereas there were larger increases at the other rail sites. Thus, wheel wear alone did not account for the increase in effective conicity, and rail geometry had an effect. Determination of the precise reasons for these large increases is beyond the scope of this report, but it should be noted that at stations R59 and R67, the rails were slightly further apart than the nominal rail gage, whereas the other sites showed a narrower gage.

From the data shown in Figures 3-26 and 3-27 and the nominal wheel diameters, a rolling radius difference graph can be computed as shown on the right side of Figure 3-28. Because the wheels were nearly new and the rail profiles were design case, the graph looks similar to our idealized one. The dotted line has been drawn manually to determine the slope of the graph. Since the vertical axis has been non-dimensionalized by dividing by rail gage,

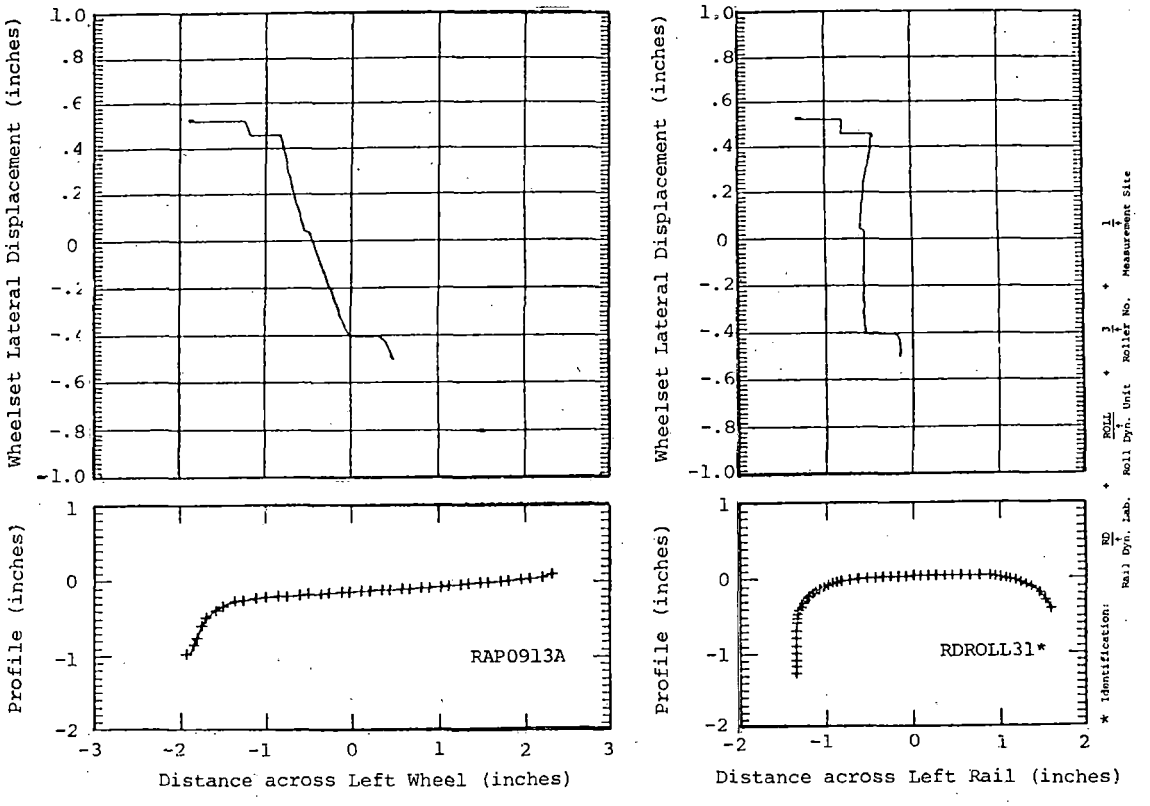

FIGURE 3-26. CONTACT POINT SHIFT OF RAPT AXLE #3 LEFT WHEEL (10-24-80 PROFILE) ON NEW 136 lb/yd RAIL.

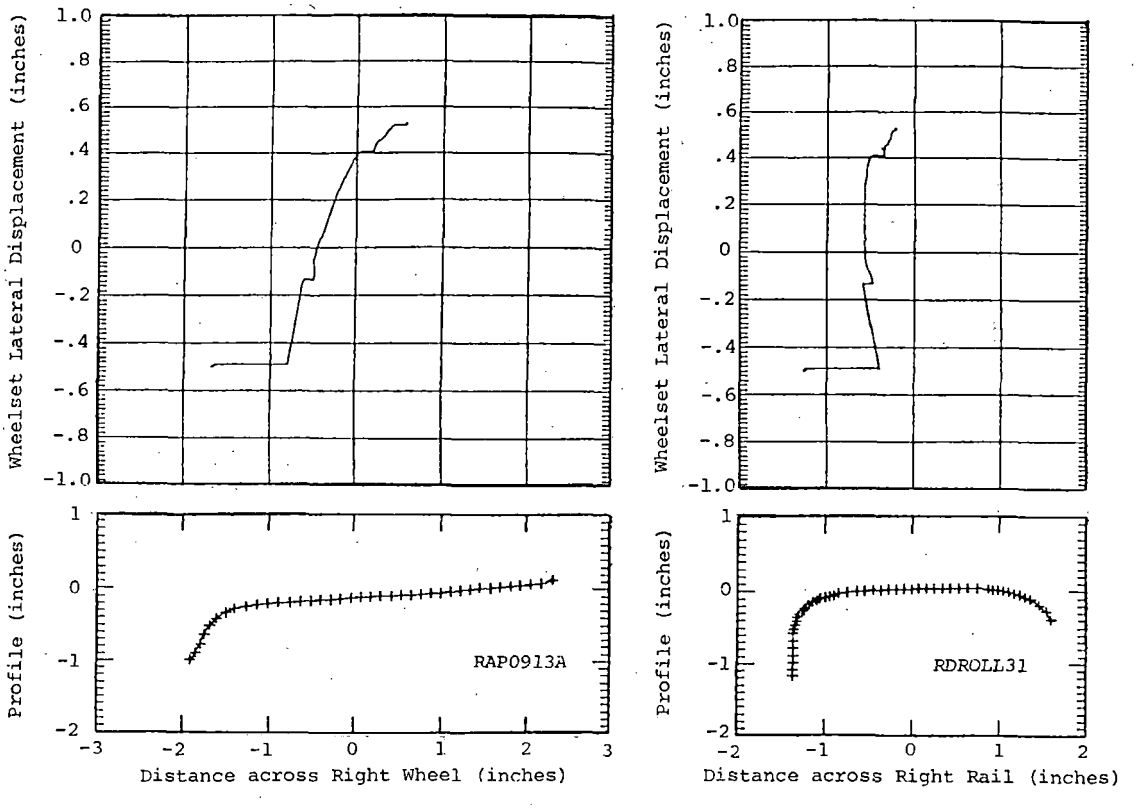

FIGURE 3-27. CONTACT POINT SHIFT OF RAPT AXLE #3 RIGHT WHEEL (2-13-81 PROFILE) ON NEW 136 lb/yd RAIL.

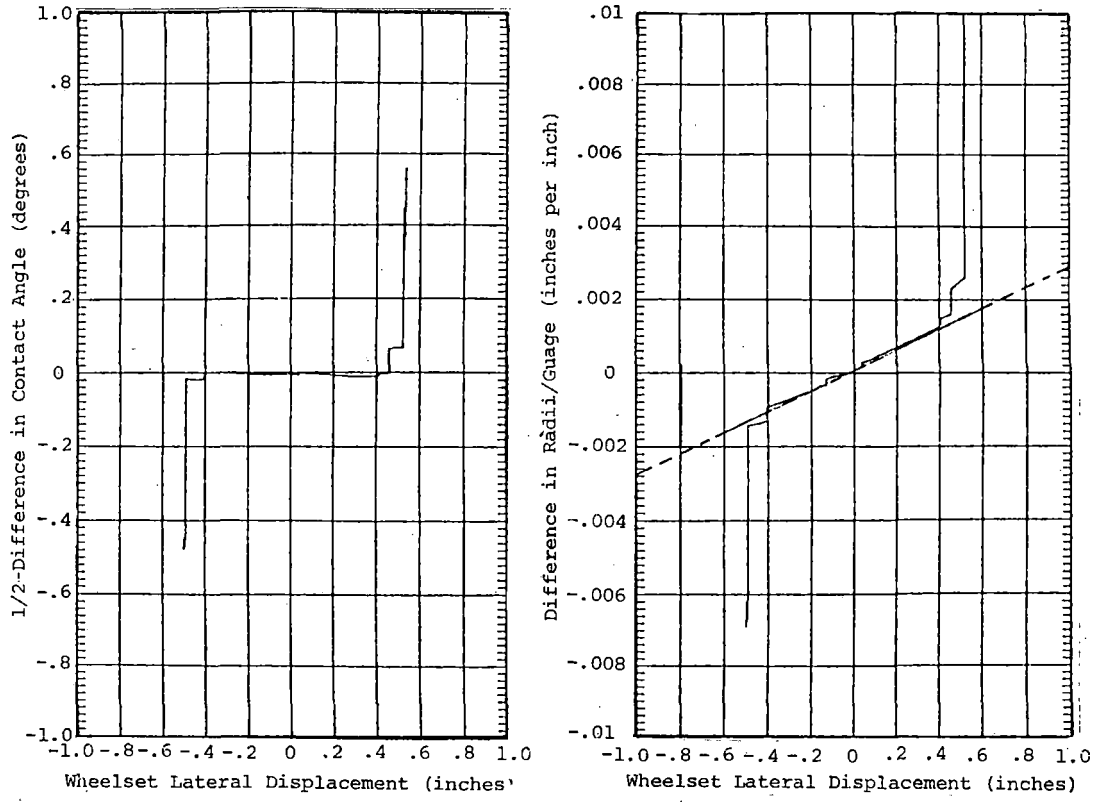

FIGURE 3-28. ROLLING RADIUS DIFFERENCE GRAPH, RAPT AXLE #3 (10-24-80 PROFILE) ON NEW 136 lb/yd RAILS.

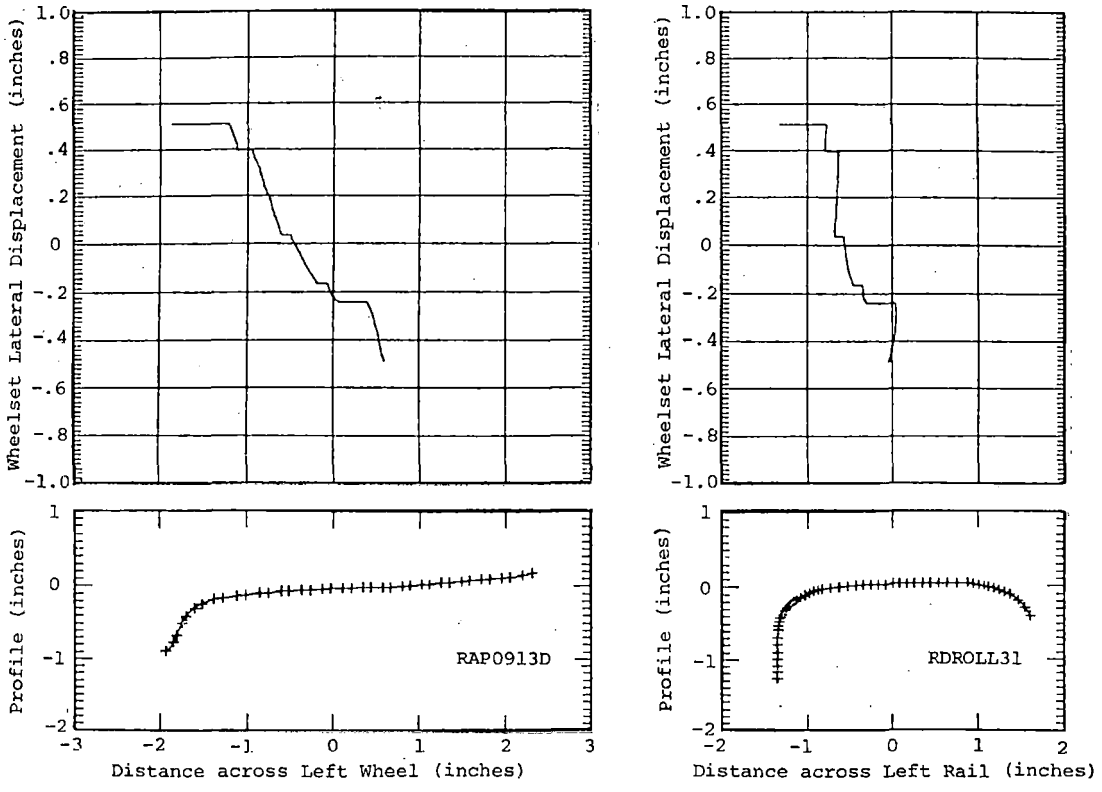

FIGURE 3-29. CONTACT POINT SHIFT OF RAPT AXLE #3 LEFT WHEEL (2-13-81 PROFILE) ON NEW 136 lb/yd RAIL.

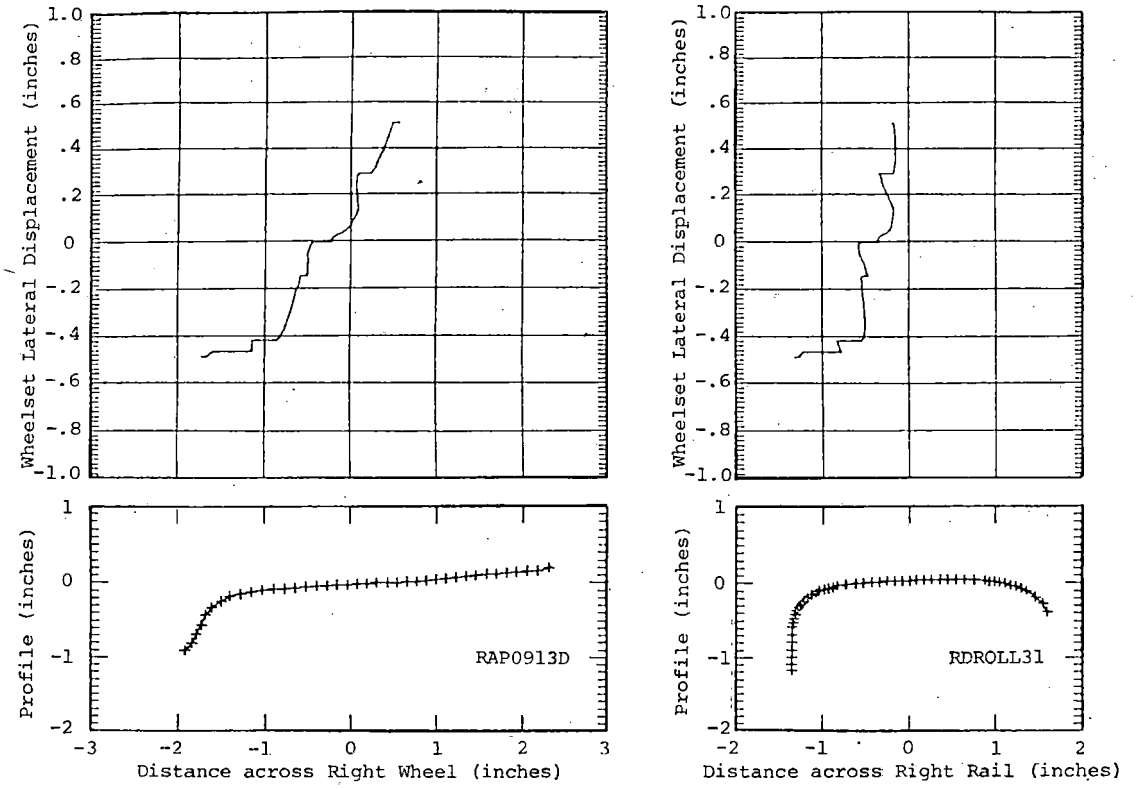

FIGURE 3-30. CONTACT POINT SHIFT OF RAPT AXLE #3 RIGHT WHEEL (2-13-81 PROFILE) ON NEW 136 lb/yd RAIL.

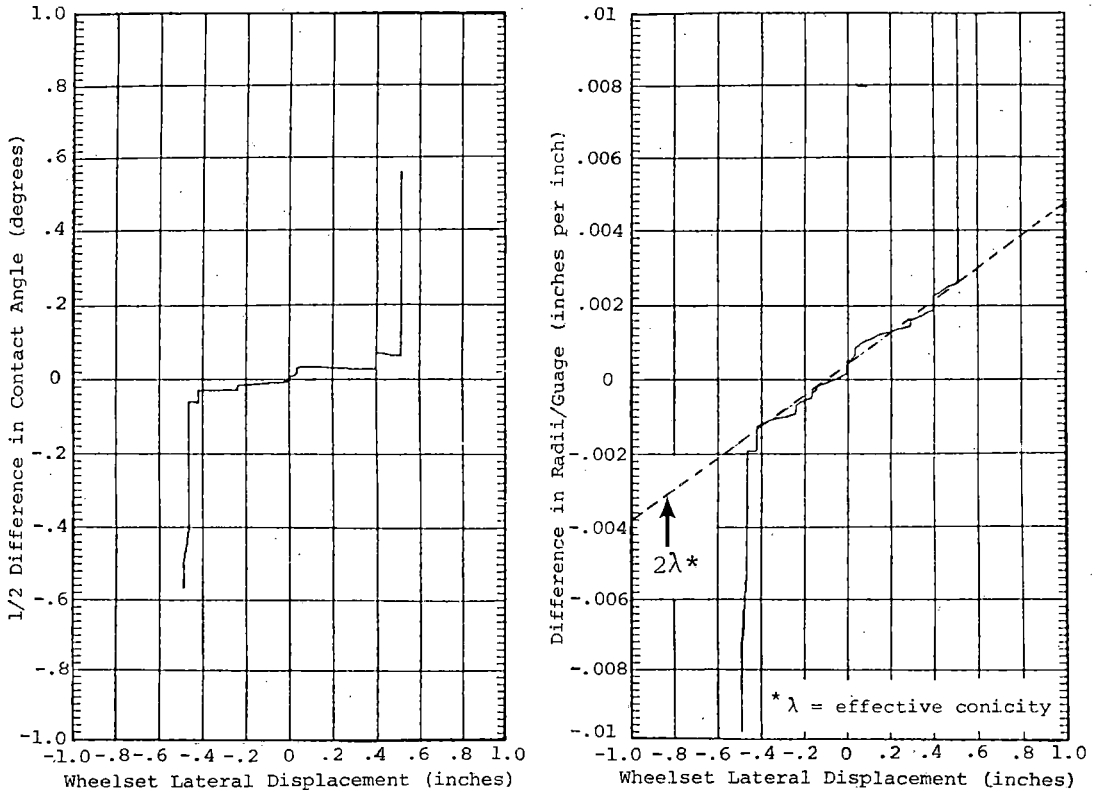

FIGURE 3-31. ROLLING RADIUS DIFFERENCE GRAPH, RAPT AXLE #3 (2-13-81 PROFILE) ON NEW 136 lb/yd RAIL.

TABLE 3-5. EFFECTIVE CONICITIES OF RAPT AXLE #3.

RTT Station	Rail Gage (in)	Effective Conicity (λ) 10/24/80 Wheel Profiles	Effective Conicity (λ) 2/13/81 Wheel Profiles	Critical Speed (V_c) 2/12/81 (mi/h)
R25	56.34	0.08	0.15	97-103
R47	56.34	0.07	0.136	100-105
R59	56.51	0.10	0.14	102-108
R67	56.57	0.10	0.13	102-108
R72	56.42	0.08	0.18	87-93

TABLE 3-6. EFFECTIVE CONICITIES OF RAPT AXLE #1.

RTT Station	Rail Gage (in)	Effective Conicity (λ) 10/24/80 Wheel Profiles	Effective Conicity (λ) 2/16/81 Wheel Profiles	Critical Speed (V_c)* (mi/h)
R25	56.34	0.08	0.16	94-100
R47	56.34	0.08	0.157	97-103
R59	56.51	0.12	0.152	99-105
R67	56.57	0.12	0.137	99-105
R72	56.42	0.11	0.182	84-90

*Critical speeds lowered by 3 mi/h as compared to those noted on 2/12/81.

the effective conicity is determined by multiplying the slope by 1/2 x rail gage. In this case,

Effective conicity = 0.00285 x 28.255 = 0.08.

In order to determine the effect of the tread wear on the conicity, the axle #3 worn profiles were run against the same design case rails; Figures 3-29 and 3-30 show the computer outputs for these cases. From Figure 3-31, the rolling radius difference plot:

Effective conicity = 0.00425 x 28.255 = 0.12.

Thus, on a new pair of rails, the tread wear experienced on the wheels of axle #3 during the life test had caused a 50% increase in effective conicity.

Table 3-5 lists the critical speeds noted during the video test on 2/12/81. These speeds are noted as a 6 mi/h range because the actual critical speed could only be determined to that accuracy. The critical speeds quoted in Table 3-6 are 3 mi/h lower than those noted on 2/12/80. These speeds have been lowered because the wheel profiles on axle #1 were not measured until 2/16/81--i.e., two full nights running after 2/12/81. The 3 mi/h critical

speed reduction is arbitrary, but the author feels that it is justified because of the rapid deterioration in wheelset stability noted at this time.

The worn wheel conicities are shown plotted against critical speed in Figure 3-32. These values are not plotted as points but as ranges because the critical speed values were not precise. There appears to be a relationship between conicity and critical speed. This theoretical relationship was determined as described below.

For the RAPT vehicle operating on the RTT, we can substitute one data pair (λ , V_c) from Table 3-5 in the expression:

$$m = \lambda V_c^2 \qquad \text{(see explanation in Section 3.4.3)}$$

and thereby determine a value for m. The data pair selected was for the RTT station R72. Critical speed V_c was 90 mi/h, and from the wheel/rail profile integration at this station, the effective conicity λ was 0.18.

$$\text{Therefore, } m = 0.18 \times 90^2$$
$$= 1458.$$

The theoretical critical speed/effective conicity relationship drawn in Figure 3-32 was constructed by using the value of m = 1458 in the transposed equation:

$$V_c^2 = \frac{1458}{\lambda}$$

This theoretical relationship appears to describe the effective conicity/critical speed relationship well. The measured values of effective conicity and the corresponding recorded critical speeds are shown superimposed on the theoretical line, and can be seen to follow the general trend well. The theoretical critical speed for an effective conicity of 0.1 is 121 mi/h, which agrees with observations that wheelset instability was infrequent at the start of the life test, when, as seen in Tables 3-5 and 3-6, effective conicities were generally less that 0.1.

3.4.5 Effective Conicity Study on Northeast Corridor Track

As an extension of the effective conicity study conducted at TTC, measurements of track and wheel profiles typical of Northeast Corridor (NEC) operation were made to determine the effective conicity values likely to be seen in service.[7] Rail profiles were measured at ten locations on Amtrak track, south of Wilmington, Delaware, in an area suspected of having high effective conicity values. A visit was also made to an Amtrak overhaul shop at Wilmington, where wheel profiles were taken on several wheelsets with hollow-worn treads. The worst case wheel profile was selected for effective conicity analysis. Using this wheel profile and the rail profiles from the NEC sites, effective conicity values were calculated in the 0.17 to 0.25 range. Comparable values using the RAPT wheel profiles and NEC track profiles were lower, in the 0.10

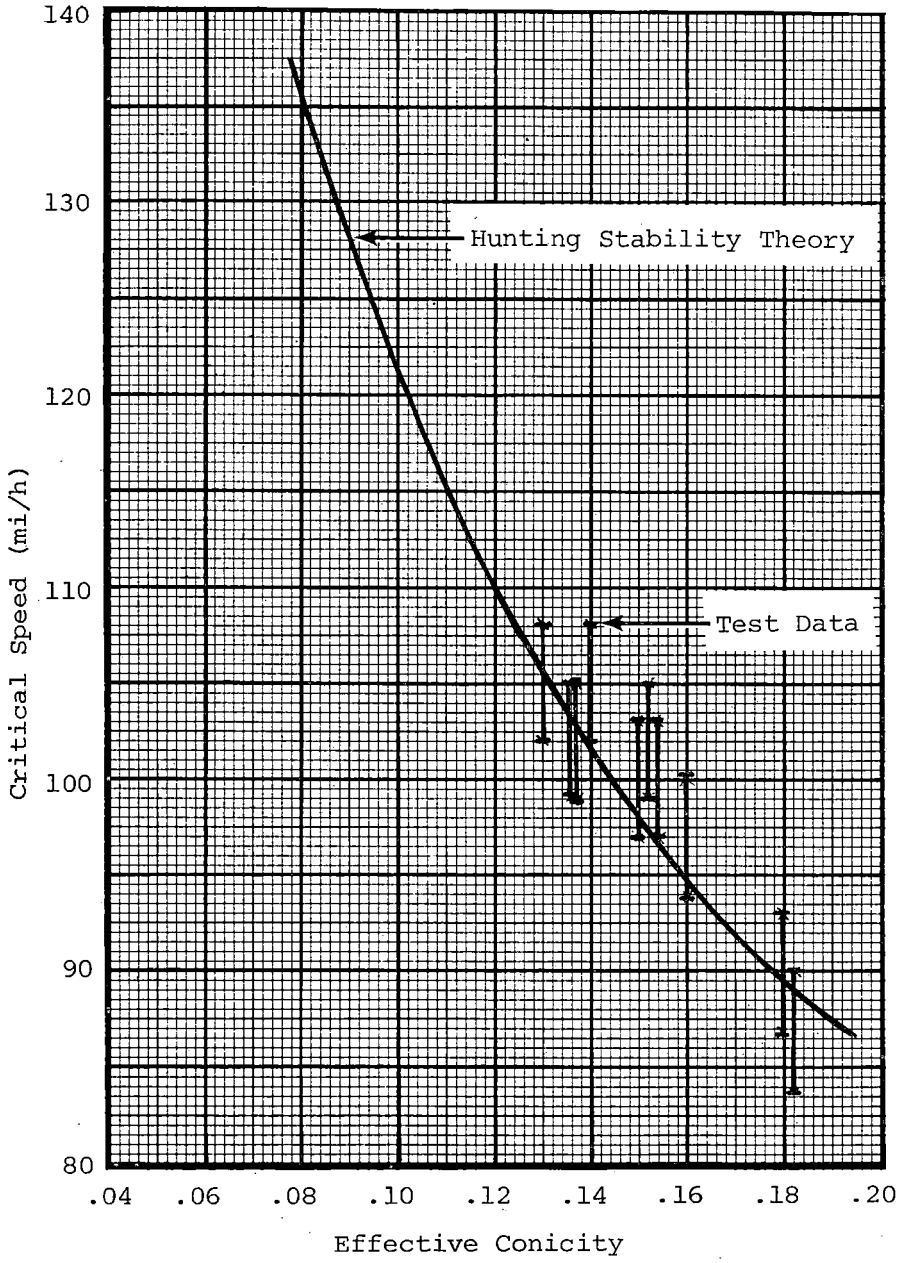

FIGURE 3-32. THE EFFECT OF CONICITY ON THE CRITICAL SPEED OF THE RAPT VEHICLE.

0.13 range. The 'worst case' effective conicity (of 0.31) was calculated from the Amtrak wheel profile and the rail profile at station R72 on the RTT.

3.4.6 Enhanced Stability Margins

In the opinion of the TTC analysts, the rapid deterioration of the RAPT car wheelset stability was due to an insufficient margin between the hunting speed and the maximum operating speed. Comparison of the modestly worn wheel profiles from the RAPT car on the RTT with the badly worn, hollow tread wheel profiles and heavily worn rail profiles from the NEC indicated that conicities of 0.3 or higher could be developed by the RAPT car on the NEC. TTC therefore suggests that a design conicity of 0.3 would be a realistic value with which to provide a 20 mi/h stability margin above the normal operating speed of 120 mi/h. Some designers[6] have used values as high as 0.4 for freight truck design studies.

The critical speed of a vehicle is dependent upon the horizontal (or plan view) stiffness values of the trucks. One of them, the primary yaw stiffness, $K\Theta$, can be related to the critical speed[4], V_c, by the equation:

$$V_c^2 \simeq m_1 K\Theta + m_2 ,$$

where

M_1 and m_2 are constants dependent upon primary stiffness, mass inertia, and effective conicity.

At the time that the original study was conducted, the suspension parameters were not known. Therefore, any proposed modifications had to be established from extrapolation to the TTC test data. From Figure 3-33 it can be predicted that, for a conicity λ of 0.3, the critical speed, V_c, would be 70 mi/h. Thus, to achieve a critical speed of 140 mi/h for $\lambda = 0.3$, the value of $(m_1 K\Theta + m_2)$ must be increased by a factor of 4. With this objective in mind, primary suspension modifications were initiated in preparation for Life Tests III and IV.

3.5 Primary Suspension Configuration Modifications (Life Tests III and IV)

Three primary suspension configurations were evaluated during the life testing phase of the RAPT program, in an attempt to increase the critical speed for axle lateral stability (hunting). As described in Section 2.0 and illustrated in Figure 2-2, the radial axle truck primary suspension is a two-part system, with vertical and horizontal motions accommodated by discrete spring systems. Vertical springing is provided by chevron steel/rubber elastomeric springs assisted by steel coil springs, operating between an upper journal box and the truck frame. This system is relatively stiff in the horizontal plane, but still affects horizontal shear stiffnesses, as will be shown later in this discussion. Horizontal shear springing is provided by

steel/rubber elastomeric 'sandwich' springs which attach the upper journal box to the axle journal bearing housings.

Primary suspension yaw stiffness has been shown (Section 3.4.5) to be one of the prime factors influencing axle lateral stability. As a result of the axle hunting experienced with the RAPT vehicle during Life Tests I and II, and the significant reductions in critical speed experienced with wheel wear, it became apparent that some modification of the truck was desirable to increase the inherent stability margins. Yaw stiffness changes were therefore made by modifying the horizontal shear springs. The original spring configuration used a three-layer rubber/steel sandwich. This was used for all initial performance, stability and ride quality phases of the test program, and for the Life I and II test programs. New springs were fabricated and fitted for the Life III test programs. Similar in configuration to the original springs, they were molded from a harder rubber compound, with one layer of elastomer replaced with a metal spacer plate (i.e., two rubber/steel sandwiches and one layer of steel).

For the Life IV program the springs fabricated for Life III were modified, in an attempt to further increase the primary suspension yaw spring rate. Four 3/4" diameter holes were drilled through the top steel/rubber/steel layers in each spring; dowels were then driven through the holes connecting the two steel plates. The intent was that the dowels would carry shear loads from the first steel plate to the second, thereby isolating one layer of rubber and increasing the shear stiffness. This configuration is referred to as the one-layer sandwich.

Each incremental change in yaw stiffness increased the critical speed at which axle hunting occurred by approximately 10 mi/h; however, the dominating effect remained the wheel wear, which increased the effective conicity and thereby reduced the lateral stability. The speed restrictions applied during each life test program illustrate the trends.

3.6 CURVING AND STABILITY OF MODIFIED YAW STIFFNESS

The curving performance and truck stability of the RAPT vehicle, with the original configuration of horizontal primary suspension springs, have been discussed in Sections 2.6 and 3.4, respectively. The curving performance tests examined high rail lateral forces during curve negotiation, and truck stability was examined by establishing a relationship between effective conicity (derived from wheel and rail profile measurements) and the critical speeds for the onset of axle hunting. Similar curving performance and stability studies were carried out for the modified primary suspensions evaluated in Life Tests III and IV. The results and conclusions of the studies are reported in the following sections.

3.6.1 High Rail Lateral Forces

The lateral forces generated at the rail during curve negotiation are a

measure of the effectiveness of the radial truck concept. The effect of increasing the truck yaw stiffness (to gain high-speed axle stability) on the lateral forces was therefore of prime concern. The high rail lateral forces were measured on the FAST track as described previously in Section 2.5, over the speed range 10 to 45 mi/h for each of the horizontal spring configurations. The test results are presented in Figures 3-33 and 3-34 for clockwise and counterclockwise directions of travel; the data are compared to the lateral forces developed by a coach in the test consist equipped with Pioneer III trucks. The plots show the lateral force trends with speed, for each axle of both trucks, during the negotiation of a 5° curve, 4" superelevation. The three-layer horizontal spring configuration (the original configuration used for Life Tests I and II) are compared to the two-layer configuration (Life Test III) and the one-layer configuration (Life Test IV). The following observations were made from the data:

- As was expected, the lead axle of each truck produced the highest lateral force. There were no discernible lateral force trends due to spring configuation, within a data scatter band of 1,000 pounds force.

- The lateral forces generated by the Pioneer III truck leading axles were 1 1/2 to 2 times greater than those generated by the radial trucks, across the speed range. Poor repeatability was noted for the Pioneer III data taken concurrently with the two-layer spring RAPT truck data, compared to that taken concurrently with the one-layer spring data. This was thought to be due to axle alignment on the Pioneer III trucks and the fact that the reference coaches were turned around between tests to equalize wheel wear.

- The counterclockwise direction data for the one-layer spring (A truck leading axle) showed a 2,000 lb increase in lateral force compared to the clockwise data across the speed range. The B truck leading axle data showed similar inconsistencies at low speeds. This was again thought to be due to axle alignment inconsistencies.

3.6.2 Stability/Yaw Stiffness Trends

Early life test running of the trucks (Life Tests I and II) showed that they were susceptible to wheelset hunting; the critical speed at which hunting became sustained reduced progressively with increasing mileage and wheel wear. The effective conicity study, which correlated measured wheel and rail profiles with critical speed data, showed that there was a relationship between critical speed and effective conicity. The literature review of Section 3.4.6 showed that primary suspension yaw stiffness is a prime factor influencing axle stability. The increased primary suspension yaw stiffnesses implemented in Life Tests III and IV were incorporated in an attempt to improve the stability of the radial truck. The effective conicity/critical speed data gathered during these test phases is presented in Figure 3-35, and supports this hypothesis. The critical speeds are plotted with a 5 mi/h tolerance to represent the speed range over which sustained hunting was established; the effective conicities were calculated using the track profiles through the core area of the RTT, between stations R70 to R75. The techniques used to determine

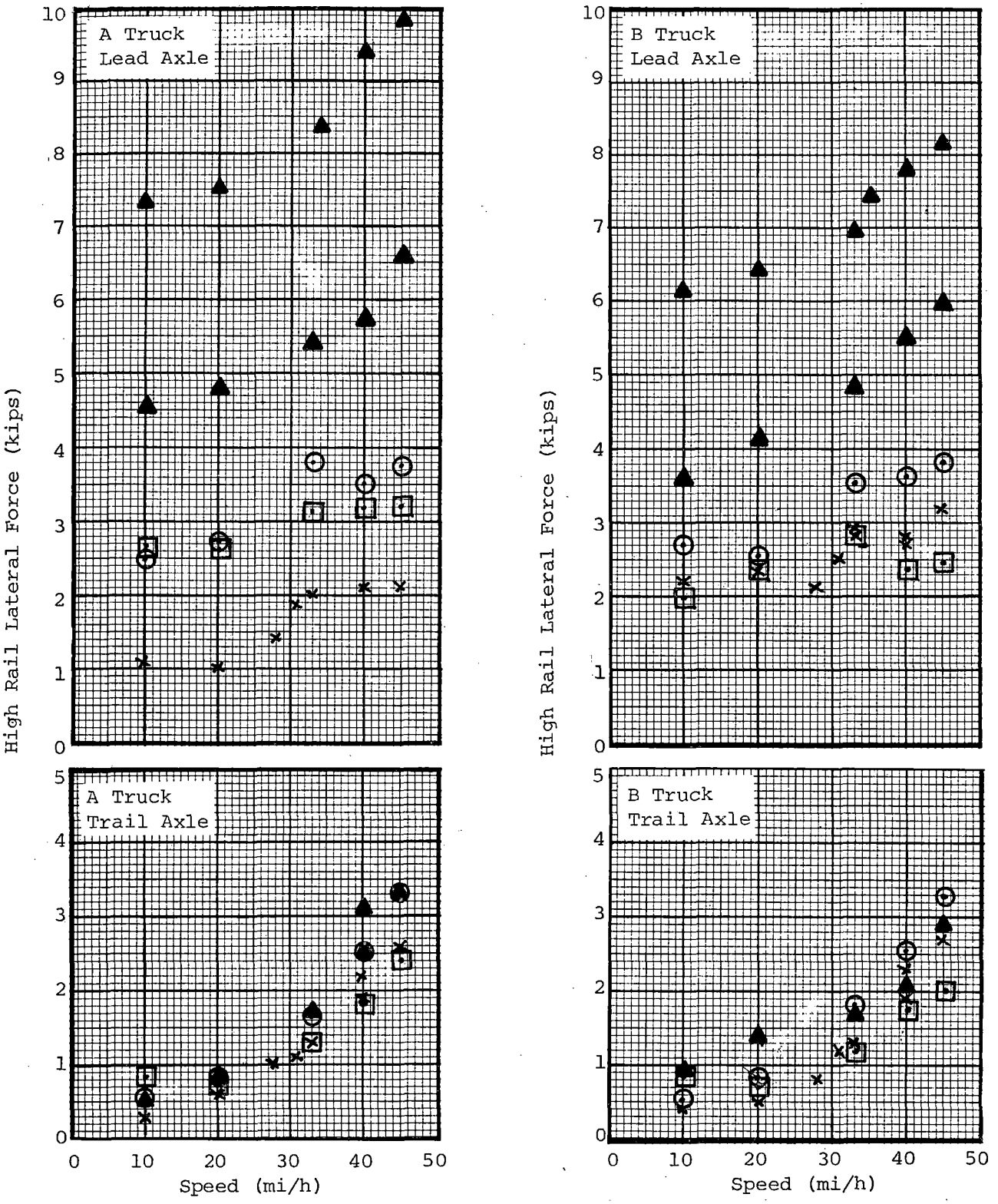

FIGURE 3-33. HIGH RAIL LATERAL FORCES, COMPARISON OF SPRING TYPES, CLOCKWISE RUNNING.

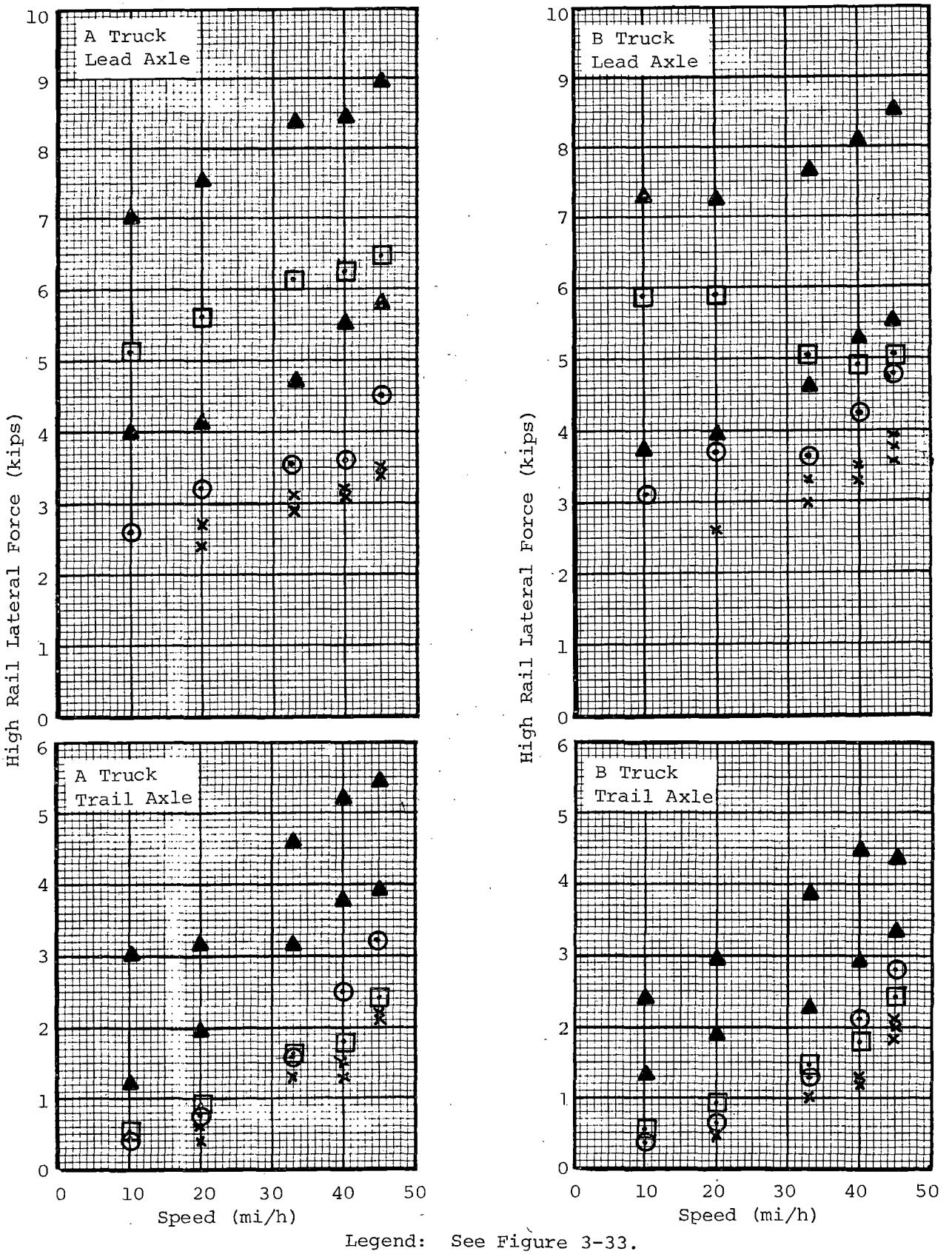

Legend: See Figure 3-33.

FIGURE 3-34. HIGH RAIL LATERAL FORCES, COMPARISON OF SPRING TYPES, *COUNTERCLOCKWISE RUNNING*.

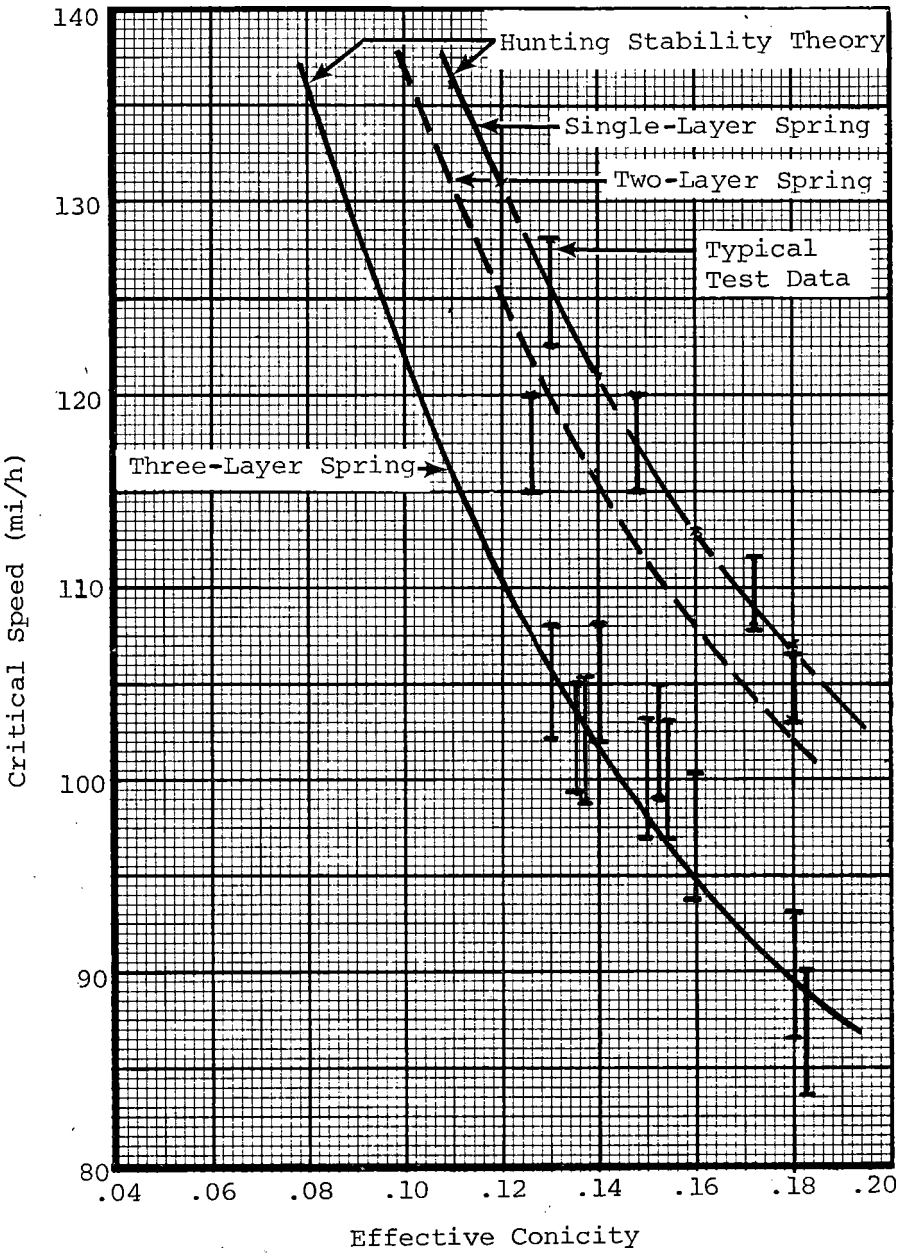

FIGURE 3-35. EFFECTIVE CONICITY/CRITICAL SPEED TRENDS FOR THREE PRIMARY SUSPENSION CONFIGURATIONS.

effective conicities were those used previously for the effective conicity study of Life Test II, described in Section 3.4. Using the simplified hunting stability algorithm (also Section 3.4) together with the test data, theoretical critical speed/effective conicity trends were established for the modified horizontal spring configurations.

The data and the trend lines show that increasing yaw stiffness of the primary suspension did increase the critical speed for sustained axle hunting. For example, at an effective conicity of 0.12, the critical speed went from 110 mi/h with the three-layer springs, to 125 mi/h with the two-layer springs, and finally to 130 mi/h for the single-layer configuration. The change from three-layer to one-layer spring represents an approximate doubling of the primary yaw stiffness. The dominant trend however was due to changes in effective conicity brought about by wheel wear. At the conclusion of Life Test IV, the single-layer spring configuration, i.e., the configuration with the best stability margin, was operating at an effective conicity of 0.17, and the critical speed was in the 108 to 112 mi/h range. This is below the 120 mi/h design operating speed of the truck.

3.6.3 Conclusions and Recommendations

Based on the test results of the RAPT vehicle life test series, the following conclusions and recommendations can be made:

- As originally configured, the trucks had insufficient stability margin to operate at their design speed of 120 mi/h in a stable condition, with effective conicities greater than 0.10. The predominant instability was wheelset hunting.

- The stability was improved by stiffening the horizontal primary suspension; with a yaw stiffness approximately double that of the original configuration the truck was stable at 120 mi/h with effective conicities up to 0.14.

- The dominant factor influencing wheelset stability was shown to be effective conicity. Wheel and rail profile measurements made on a section of track on the NEC have shown that effective conicities up to 0.3 can be expected in service; the truck will require further modification to operate in a stable mode in this regime.

- Future test programs should include an evaluation of truck stability over the range of effective conicities likely to be found in service.

- Rail lateral forces in a curving situation were not affected by changes in primary suspension yaw stiffness, over the range evaluated. It is therefore likely that further increases in stiffness could be made without substantially changing the curving performance. With the current design, the limiting factor to increasing yaw stiffness may be the horizontal stiffness of the primary vertical springs.

- The early flanging problems of the truck indicate a sensitivity to axle alignment. A series of tests should be conducted with axle alignment as a

variable, to quantify the effect of alignment on curving performance.

- The simplified theoretical discussion contained herein indicates that a four-fold increase in yaw stiffness may be required. An increase of this magnitude may be detrimental to the vehicle's curving performance, and therefore suspension stiffness should be the subject of a parametric study, using curving and stability math modeling analysis.

3.7 TRUCK CHARACTERIZATION

Concurrent with the testing of modified primary suspension spring rates, an analytical study was proposed using two math models--one a hunting instability model, the other a curving performance model. As a prerequisite to the study, a truck characterization test program was accomplished to provide truck parameter inputs to the models; tests were carried out to determine primary longitudinal stiffness, primary lateral stiffness, truck rotational break-away torque, axle-to-axle shear stiffness, and longitudinal bending stiffness for each primary suspension configuration. In addition to the test configurations described earlier, longitudinal and lateral stiffness tests were conducted with the rubber/steel sandwich springs replaced with steel blocks, to determine the contribution of the vertical chevron springs to the horizontal spring rates. Table 3-7 details the truck characterization tests carried out on each suspension configuration. The tests are described in brief in the following paragraphs.

TABLE 3-7. SUMMARY OF TRUCK CHARACTERIZATION TESTS PERFORMED.

	Sandwich Configuration			Chevron
	1 Layer	2 Layer	3 Layer	Pad **
Primary Longitudinal Stiffness	x*	x	x	x
Primary Lateral Stiffness	x	x	x	x
Truck Rotational Breakaway Torque	x	x	x	x
Shear Stiffness	x	x		
Longitudinal Bending Stiffness		x		

* tests performed.
** Sandwiches were replaced by solid steel blocks.

3.7.1. Truck Spring Stiffness Tests

All tests, with the exception of the primary longitudinal stiffness tests, were conducted with the steering cross-links in place. Measurements were performed only on the A-end truck. All tests, with the exception of the lateral primary suspension spring rate, were conducted by supporting the truck axles on one or two air tables. These devices provide a frictionless cushion of air

to support the axles, when activated by means of a shop air line. Thus, friction forces between the axle and rail are reduced to zero and the true suspension parameters can be measured.

Primary Longitudinal Stiffness. The test setup is illustrated in Figure 3-36. With both axles of the truck resting on separate air tables, a longitudinal force was applied between wheel L-3 and the side frame, by means of a hydraulic cylinder. The applied force was measured by a load cell mounted in series with the hydraulic cylinder; longitudinal displacements of both wheels of the loaded axle relative to the truck side frame were measured with dial gage indicators. The test was repeated for wheels L-4, R-4, and R-3.

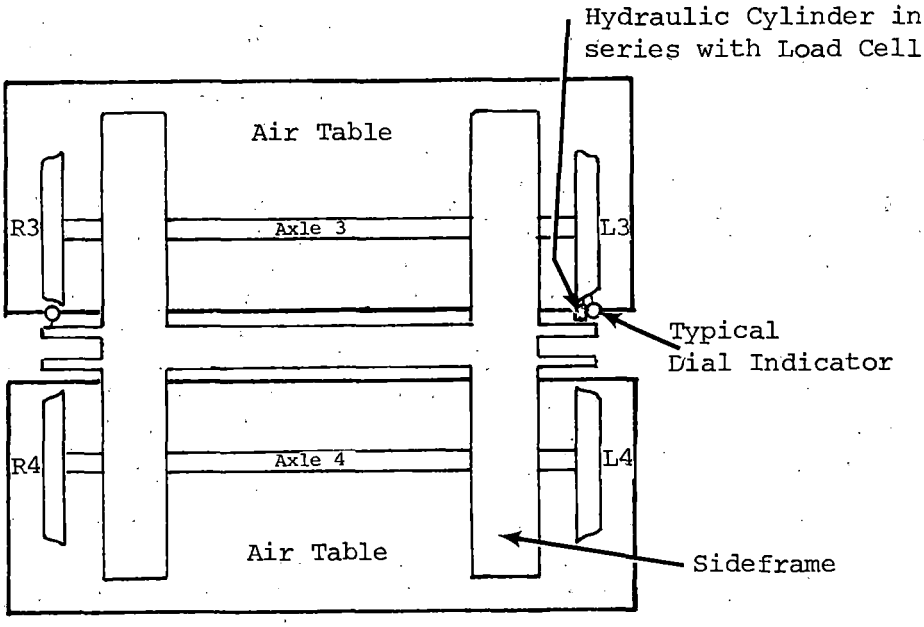

FIGURE 3-36. LONGITUDINAL STIFFNESS TEST SETUP.

Primary Lateral Stiffness. The schematic of Figure 3-37 illustrates the test setup. With the truck wheels resting on the track, a lateral force was applied to the center of the truck sideframe by means of a hydraulic cylinder attached with steel cables. Lateral force was measured with a load cell mounted in series with the hydraulic cylinder, while lateral displacements of all four wheels were measured relative to the sideframe with dial gage indicators.

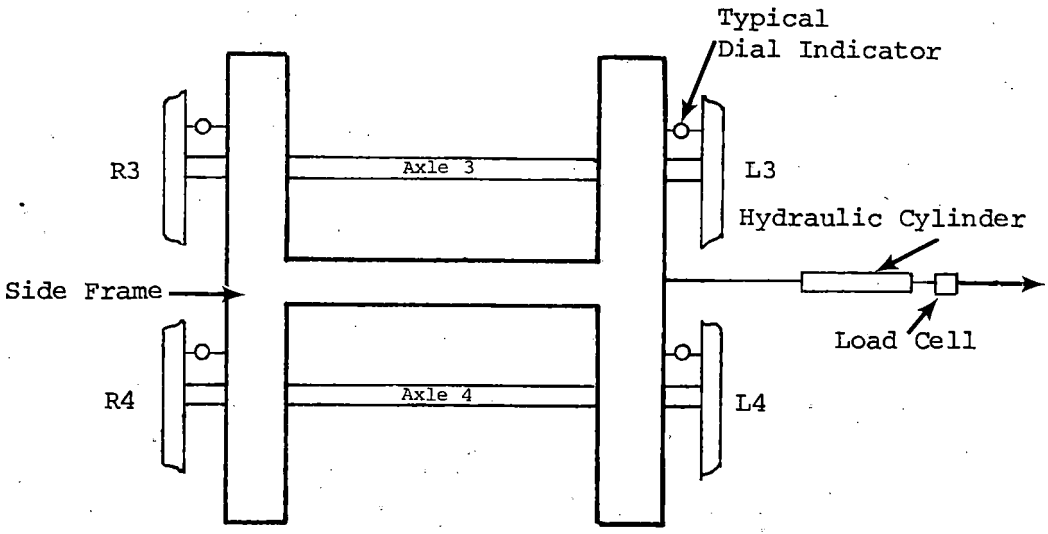

FIGURE 3-37. LATERAL STIFFNESS TEST SETUP.

Truck Rotational Breakaway Torque. This test was conducted to determine the torque necessary to overcome the frictional restraints between the truck bolster and the carbody bolster. With both axles of the truck resting on a common air table, a rotational torque was applied to the truck by two hydraulic cylinders attached to opposite corners of the table (Figure 3-38). The applied force of each cylinder was measured by load cells mounted in series. The point of friction breakaway was determined by a string-pot type displacement transducer mounted between the sideframe and the carbody underframe. Load cell readings were recorded at the point of break-away as indicated by the displacement transducer.

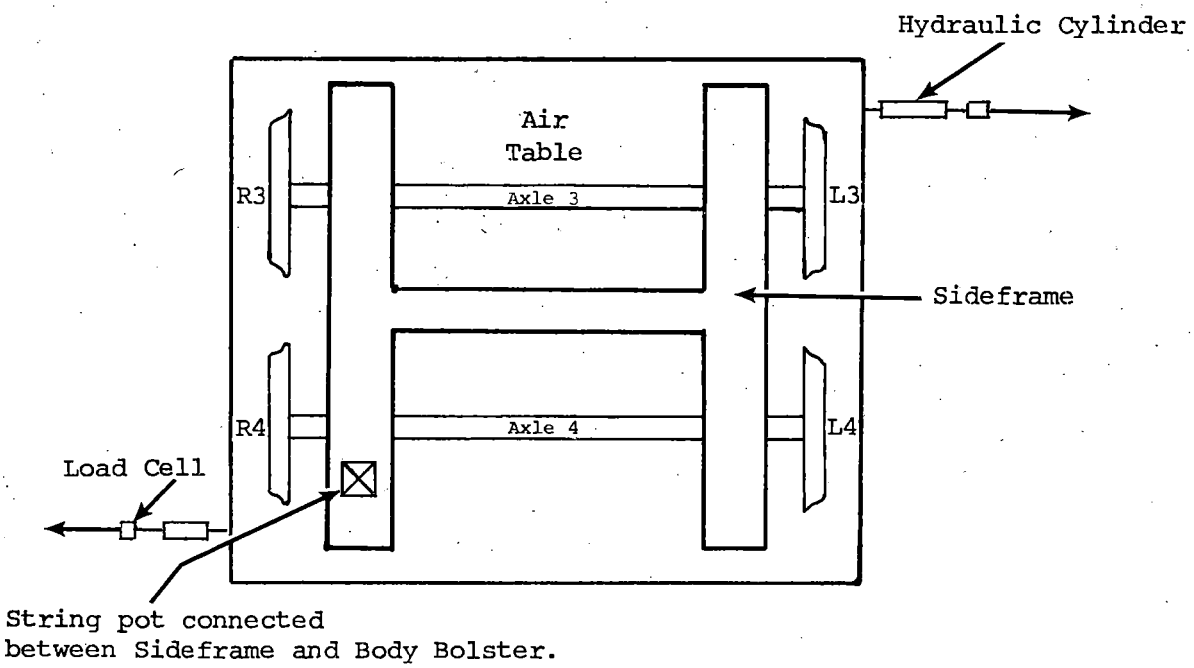

FIGURE 3-38. TRUCK ROTATIONAL TORQUE TEST SETUP.

Shear Stiffness. With both axles of the truck resting on separate air tables and the truck frame restrained from yawing by wood blocks wedged between the side frame and the carbody center sill, equal and opposite shear forces were applied at the axles (Figure 3-39). The forces were applied by means of two hydraulic cylinders and measured by two load cells mounted in series with the cylinders. The relative lateral displacement between the axles was measured with a dial gage indicator.

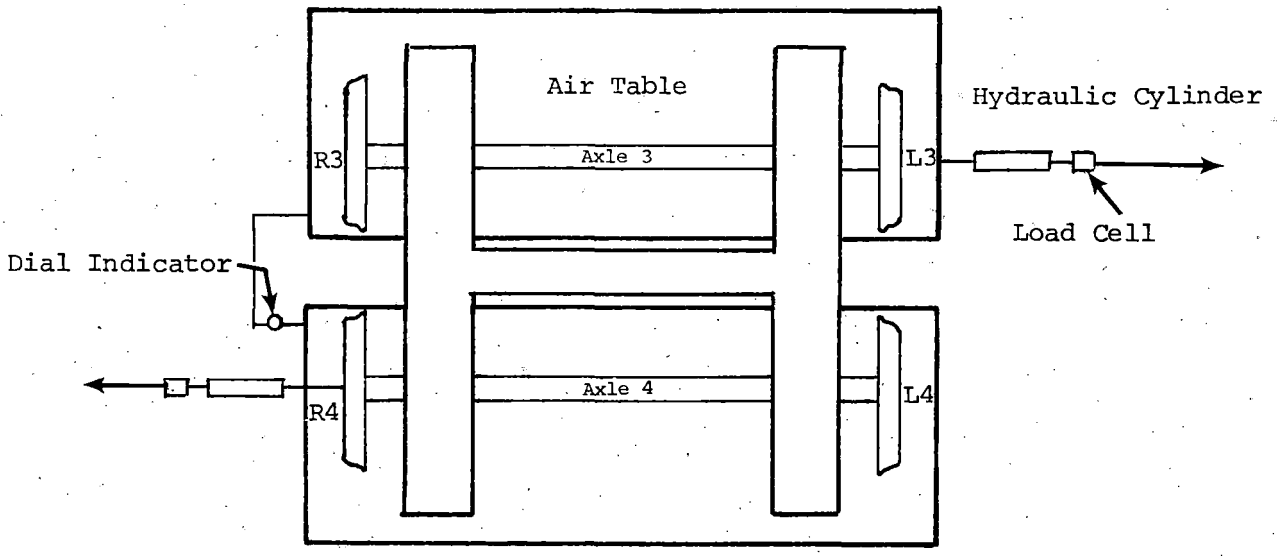

FIGURE 3-39. PRIMARY SUSPENSION SHEAR STIFFNESS TEST SETUP.

Longitudinal Bending Stiffness. With both axles of the truck resting on separate air tables, spreading forces were applied to the axles through two hydraulic cylinders. Each cylinder was attached to an axle at an offset from its longitudinal centerline. The applied forces were measured with load cells while the longitudinal displacements of each wheel relative to the sideframe were measured with dial indicators (Figure 3-40).

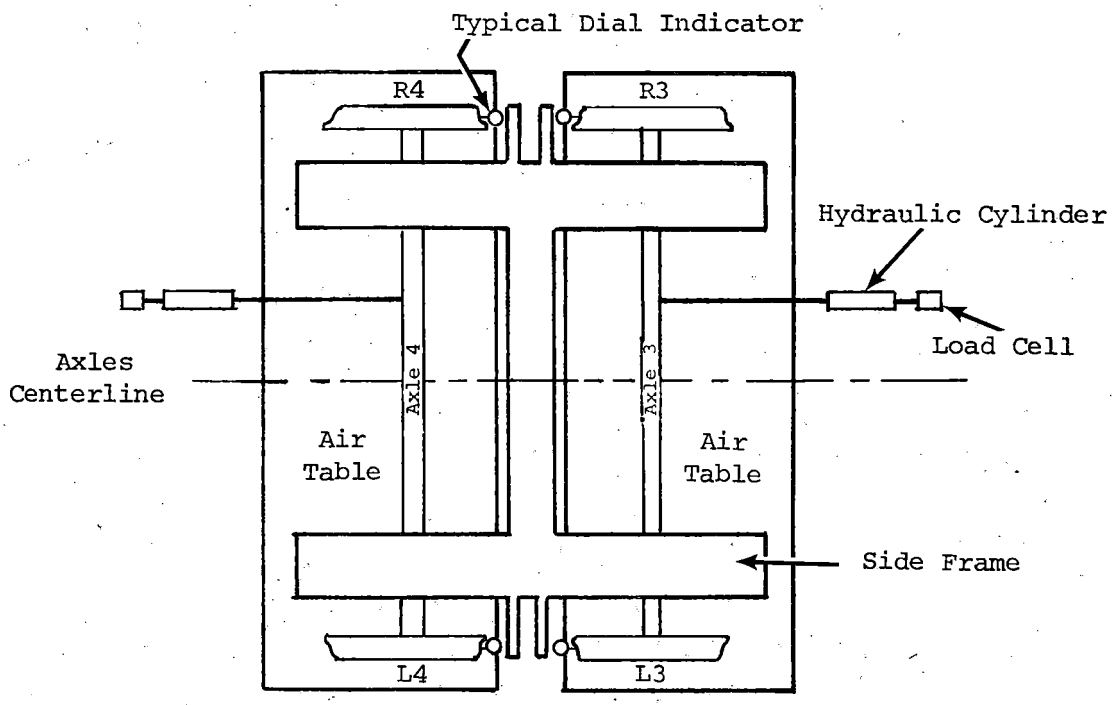

FIGURE 3-40. LONGITUDINAL BENDING STIFFNESS TEST SETUP.

3.7.2 Characterization Test Results

The results of the truck primary suspension tests are tabulated in Table 3-8. The numbers quoted are for an individual spring. In the case of the longitudinal stiffness determination, where forces and deflections were measured at the wheels rather than at the journals, moments were computed to determine the loads at the journals. The deflections at the jounals were then determined by proportionality. Lateral stiffness was determined by using the average displacement for all four wheels, and (assuming that the force is equally divided between wheels) one-fourth of the applied load. In each case load/deflection curves were plotted, and the slopes were computed from linear regression techniques.

TABLE 3-8. TRUCK CHARACTERIZATION TEST RESULTS.

Spring Configuration	Average** Longitudinal Stiffness (kip/in)	Average** Lateral Stiffness (kip/in)	Shear Stiffness With Cross-links (kip/in)	Shear Stiffness Without Cross-links+ (kip/in)	Longitudinal Bending Stiffness w/ Cross-links (kip-in/°)	Longitudinal Bending Stiffness w/o Cross-links+ (kip-in/°)	Truck Break-Away Torque (kip.ft)
3-Layer	17.96	8.52					12.95
2-Layer (plus Steel Spacer Plate)	35.31	11.41	60.02	11.41	343.9	284.45	12.95
2-Layer (1-Layer pinned)	40.83	13.11	58.22	13.11			12.95
Chevron Springs*	63.63	16.96					12.95

* Horizontal shear springs replaced with steel blocks.
** Average of 4-spring stiffness measurements.
\+ Derived values.

3.7.3 Discussion of Truck Stiffness Parameters

Primary Longitudinal and Lateral Stiffness. Despite the expectation that the primary longitudinal stiffness would be increased significantly by converting the 2 layer sandwich to a single-layer sandwich, the measured results indicate only an average increase of 15.6%. This is because the series stiffness of the chevron is fairly low and therefore limits the overall suspension system stiffness, as explained in the following discussion.

The primary longitudinal stiffness of the RAPT vehicle could be closely represented by the following relationship:

$$\frac{1}{K_{sys}} = \frac{1}{K_s} + \frac{1}{K_c} \qquad (1)$$

where,

K_{sys} = primary longitudinal stiffness,
K_s = longitudinal stiffness of sandwich, and
K_c = longitudinal stiffness contributed by the chevron pad and the rest of the suspension system.

and,

$$K_s = \frac{K_r}{2} \quad \text{for 2-layer sandwich} \qquad (2)$$

$$K_s = K_r \quad \text{for 1-layer sandwich} \qquad (3)$$

where,

K_r = longitudinal stiffness of each rubber layer of the sandwich.

Substituting from Table 3-8

K_{sys} = 35.31 kip/in for the 2-layer sandwich

and

K_c = 63.63 kip/in

into equation (1),

$$K_s = 79.33 \text{ kip/in.} \qquad (4)$$

Substituting equation (4) into equation (2),

$$K_r = 158.66 \text{ kip/in} \qquad (5)$$

Then using equations (3) and (5), the longitudinal stiffness of the 1-layer sandwich is:

$$K_s = K_r = 158.66 \text{ kip/in.} \quad (6)$$

Substituting

$K_s = 158.66$ kip/in for the 1-layer sandwich

and

$K_c = 63.63$ kip/in

into equation (1), the calculated primary longitudinal stiffness K_{sys} for the 1-layer sandwich is

$K_{sys} = 45.42$ kip/in

while the measured value is 40.83 kip/in.

The calculated value of the primary longitudinal stiffness for the 1-layer sandwich agrees fairly closely with the measured data. The slight discrepancy could be contributed in part to system non-linearities and in part to measurement tolerances. Thus, the value of K_{sys} for the 1-layer sandwich is limited by the value of K_c. A higher chevron pad stiffness would have produced a larger change in K_{sys} when changing from 2-layer to 1-layer sandwiches.

The same could be said about the primary lateral stiffness, using

$K_{sys} = 11.41$ kip/in for the 2-layer sandwich

and

$K_c = 16.96$ kip/in,
$K_s = K_r = 69.73$ kip/in for the 1-layer sandwich.

Again, using

$K_s = 69.73$ kip/in for the 1-layer sandwich

and

$K_c = 16.96$ kip/in,

the calculated primary lateral stiffness K_{sys} for the 1-layer sandwich is

$K_{sys} = 13.64$ kip/in

while the measured value is 13.11 kip/in.

Shear Stiffness. There is practically no difference between the shear stiffness with 1-layer and 2-layer sandwiches. The small discrepancy between the two values could easily be explained through measurement tolerances. It is also apparent that the cross-links are the principal contributors to the

shear stiffness, while the effects from the sandwiches are considered to be minimal.

Longitudinal Bending Stiffness. The data indicate that the longitudinal bending stiffness is increased by 59.5 kip-in/degree (or 21%) when the cross-links are in place for the 2-layer sandwich configuration. Furthermore, it is believed that the amount of increase with the other sandwiches will be the same (i.e., 59.5 kip-in/degree), but the percentage of change will be different. Thus, the shear stiffness and longitudinal bending stiffness results confirm the radial truck design philosophy. The cross-links have significantly increased the shear stiffness, without increasing the axle bending stiffness.

REFERENCES

1. Elkins, J.A., and Eickholf, B.M., Advances in Non-Linear Wheel/Rail Force Prediction Methods and Their Validation, ASME Winter Meeting, New York, December 1979.

2. Blake, Alexander, Design News, June 1974

3. Timoshenko,S. Strength of Materials, Part II, Robert E. Krieger Publishing Company, Huntington, New York, 1976.

4. Cooperrider, N.K., and Law, E.H., Dynamics of Wheel-Rail Systems, class notes for TTC course, January 7-11, 1981.

5. Heller, R., and Cooperrider, N.K., Users' Manual for Asymmetric Wheel/Rail Contact Characterization Program, FRA/ORD-78/05, December 1977.

6. Pollard, Dr. M.G., "The Development of Cross-Braced Freight Bogies," Rail International, September 1979.

7. "Further Conicity Measurements for the RAPT Program", TTC/TDAS Internal Memo W-2420-0006, March 27, 1981.

GPO 835-824

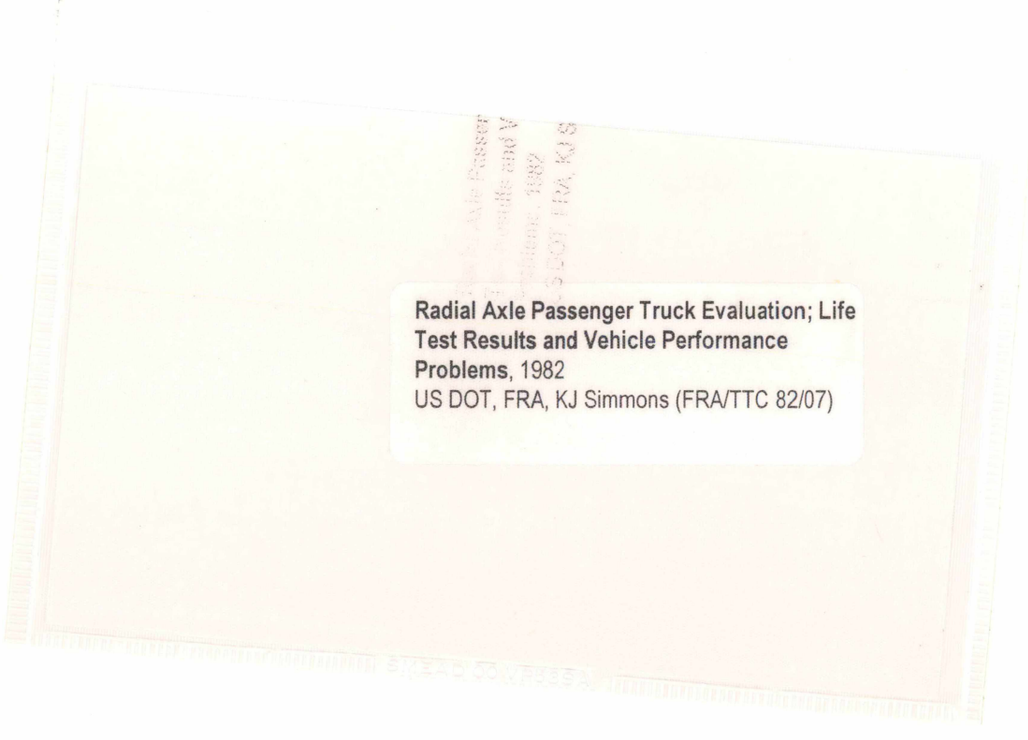

Radial Axle Passenger Truck Evaluation; Life Test Results and Vehicle Performance Problems, 1982
US DOT, FRA, KJ Simmons (FRA/TTC 82/07)